Preparation of mineral-binding poly (ethylene sodium phosphate) conjugates for biomedical applications

	Noree Susita
year	2020-03-31
	34416 772
URL	http://doi.org/10.32286/00021319

2020 年 3 月
関西大学審査学位論文

Preparation of mineral-binding poly(ethylene sodium phosphate) conjugates for biomedical applications

Susita Noree

Graduate School of Science and Engineering

Kansai University

ABSTRACT

Polyphosphoesters (PPEs) have been used in medical applications owing to their diverse features, including biocompatibility, biodegradability, and facile modification of their side chains with various functional groups. Poly(ethylene sodium phosphate) (PEP·Na), a class of water-soluble PPEs, possesses a backbone of anionic phosphodiester providing excellent biomineral affinity to hydroxyapatite (HAp) which is the main mineral of human bone and tooth. The potential of nontoxic materials made from PEP·Na for mineral targeting was explored in order to demonstrate the effectiveness of a nanocomplexation of protein–amphiphilic PEP·Na as a protein carrier and the immobilization of zwitterionic PPE containing PEP·Na on mineral surfaces for anti-erosion and bacterial anti-adhesion. In order to deliver medically therapeutic proteins, proteins were conjugated with polymers to inhibit denaturation and aggregation due to the susceptibility of the proteins. The thermo-assisted complexation of proteins with amphiphilic cholesterol-terminated PEP·Na (CH-PEP·Na) was proposed as a novel strategy to enhance their durability. A nanocomplex of CH-PEP·Na with protein was formed through hydrophobic interactions between partially lipophilic proteins and the cholesteryl appendages of CH-PEP·Na, induced by thermal treatment. The complexes exhibited size stability for long-term storage in an aqueous solution. CH-PEP·Na efficiently prevented the thermal aggregation of proteins and sheltered the complex proteins from proteolytic attack. The protein−CH-PEP·Na complexes adsorbed well onto HAp surfaces even in the presence of albumin. To broaden the potential effectiveness of PEP·Na, zwitterionic phosphorylcholine (PC)-modified PPE was created as a coating polymer inhibiting oral bacterial adhesion on HAp for the prevention of tooth decay. It was anticipated that this would provide both a mineral affinity for HAp and antifouling activity arising from PEP·Na and PC motifs, respectively. The zwitterionic PPE was synthesized *via* thiol-yne click chemistry of alkyne-containing PPE copolymer and thiol-terminated PC (PC-SH). Immobilization of the zwitterionic PPE on HAp could be performed through an affinity of PEP·Na for HAp surfaces. After the immobilization of the PC-bearing PPE, the polymer exhibited not only great adsorption onto HAp surfaces but also a decrease in mineral loss in acidic conditions. The HAp with the immobilization of the PC-bearing PPE effectively inhibited *Streptococcus mutans* adhesion*,* evaluated by counting bacterial colonies. In addition, the thickness of the biofilm on the immobilized HAp was significantly lower than that on the non-immobilized HAp surface, suggesting the advantages of PEP·Na conjugation for bone- and tooth-related applications.

CONTENTS

Contents

ABBREVIATIONS

BSA	Bovine serum albumin
BYP	2-(But-3-yn-1-yloxy)-2-oxo-1,3,2-dioxaphospholane
CCK-8	Cell Counting Kit-8
CD	Circular dichroism
CFU	Colony-forming units
CH-PEP·Na	Cholesterol-terminated poly(ethylene sodium phosphate)
CH-PMP	Cholesterol-terminated poly(2-methoxy-2-oxo-1,3,2-dioxaphospholane)
CLSM	Confocal laser scanning microscopy
COP	2-Chloro-2-oxo-1,3,2-dioxaphospholane
DBU	1,8-Diazabicy-clo[5.4.0]-undec-7-ene
DLS	Dynamic light scattering
FITC-BSA	Albumin–fluorescein isothiocyanate conjugate protein bovine
HAp	Hydroxyapatite
M_n	Number-average molecular weight
M_w	Weight-average molecular weight
MALDI TOF MS	Matrix assisted laser desorption ionization time of flight mass spectrometer
MP	2-Methoxy-2-oxo-1,3,2-dioxaphospholane
MPC	2-Methacryloyloxyetyl phosphorylcholine
PBS	Phosphate buffered saline
PC	Phosphorylcholine
PC-SH	Thiol-terminated-phosphorylcholine

PDI	Polydispersity index
PEB	Poly(ethylene sodium phosphate-*co*-2-(but-3-yn-1-yloxy)-2-oxo-1,3,2-dioxaphospholane)
PEB-PC	Phosphorylcholine-modified PEB
PEP·Na	Poly(ethylene sodium phosphate)
PMB	Poly(2-Methoxy-2-oxo-1,3,2-dioxaphospholane-*co*-2-(but-3-yn-1-yloxy)-2-oxo-1,3,2-dioxaphospholane)
PMB-PC	Phosphorylcholine-modified PMB
PMP	Poly(2-methoxy-2-oxo-1,3,2-dioxaphospholane)
PPE	Polyphosphoester
SEC-MALS	Size exclusion chromatography with multiangle light scattering
TEM	Transmission electron microscopy
XPS	X-Ray photoelectron spectroscopy

CHAPTER I

GENERAL INTRODUCTION

1.1 Problem statement

One of the challenges in the development of biomaterials for medical treatments, such as nanoparticles, is how to selectively target them at specific pathogenic sites. The application of therapeutic materials off-target is wasteful and may be toxic for healthy surrounding tissues.[1] The functionalization of polymers with targeting ligands is an effective method to address this problem. The protocols, however, often require complicated synthesis and purification procedures. Employing polymers with an inherent affinity for the selected tissue is a more effective biomaterial design approach. However, inherent affinity for bone and teeth is found in a limited number of materials. Currently, phosphate-based molecules are used to target bone and teeth by utilizing the electrostatic interaction between calcium ions and phosphate ions arising from the hard tissues and such polymers, respectively.[2–5] However, some phosphate-based polymers are not biodegradable, leading to the risk of nonbiodegradable polymer accumulation in the kidneys.[6] Poly(ethylene sodium phosphate) (PEP·Na) is a PPE with a negatively charged and biodegradable backbone. Interestingly, PEP·Na has exhibited high affinity toward hydroxyapatite (HAp) and bone with an excellent cytocompatibility owing to its structural similarity to naturally occurring nucleic acids.[7–9] Although PEP·Na exhibits various useful properties, especially binding affinity to calcium mineral surfaces, few studies have researched its application to the field of dental caries. Therefore, in the first section of this thesis, a nanocomplex of protein–amphiphilic PEP·Na with a binding affinity to HAp is studied. In another topic, the properties of zwitterion-containing PPEs on a mineral substrate that help in minimizing acid erosion and bacterial adhesion to oral tissue are investigated. These knowledge bases were combined and adapted to generate antimicrobial peptide-conjugated PEP·Na nanoparticles for dental applications. It is anticipated that this approach will prove effective in combating the oral bacteria that are the major cause of serious diseases in oral cavities but show great biocompatibility for human cells.

1.2 Theory and literature review

1.2.1 Polyphosphoesters (PPEs)

Polyphosphoesters have been investigated for use in a variety of biomedical applications, such as regenerative therapeutics, drug delivery, and protein delivery, owing to the degradability of phosphoester linkages through spontaneously hydrolytic and enzymatic (i.e., phosphatases and phosphodiesterases) mechanisms under physiological conditions.[5,10–12] This can reduce the problem of renal tubular vacuolization caused by the accumulation of nonbiodegradable macromolecules in the kidney and persistence by compounds.[13] PPEs are biocompatible polymers consisting of nucleic acid-mimetic building blocks; the functionality of their side-chain groups are easily tunable, endowing them with desirable mechanical, chemical, and biological potential, in contrast to other biodegradable polyesters (e.g., polylactide and polycaprolactone).[4] Examples of PPE analogs with different functionalities are presented in **Table 1.1**. The polymers can be prepared simply *via* ring-opening polymerization of cyclic phospholane monomers, offering well-controlled molecular weight and distribution.[14]

In this thesis, we mainly focus on PEP·Na. PEP·Na is negatively charged along its phosphate diester backbone, enabling calcium-binding ability. PEP·Na is a hygroscopic polymer that does not disintegrate mammalian cell membranes.[15] PEP·Na has been applied in bone-targeted nanoparticles[8], bone imaging[7], and osteoporosis treatment.[16]

Table 1.1 The examples of PPEs analogue with different functionalities and their applications.
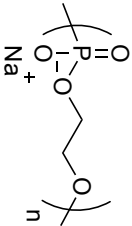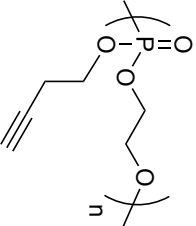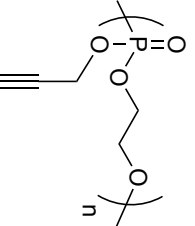
Structures	Aim of applications	Authors
Poly(ethylene sodium phosphate) (PEP·Na)	PEP·Na diminished osteoclast cells and their activity to bone resorption. Also, it showed *in vivo* bone affinity that is benefit for bone-targeted therapies.	Kootala et al.[16] Iwasaki et al.[7]
Poly(2-(but-3-yn-1-yloxy)-2-oxo-1,3,2-dioxaphospholane) (PBYP)	Pendant butynyl and propargyl moieties of the polyphosphoesters were employed as a clickable side chains for thiol-yne and azide-alkyne cycloaddition using thiol- and azide-functionalized compounds such as poly(ethylene glycol)-azide, and sulfhydryl antimicrobial peptide.	Wang et al.[17] Zhang et al.[14] Pranantyo et al.[18]
Poly(2-propynoxy-2-oxo-1,3,2-dioxaphospholane) (PPEP)		

Table 1.1 The examples of PPEs analogue with different functionalities and their applications. (Continued)
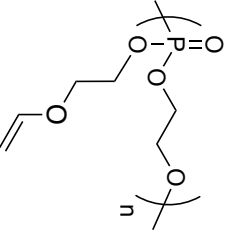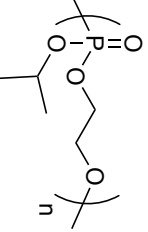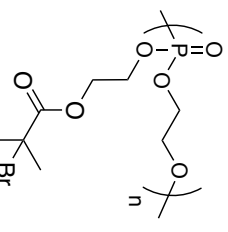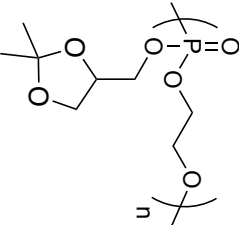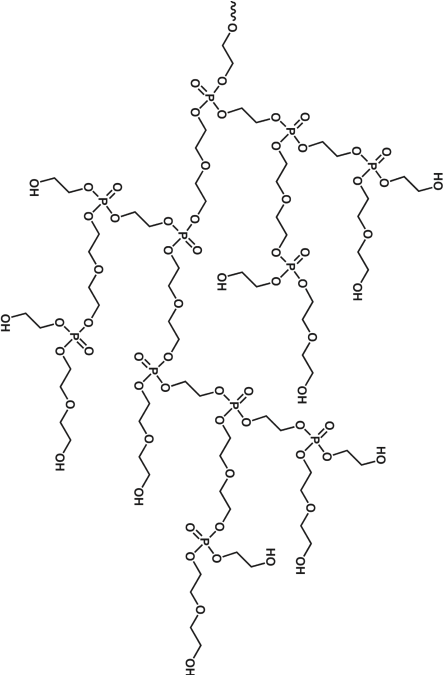
Structures		Aim of applications	Authors
Poly(ethylene glycol vinyl ether phospho-triester) (PEVEP)		PEVEP with a vinyl ether side chains was designed as a versatile polymer for post-polymerization modification allowing beside a functionalization by thiol-ene click reaction also the subsequent introduction of acid labile functionalities, e.g., acetals and thio-acetals, respectively.	Lim et al.[23]
Poly(2-isopropoxy-2-oxo-1,3,2-dioxaphospholane) (PIPP)		PIPP exhibited thermo-responsive behavior for use in biological applications such as drug delivery.	Iwasaki et al.[21] Hiranphinyophat et al.[22]
Poly(2-(2-xo-1,3,2-dioxaphosphoroyloxyethyl-2-bromoisobutyrate)) (POPBB)		Macroinitiator for atom transfer radical polymerization (ATRP) provided grafted polyphosphoester.	Iwasaki et al.[19,20]

5

Table 1.1 The examples of PPEs analogue with different functionalities and their applications. (Continued)

Structures	Aim of applications	Authors
Poly(2-(2,2-dimethyl-1,3-dioxolan-4-yl-meth-oxy)-2-oxo-1,3,2-dioxaphospholane) (PGEP) 	PGEP whose hydroxyl pendant groups were protected by the 1,3- dioxolane ring. After deprotection under acidic conditions, the polyphosphoester bearing functional hydroxyl pendant groups were obtained for further biological modification.	Song et al.[26]
Hyperbranched poly(2-(2-hydroxyethoxy)ethoxy-2-oxo-1,3,2-dioxaphospholane) (HPHEEP) 	A biocompatible hyperbranched HPHEEP was covalently conjugated with anticancer drug, chlorambucil. The significant ability of the conjugate can be attributed to the biodegradability of HPHEEP, which releases free chlorambucil in breast cancer cells.	Liu et al.[24,25]

1.2.2 Mineral composition of hard tissues

Human hard tissues, namely, bone and tooth enamel, are tissues that are mineralized supporting and protecting the various organs of the body. Bone is a specialized form of connective tissue, composed of inorganic components (60%), organic components such as proteins (30%), and water (10%),[27] whereas tooth enamel is the hardest material in the body comprising approximately 96% inorganic matter and 4% organic matter and water.[28] The biominerals found in hard tissues that give them their strength and hardness belong to a group of mineralized substances named apatites. Hydroxyapatite (HAp), a form of calcium phosphate mineral ($Ca_{10}(PO_4)_6OH_2$), is the main component in mineral formations found in calcified tissues (bones and teeth).[29,30] HAp provides a site of positively charged calcium for binding negative molecules as demonstrated in **Figure 1.1**. This enables PPEs, such as PEP·Na, to strongly adsorb onto HAp-based surfaces through ionic interaction between calcium ions and phosphate ions. Therefore, in this work, HAp substrates were used as a representative tooth model. Nevertheless, HAp surfaces are not stable at low pH because of mineral resorption by acid.[31]
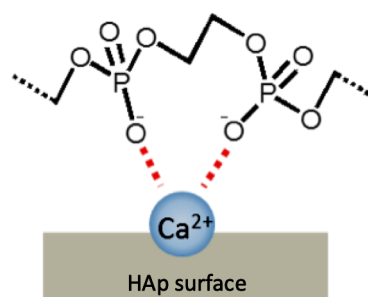
Figure 1.1 Schematic diagram of chelation between PEP·Na and calcium ion on the HAp surface.

1.2.3 Bone and tooth therapies with proteins

Protein-based therapeutics offer a unique approach for manipulating specific and biologic actions that cannot be achieved by general devices or chemical agents. Bone morphogenetic proteins (BMPs) are known transforming growth factors. BMPs play a crucial role in tissue regeneration[32,33] and have attracted interest owing to their clinical applications in bone healing.[34] Since BMP-2s received approval from the United States Food and Drug

Administration, the efficacy of these proteins in restoring bone defects,[34,35] including bone grafting in dentistry,[36,37] has been reported. However, proteins are sensitive to proteolytic enzymes and have a short circulating half-life, and their side effects, such as too high concentration of the proteins, need to be prevented. For example, Ning et al.[38] described the treatment of medication-related osteonecrosis of a mouse jaw using cellulose hydrogels loaded with stem cells and BMP-2. After the hydrogel was applied to the lesion site on the jaw, it encouraged mucosal recovery, bone tissue reconstruction, and osteoclastogenesis. Apart from BMP-2, other therapeutic proteins and peptides have been used in therapies for mineralized tissues, such as amelogenin analogs, enamelin, and ameloblastin. Amelogenin is the key protein in enamel and cementum formation that regulates crystallization, thus leading to enamel biomineralization.[39,40] Moreover, treatment with amelogenins supersedes conventional preventive fluoride treatments, due to the lower risk of toxicity, biointegration, promotion of functional responses, and improved permeation of minerals to treat deeper subsurface lesions.[41,42] Thus, these proteins provide great benefits for remineralization, regeneration, and repair of natural tooth structures.

1.2.4 Protein denaturation

In the drug delivery environment, protein denaturation can be caused by several factors, such as heat, protease digestion, pH, and solvents, leading to irreversible protein aggregation. In this study, we have focused on the thermal denaturation of proteins. Heating initially allows the protein to expose its hydrophobic part to form complexes with amphiphilic polymers through hydrophobic associations. Therefore, polymers can inhibit aggregation of unfolded proteins.[43] Because of the relatively fragile nature of the protein, the polymer also acts as a protective barrier against proteolytic digestion.

Circular dichroism (CD) spectroscopy, the differential absorption of left- versus right-handed polarized light, is an effective technique for the determination of the retention of protein secondary structures due to its sensitivity to the structural asymmetry.[44] The secondary structure of molecules, such as proteins and nucleic acid, can be estimated by CD spectroscopy in the far-UV spectral region (190–250 nm). Alpha-helix, beta-sheet, and random coil structures (**Figure 1.2A**) each offer a characteristic signal and magnitude on the CD spectrum. **Figure 1.2B** illustrates spectra for proteins in three different structures: myoglobin, prealbumin, and acid denatured staphylococcal nuclease, representing α-helix, β-sheet, and random coil structures, respectively.
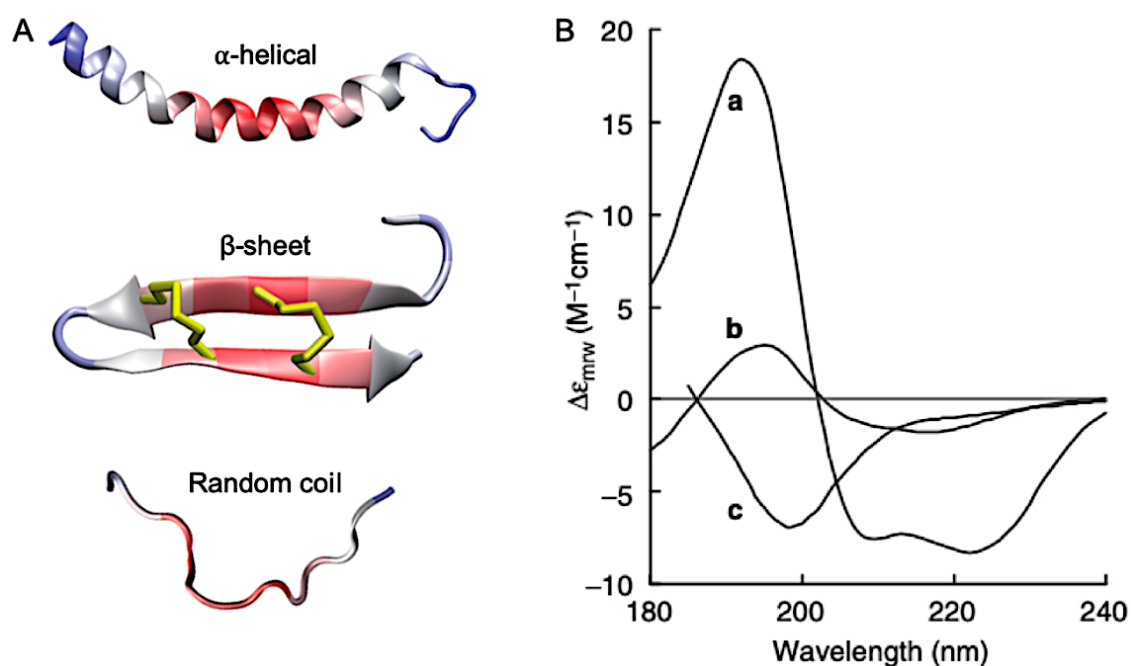
Figure 1.2 (A) Representative secondary structures.[45] (B) CD spectra of a) myoglobin (all-α); b) prealbumin (all-β), and c) acid denatured staphylococcal nuclease at pH 6.2 and 6 °C (unordered).[44]

1.2.5 Conjugation of proteins with polymers

A number of polymers have been utilized to conjugate with proteins in order to reduce immune response, preserve protein activity, and prolong circulation time during delivery to the target site.[46] Conjugation of proteins with polymers can occur *via* chemical or physical interactions. For instance, PEGylation, a permanent conjugation of poly(ethylene glycol) (PEG) to biologics,[47] is one of the most well-known and widely used platforms to improve the pharmacokinetics of the delivered proteins. Unfortunately, nonbiodegradable PEG may lead to PEG accumulation in the body.[48] Therefore, degradable PPEylated conjugates have been proposed as an alternative avenue for protein conjugations using biodegradable PPE with the highly remaining bioactivity.[6,19] On the other hand, noncovalent bioconjugations have been deployed using various methods, namely, electrostatic interactions, hydrogen bonding, and hydrophobic attractions providing assemblies of particles, vesicles, and cages.[50] Akiyoshi et al.[51] utilized a facile heat-induced method to form a selective complex of carbonic anhydrase B: (CAB) and amphiphilic cholesterol-bearing pullulan (CHP) (**Figure 1.3**). The self-assembly

of the cholesteryl groups provided CHP nanogels with crosslinking, arising from the hydrophobic association of the pendant cholesterol, which was first synthesized by Akiyoshi.[52] These nanogels have also been shown to spontaneously form with proteins through the binding of partly hydrophobic CAB and cholesterol. By increasing the temperature, the nanogel perfectly suppressed the irreversible aggregation of CAB. The CAB was released by the nanogel disassembly after the addition of β-cyclodextrin, which can bind specifically with a cholesteryl group. The result demonstrated that the released protein could refold to almost native form. The thermal stability of the protein was enhanced by the capture of the unfolded structure which was subsequently released with a refolded structure. Hence, the preparation of protein/polymers assisted by thermal treatment can be an easy method of protein protection *via* thermal stabilization by the amphiphilic polymer.
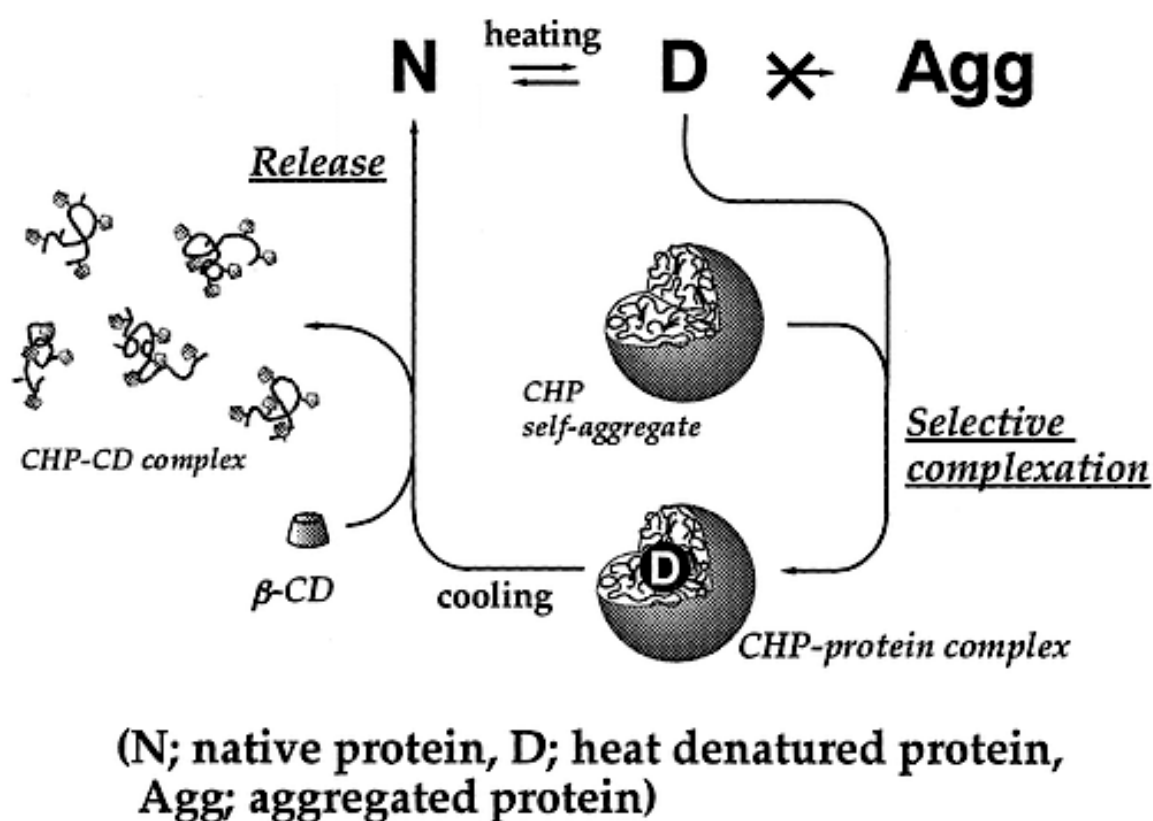
Figure 1.3 Schematic representation of controlled association between cholesteryl group-bearing pullulan nanoparticles and protein.[51]

1.2.6 Click chemistry

Click chemistry is a versatile tool for diverse synthetic methodologies, biofunctionalization, surface modification, and polymerization, including catalyzed and non-catalyzed coupling between an alkyne and an azide, cycloaddition reactions, and a class of thiol-based chemistries, such as thiol-ene and thiol-yne reactions.[53] This platform has been used frequently for grafting numerous types of functionality onto polymers given its quantitative yield, absence of offensive byproducts and side reactions, and faster reactions in mild conditions.[54–56] In this thesis, we have focused on thiol-yne reactions and azide–alkyne Huisgen cycloaddition, the two classical components of click chemistry, for the functionalization of alkyne-pendant PPEs.

The click conjugation of pendant propargyl or butynyl analogs of PPEs with cysteine under UV irradiation was successfully synthesized, offering biodegradable PPE-antimicrobial peptide conjugates[18] and zwitterionic PPE as coating materials for gold nanoparticles,[57] respectively.

Four different charged and uncharged thiols were subjected to reactions with PPEs containing clickable 2-(but-3-yn-1-yloxy)-2-oxo-1,3,2-dioxaphospholane (BYP) to yield amphiphilic PPEs that self-assemble into nonionic, anionic, cationic, and zwitterionic micelles in aqueous media (**Figure 1.4**).[58]
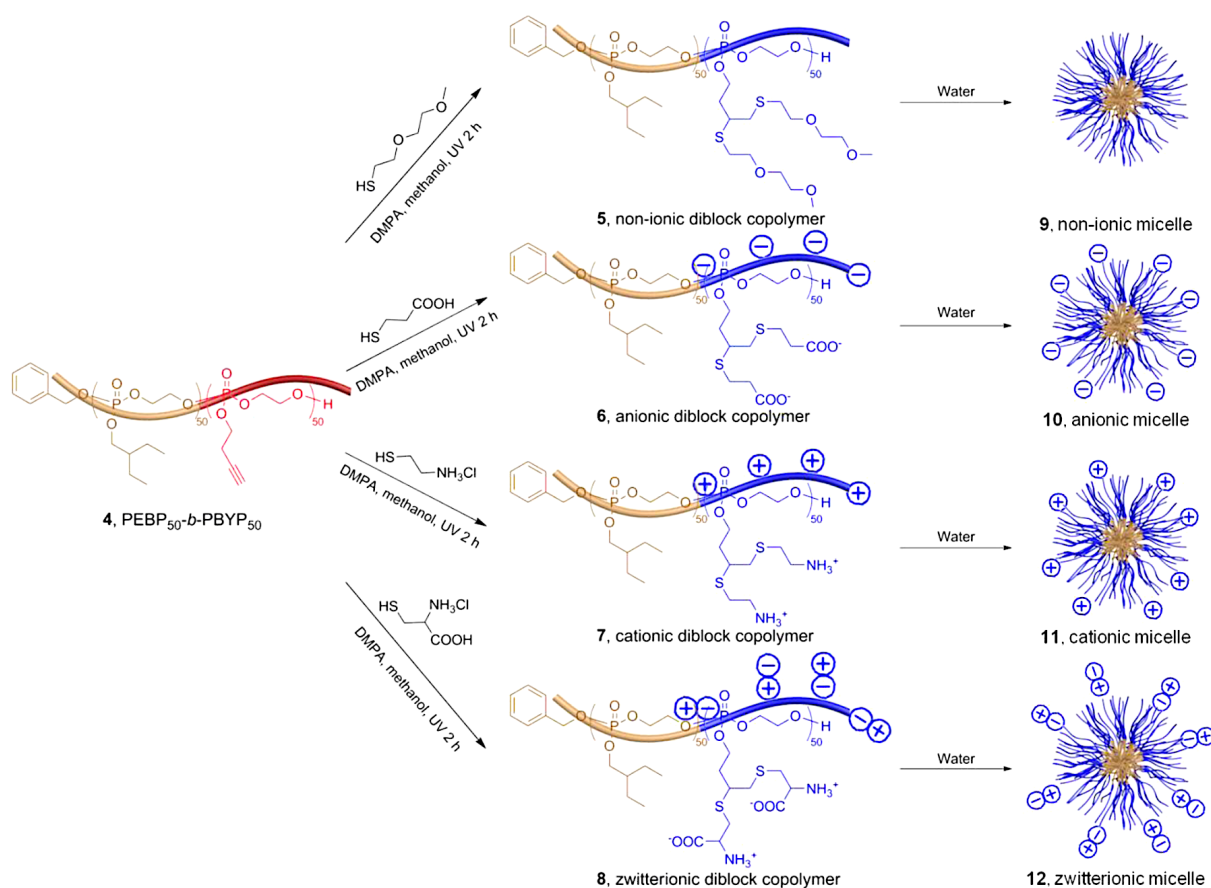
Figure 1.4 functionalization of a PPE copolymers with four thiols (with and without charges) yielding amphiphiles that self-assembly into micelles with different surface charges.[58]

Both thiol-yne reactions and azide–alkyne reactions have been employed to functionalize clickable PBYP with thiol- and azide-containing molecules (methoxyethoxyethanethiol and benzyl azide, respectively) as presented in **Figure 1.5**.[14] This demonstrated a simple route for the synthesis of clickable, water-soluble, and degradable PPEs, which can be adjusted for desired applications.
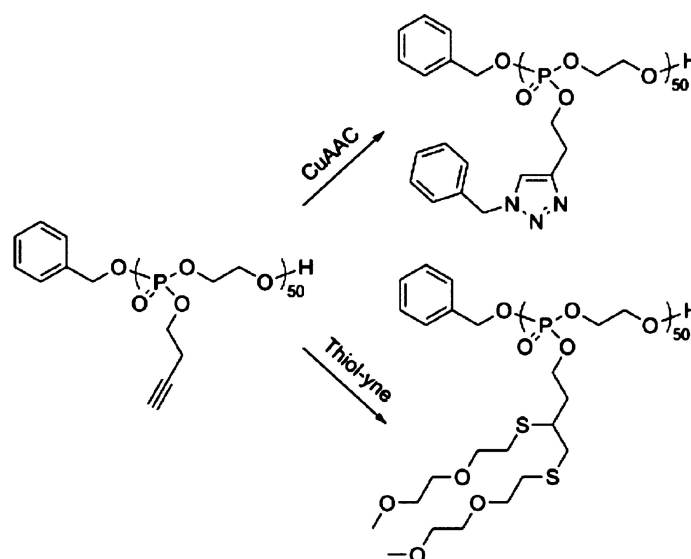
Figure 1.5 Azide-alkyne click reaction of PBYP and benzyl azide using copper catalyst (top) and thiol-yne click reaction of PBYP and methoxyethoxyethanethiol.

1.2.7 2-Methacryloyloxyethyl phosphorylcholine (MPC) and MPC-based molecules

2-Methacryloyloxyethyl phosphorylcholine (MPC) is a hygroscopic monomer possessing both positive and negative electrical charges in structures called zwitterions. Ishihara and Nakabayashi et al.[59–61] synthesized MPC polymers inspired by the natural cell membrane. The membrane consisted of a phospholipid bilayer bearing an outer surface of hydrophilic phosphorylcholine (PC) domains as presented in **Figure 1.6**. Thenceforth, MPC-based polymers have been widely used for bio-related applications owing to their excellent hydrophilicity, biocompatibility, and antifouling properties.[62–64] MPC polymers also exhibited affinity to the C-reactive protein (CRP) that can be applied in CRP detection.[65,66] In addition, MPC has been applied as an anti-adsorptive platform in dentistry. Kang et al.[67] presented copolymers of MPC and 2-methacryloyloxyethyl phosphate (MOEP) as antifouling and Ca^{2+} binding moieties, respectively, for immobilization on a hydroxyapatite surface. The surface immobilized with anti-biofouling MPC-based polymer performed well in the prevention of protein adsorption, cell attachment, and oral bacterial adhesion.
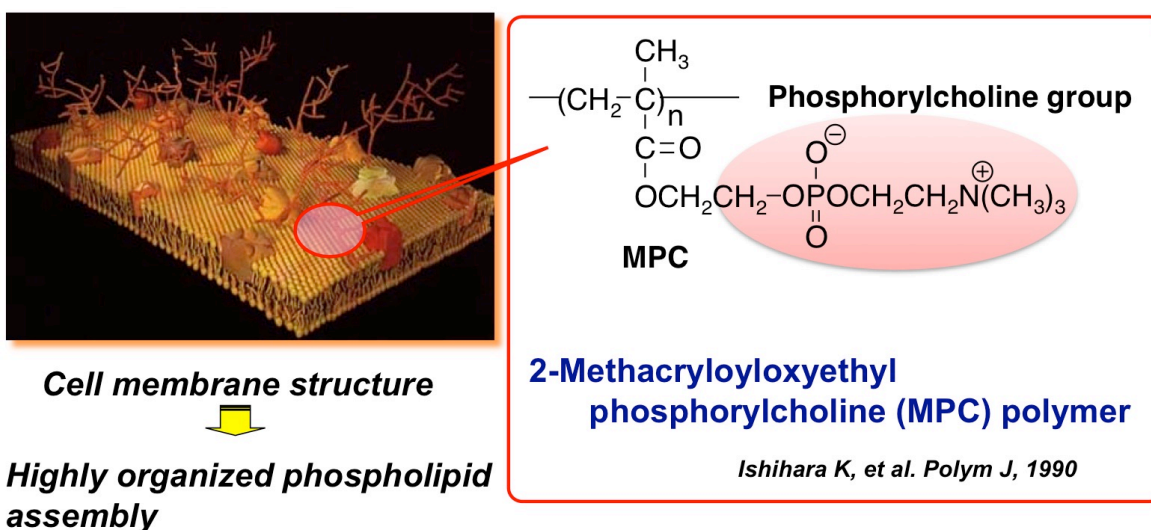
Figure 1.6 Chemical structure of MPC designed by inspiration from cell membrane surface.[68]

Moreover, MPC has been reported as a building block for protein- and cell-repellant self-assembled monolayers modified through Michael addition of MPC and alkane dithiol to obtain thiol-terminated MPC (PC-SH), as presented in **Figure 1.7**.[69] Furthermore, Sangsuwan et al.[70] used antimicrobial silver nanoclusters protected with PC-SH, resulting in excellent biocompatibility with fibroblast cells.
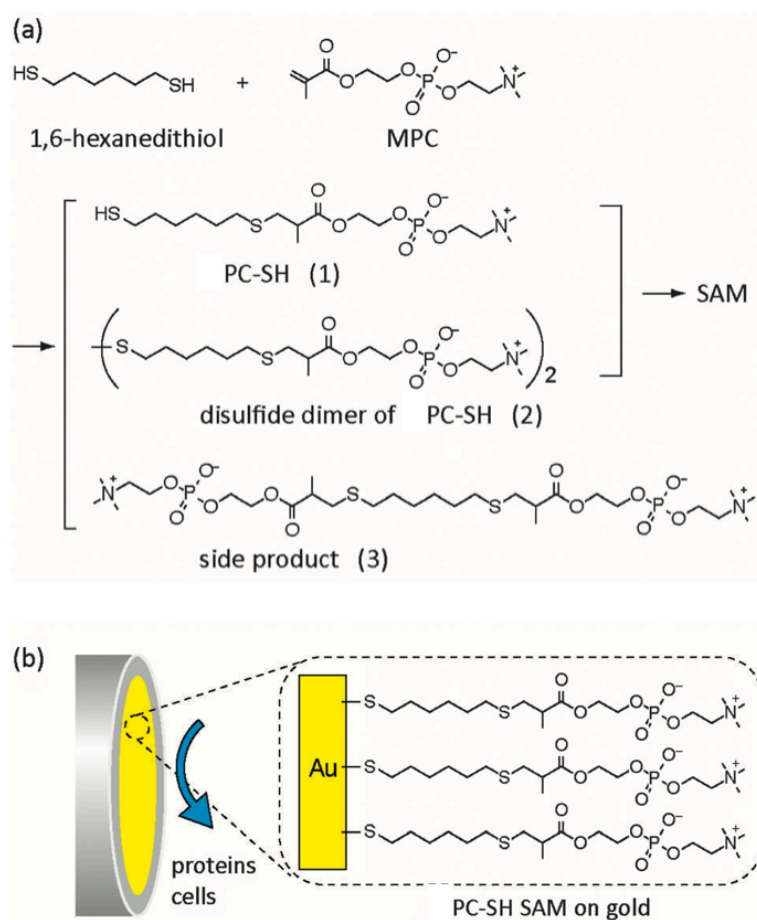
Figure 1.7 (a) Synthetic route of PC-SH. (b) Schematic representation of antifouling PC-SH SAM on gold electrode.[69]

1.2.8 Dental carries and the solution
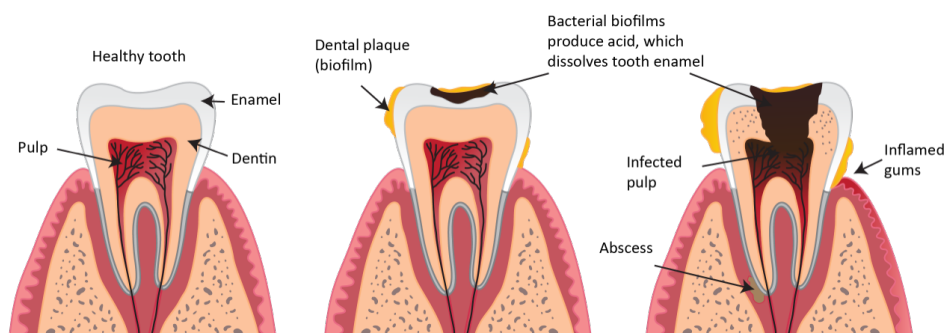
Figure 1.8 Bacterial biofilm is formed on surface of the tooth where acid produced by the oral bacteria dissolves the enamel promoting dental caries and infections.[71]

One of the main factors in tooth loss is dental caries. The accumulation of biofilms on tooth surfaces is a condition that plays a vital role in the development of dental caries.[72] During bacterial adhesion, dental enamel is exposed to organic acids, such as lactic acid and propionic acid, generated by oral bacteria known as cariogenic bacteria; this can erode the surface leading to demineralization, tooth decay, and infection.[73] The steps in the formation of tooth decay by bacteria is illustrated in **Figure 1.8**. Furthermore, acidic foods and drinks, for example, citrus fruits, soda, and tea, can also harm tooth enamel. In order to protect the mineral surface, the standard method for the prevention of enamel erosion is fluoride treatment, which forms fluorapatite ($Ca_{10}(PO_4)_6F_2$) to protect the enamel surface from dissolution. However, overexposure to fluoride adsorption may result in fluorosis and the risk of fracture.[74,75] Non-fluoride polymers may be promising alternative protective agents.

Lei et al.[76] designed amphiphilic copolymers of hydrophilic methacryloyloxyethyl phosphate (MOEP) and a hydrophobic methyl methacrylate (MMA) to prevent tooth decay caused by acidic erosion. MOEP can immobilize onto the enamel surface, thus increasing the retention time of the immobilized polymer. Additionally, a hydrophobic domain was incorporated to form a hydrophobic barrier, resulting in a reduction in acid attacks on the tooth enamel (**Figure 1.9**).

Figure 1.9 The proposed mechanism of phosphate block copolymer on protecting enamel.[76]

Cui et al.[3] modified HAp and tooth surfaces with copolymers of poly(ethylene glycol) methyl ether methacrylate (PEGMA) and ethylene glycol methacrylate phosphate (Phosmer). The synthesized polymers were immobilized on HAp and the tooth enamel by the affinity of phosphate segments to HAp in order to form stable and durable polymer brushes on the surfaces (**Figure 1.10**). Due to the anti-biofouling ability of PEG, PEGMA moieties exhibited a considerable inhibitory effect on the bacterial adhesion of *Staphylococcus epidermidis.*
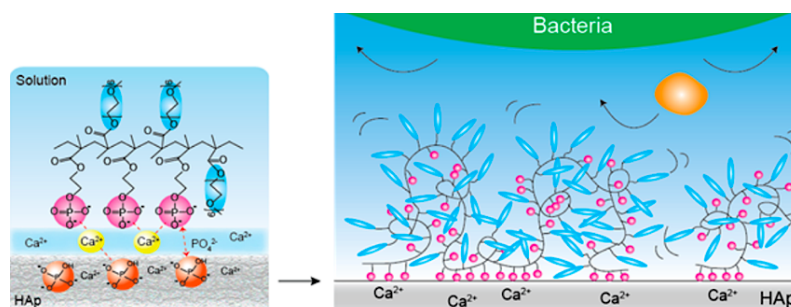
Figure 1.10 Schematic of bacterial anti-adhesion on HAp model teeth by surface modification with PEGMA-phosmer copolymers.[3]

1.3 Contents of this thesis

This thesis consists of five chapters shown below.

Chapters I is a general introduction providing a statement of biomaterial problems and a description of an alternative method to solve these problems, using PPEs. This chapter also includes a literature review that covers PPEs and their applications, mineral apatite, protein denaturation and its characterization by CD spectroscopy, conjugates of proteins and polymers, click chemistry, MPC and MPC-based molecules, and dental caries.

Chapter II described the thermally assisted generation of protein–amphiphilic PEP·Na conjugates, the size of complex, the complex stability against protease, and the binding affinity of the complex for hydroxyapatite substrate.

Chapter III describes the immobilization of zwitterionic PPEs on mineral substrates prepared by click reaction between alkyne-pendant PPE and thiolated PC groups. The introduction of zwitterionic PPEs on the surface resulted in reduction of acid erosion and oral bacterial adhesion.

Chapter IV is the conclusion of this thesis. The advantages of PEP·Na, protein-PEP·Na conjugation, and zwitterionic PPEs in the reduction of acid erosion and oral bacterial adhesion are summarized.

CHAPTER II

THERMALLY ASSISTED GENERATION OF PROTEIN–POLY(ETHYLENE SODIUM PHOSPHATE) CONJUGATES WITH HIGH MINERAL AFFINITY

2.1 Introduction

Protein therapeutics has attracted interest in numerous medical treatments. The specificity and bioactivity of such proteins have positively affected on the treatments for autoimmune diseases, cancers, and other human disorders.[77–81] However, most protein suffer from a limited blood circulation time and their susceptibility, especially in proteolytic condition.[46,82,83] In order to improve their stability, diverse bioconjugation approaches, such as the poly(ethylene glycol) (PEG) immobilization as known as PEGylation,[47,84] have been attempted to develop the delivery of protein. Despite the improved intravascular half-life of the delivered proteins, the decreased bioactivity owing to permanent conjugates and nonbiodegradability of PEG which can cause long-term effects to the body are a serious issue.[82,85] As an alternative strategy, bioconjugates of proteins (myoglobin[49], bovine serum albumin (BSA), and uricase[6]) with fully degradable polyphosphoester (PPE) have been proposed. To overcome the inherent shortcoming of PEG, the biodegradable PPE could be designed as the protective polymer shell for such proteins resulting in a relatively high bioactivity retention under physiological condition. Protein–polymer conjugations, however, often require onerous procedures. Noncovalent binding is an alternative formation for the protein delivery involving hydrogen bonding, electrostatic forces, and hydrophobic interactions. The thermally assisted complexation of proteins with amphiphilic polymers is a simple and timesaving route to generate protein carriers, but its challenge lies in inhibiting the protein aggregation and preserving the protein activity according to thermal denaturation. In previous work, Akiyoshi and coworkers[51] have demonstrated a cholesterol-bearing pullulan (CHP) nanogel having a chaperone-like activity for the thermal stabilization of carbonic anhydrase B: (CAB). The self-assembly of the cholesteryl domains provided physical cross-linking to form stable CHP nanogels in aqueous media. During heating, the nanogel completely suppressed the irreversible aggregation of CAB. The encapsulated CAB was released by disassembly of the nanogel after the addition of β-cyclodextrin. Compellingly, the released protein refolded to almost native form. The thermal stability of the protein was enhanced by capture of the unfolded structure which was subsequently released with refolded structure. Accordingly, employing amphiphilic polymer in order to create the thermostabilizer for the delivered proteins can be a significant strategy.

On the other hand, PPEs are unique polymers in the field of biomedical materials due to their biocompatibility, biodegradability, and mimetic building blocks of natural compound

as nucleic acids.[57,86,87] In contrast to biodegradable polycarboxylic acid esters such as poly(lactic acid), poly(glycolic acid), and poly(ε-caprolactone), diverse functionalities can be introduced to the PPE structures.[4,5] Poly(ethylene sodium phosphate) (PEP·Na) is a class of negatively charged PPE possessing a phosphodiester backbone. PEP·Na has provided high affinity toward bone in both *in vitro* and *in vivo*. Moreover, it exhibited high cell viability against bone cell (MC3T3-E1 cell line).[7,8,16] PEP·Na can be synthesized via the ring-opening polymerization (ROP) of cyclic phosphoester monomers by using organocatalysts and alcohols as initiators,[7,16,58,88–90] whereas its polarity can be conveniently adjusted to be hydrophilic or amphiphilic by using desired hydroxyl-containing initiators. Cholesterol, which is a ubiquitous lipid molecule presented in body systems, was used as an initiator to prepare amphiphilic cholesterol-terminated PEP·Na (CH-PEP·Na).

In this work, amphiphilic CH-PEP·Na was newly introduced to form complexes with proteins assisted by thermal treatment. Once the temperature rose, the interior hydrophobic amino acids of the proteins became exposed. The hydrophobic interactions between the nonpolar segments of the amphiphilic polymer and the exposed lipophilic proteins spontaneously occurred. At that time, the hydrophilic PEP·Na chains stabilized such micelle-like complexes at the periphery because of the electrostatic repulsive force of the anionic phosphate domains and the polymeric chains also hindered the aggregation of the unfolded proteins.[43] BSA formed a complex with CH-PEP·Na without the need for protein modification and organic solvents. After the thermally assisted complexation, CH-PEP·Na exhibited a potential ability to form complexes with BSA upon a treatment at high temperature (90°C) without BSA thermal aggregation and the peripheral CH-PEP·Na protected the complexed BSA well under proteolytic conditions. Additionally, the obtained complexes showed affinity for hydroxyapatite (HAp), which is the major mineral component of bone and tooth, by adsorbing onto HAp surface as illustrated in **Scheme 2.1**.
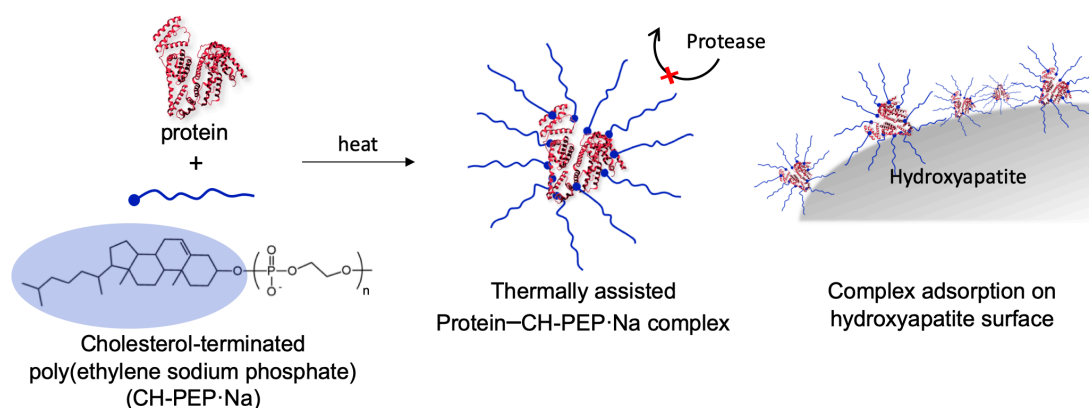
Scheme 2.1 Complexation of protein–CH-PEP·Na for adsorption on HAp surface.

2.2 Materials and methods

2.2.1 Materials

2-Chloro-2-oxo-1,3,2-dioxapholane (COP) was kindly donated by NOF Co., Ltd., Tokyo, Japan. The water used throughout the experiments was purified using a Millipore Milli-Q system (resistivity 18.2 MΩ·cm), involving ultraviolet irradiation, ion exchange, and filtration. Ceramic hydroxyapatite, type II, 40 μm (Bio-Rad) was used as substrates for the complex adsorption. 1,8-Diazabicy-clo[5.4.0]-undec-7-ene (DBU) was purchased from FUJIFILM Wako Pure Chemical Co., Osaka, Japan and distilled under reduced pressure, where the fraction with a bp of 130 °C/3.0 mmHg (lit.: bp 80 °C/0.6 mmHg) was collected. 2,6-Lutidine was purified by vacuum distillation. Ion exchange Amberlite IR-120 (Merck KGaA) was rinsed with water before use. An aqueous solution of trimethylamine (TMA) (30%) was purchased from Nacalai Tesque, Tokyo, Japan. Albumin–fluorescein isothiocyanate conjugate protein bovine (FITC-BSA) and bovine serum albumin (BSA) were purchased from Sigma-Aldrich Co., St. Louis, MO, USA. The quantity of BSA in the complexes was quantified using the Pierce BCA Protein Assay Kit (Thermo Scientific). Other chemicals were purchased from FUJIFILM Wako Pure Chemical Co., Osaka, Japan and used without further purification.

2.2.2 Preparation and characterization of materials for generation of protein−PPE complexes

2.2.2.1 Synthesis and characterization of polyphosphoesters (PPEs)

Cholesterol-terminated poly(2-methoxy-2-oxo-1,3,2-dioxaphospholane) **(CH-PMP)** was synthesized via the ring-opening polymerization (ROP) of MP (60 mmol, 70 eq.) using cholesterol (0.86 mmol, 1 eq.) and DBU (0.86 mmol, 1 eq.) as initiator and organo-catalyst,

respectively. Synthetic route of MP monomer was described in Chapter 3. The solution was dissolved in dehydrated dichloromethane (5 mL) and the reaction was allowed to proceed under an argon gas in an ice bath for 1 h and subsequently stirred at room temperature for 2 h. Then, CH-PMP was reprecipitated in toluene followed by diethyl ether and dried under vacuum, resulting in a viscous colorless liquid that was stored at 4 °C. To prepare negatively charged cholesterol-terminated poly(ethylene sodium phosphate) (CH-PEP·Na), the purified CH-PMP was further demethylated with trimethylamine (TMA) (120 mmol, 140 eq.) for 24 h, and the mixture was then stirred with cation exchange resins twice to replace the quaternized ammonium with hydrogen ions. The polymer was subsequently purified using a Spectra/Por 3® membrane against DI water with molecular weight cut-off (MWCO) 3500 (Spectrum, Rancho Dominguez, CA, USA). The so-obtained polymer was neutralized with an NaOH solution, dialyzed against DI water (MWCO 3500), and lyophilized to obtain CH-PEP·Na. PEP·Na was also synthesized as described for CH-PEP·Na using MP (36 mmol, 70 eq.), methanol (0.51 mmol, 1 eq.), and DBU (0.51 mmol, 1 eq.). Both purified CH-PEP·Na and PEP·Na were finally obtained as white solids and stored at 4 °C. The molecular weight, degree of polymerization, and percentage of demethylation of the synthesized PPEs were calculated from the proton nuclear magnetic resonance (^{1}H-NMR) spectra, obtained using a JEOL (Japan) operating at 400 MHz. CH-PEP·Na and PEP·Na were dissolved in D_2O while CH-PMP was analyzed in $CDCl_3$. The molecular weight and the dispersity of the polymers were determined by a gel permeation chromatography (GPC) equipped with an RI-2031 refractive index detector (JASCO, Japan). For the analysis of CH-PEP·Na and PEP·Na, acetate buffer containing 0.1 M CH_3COONa, 0.3 M NaCl and 1.0 mM EDTA·2Na was selected as eluent and poly(ethylene glycol) (PEG) standards (7.5×10^2 to 1.4×10^5 Da) were used to generate a calibration curve, whereas for CH-PMP, chloroform as eluent and polystyrene standards (2.8×10^3 to 1.3×10^6 Da) were used.

The critical micelle concentration (cmc)'s of the cholesterol-containing PPEs, namely CH-PMP and CH-PEP·Na, were determined using pyrene as a fluorescent probe, according to a previously published method.[91,92] The concentrations of the polymer solutions were varied in the range of 2×10^{-5} - 5 mg/mL. A pyrene solution dissolved in acetone was added to each sample and the resulting mixtures were dissolved in phosphate-buffered saline (PBS; pH 7.4). The spectra were recorded with a fluorescence spectrophotometer using an F-2500 spectrophotometer (Hitachi, Japan) with an excitation wavelength of 336 nm.

2.2.2.2 Preparation and characterization of BSA–PPE complexes

BSA (120 μmol, 1 eq.) was dissolved in 1 mL of PBS, pH 7.4. Each PPE including CH-PMP, CH-PEP·Na, and PEP·Na (0 μmol, 0 eq.; 240 μmol, 2 eq.; 600 μmol, 5 eq.; 1200 μmol, 10 eq.) in PBS (1 mL) was prepared separately and then mixed with the BSA solution, affording final BSA concentration of 60 μM. The mixtures were heated at 90 °C with agitation for 15 min. The free polymers were eliminated by centrifugal filtration (MWCO 50k, Merck Millipore) and the complexes were finally re-dispersed in PBS. The complex formation was performed using a UV-2075 UV–vis detector (JASCO, Japan) recorded at 280 nm. A PBS solution containing NaCl (0.3 M) was used as the eluent. DLS was also carried out with a Zetasizer Nano-ZS (Malvern Instruments Ltd., UK) to analyze the average diameter and polydispersity index (PDI) of the complexes based on intensity. Circular dichroism (CD) spectra were recorded on a J-1500 CD spectrometer (JASCO, Japan). The secondary structures of the proteins were investigated in the 200–250 nm wavelength range using a quartz cuvette; the samples were prepared with PBS (pH 7.4) to obtain a protein concentration of 2 μM and a scan rate of 100 nm/min at 37 °C, with 8 accumulation scans, was adopted.

2.2.2.3 BSA–CH-PEP·Na ratio determination in the complexes

The weight-average molecular weight of a complex was carried out by size exclusion chromatography with multiangle light scattering (SEC-MALS; TOSOH) with column (WTC-050S5, Wyatt technology) (M_w 15 000–5 000 000) using two detectors, a refractive index detector (Optilab T-rEX, Wyatt technology) and MALS detector (DAWN HELEOS-II, Wyatt technology). Dulbecco's PBS was used as a solvent for the complexes and as an eluent for SEC analysis with a flow rate of 0.5 mL/min at 30 °C. The dn/dc value of 0.185 mL/g was used in the molecular weight calculations processed by ASTRA software. The BSA amount in the complex solution was then quantified via the BCA assay using the albumin standard curve (concentration range 125–2000 μg/mL). The content of the complexed CH-PEP·Na was calculated according to the following equation. Both the complex weight and BSA–CH-PEP·Na ratio (by mol) data were used for estimating the number of protein molecules to the CH-PEP·Na chain in a complex.

$$\text{CH-PEP·Na content (mmol)} = \frac{\text{weight of complex (mg) - weight of BSA (mg)*}}{M_n \text{ of CH-PEP·Na}}$$

* derived from the BCA assay.

2.2.2.4 Stability against trypsin digestion analyzed by matrix assisted laser desorption ionization time of flight mass spectrometer (MALDI TOF MS)

The enzymatic degradation study of native and complexed BSA was performed according to a modified version of a previously published method.[93] The samples were 10-fold diluted with acetonitrile (10%) and NaHCO$_3$ (90%) buffer at pH 8, with a final protein concentration of 0.40 mg/mL, and was then incubated with trypsin (trypsin:protein 1:25) at 37 °C for 17 h. The MALDI matrix was prepared from a mixture of acetonitrile, Milli-Q water, and trifluoroacetic acid (50:47.5:2.5) containing α-cyano-hydroxycinnamic acid (10 mg/mL). The digested samples and the matrix were mixed at a 1:1 ratio and spotted on an Anchor Chip target to undergo fragmental analysis operated by Microflex-KC (Bruker) using Flex Control software (Mode: Reflector Positive Ionization).

2.2.2.5 Binding affinity of FITC-BSA–CH-PEP·Na complexes for ceramic HAp surfaces

Hydroxyapatite (HAp) microparticles (average size 40 μm; 30 mg) were treated with the FITC-BSA–CH-PEP·Na (1:10, 500 μL) complex suspension containing different amounts of albumin (0, 2.5, 3.0, 3.5, 4.0, 4.5, 5.0, and 5.5 g/dL), as a protein model in human serum, for 3 h. The fluorescence intensity of the centrifuged supernatants was measured with a FP-6200 spectrofluorometer (JASCO, Tokyo, Japan) and derived from the initial value to determine the amount of complex adsorbed onto HAp; the excitation and emission wavelengths were 495 and 520 nm, respectively. The fluorescence micrographs of HAp treated with FITC-BSA and FITC-BSA–CH-PEP·Na complexes were observed by Olympus fluorescence microscope. The surface area coverage ratio is defined as the ratio between the total surface area of the adsorbed complexes and the HAp surface area.

2.3 Results and Discussion

2.3.1 Synthesis and characterization of PPEs
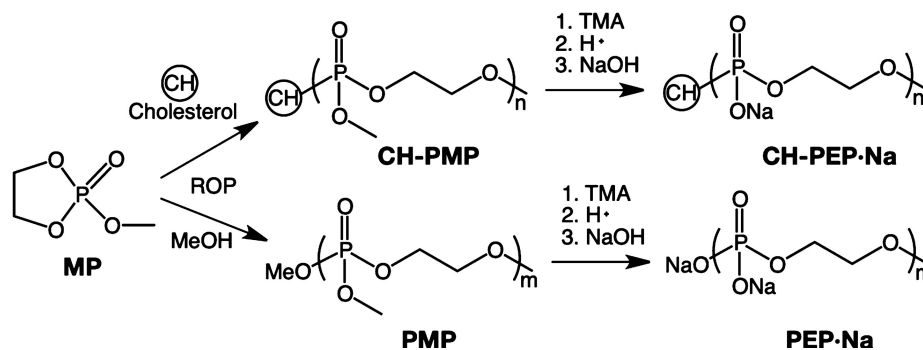
Scheme 2.2 Synthetic route of polyphosphoesters.

According to **Scheme 2.2**, three types of PPEs, cholesterol-terminated poly(2-methoxy-2-oxo-1,3,2-dioxaphospholane) (CH-PMP), CH-PEP·Na, and PEP·Na, were successfully synthesized *via* the ROP of 2-methoxy-2-oxo-1,3,2-dioxaphospholane (MP) initiated by cholesterol using 1,8-Diazabicy-clo[5.4.0]-undec-7-ene (DBU) as catalyst. Spectra of monomers including MP were displayed in chapter 4. These PPEs were examined for a targeted degree of polymerization (DP) of 70. Their molecular weights and the dispersity were evaluated by gel permeation chromatography (GPC), as summarized in **Table 2.1**. The molecular weight of PPEs detected by GPC is in the range of $8.1\text{-}9.5 \times 10^3$ with the relatively narrow dispersities and the comparable molecular weights were also estimated by proton nuclear magnetic resonance (^{1}H NMR) analysis. GPC traces of CH-PMP, CH-PEP·Na, and PEP·Na are shown in **Figure 2.1B**. The ^{1}H NMR spectra (**Figure 2.1A**) revealed the characteristic peaks of CH-PMP at 4.3, 3.8, and 0.7–1.0 ppm, which correlate respectively to the methylene and methyl protons of the PMP chain and the methyl protons of the cholesteryl group. After demethylation with trimethylamine, cation exchange and neutralization, the triester PMP was transformed into diester PEP·Na, demonstrating the upfield shift (3.9 ppm) of the methylene protons from the backbone and the disappearance of the methoxy signal. Nonetheless, slightly remained methoxyl groups can be evidenced from the peak appearing at 3.4 ppm. The percentage of demethylation calculated from an NMR spectrum is reported in **Table 2.1** as 98% and 97% for CH-PEP·Na and PEP·Na, respectively. This could be confirmed that almost MP were completely converted into EP·Na analogues.

In order to suppress the protein aggregation under thermal conditions, the self-assembly of amphiphilic polymers is necessary to stabilize the proteins by forming micelle-like particle. Hence, the critical micelle concentration (cmc) of the amphiphilic cholesterol-bearing PPEs was investigated using a pyrene as fluorescence probe in an PBS. The cmc's of CH-PEP·Na and CH-PMP were 0.04 and 0.01 g/L, respectively, and the higher value of CH-PEP·Na was probably due to the higher water-solubility of the anionic PEP·Na compared with the nonionic PMP and to its repulsion of the negative charges.[94]
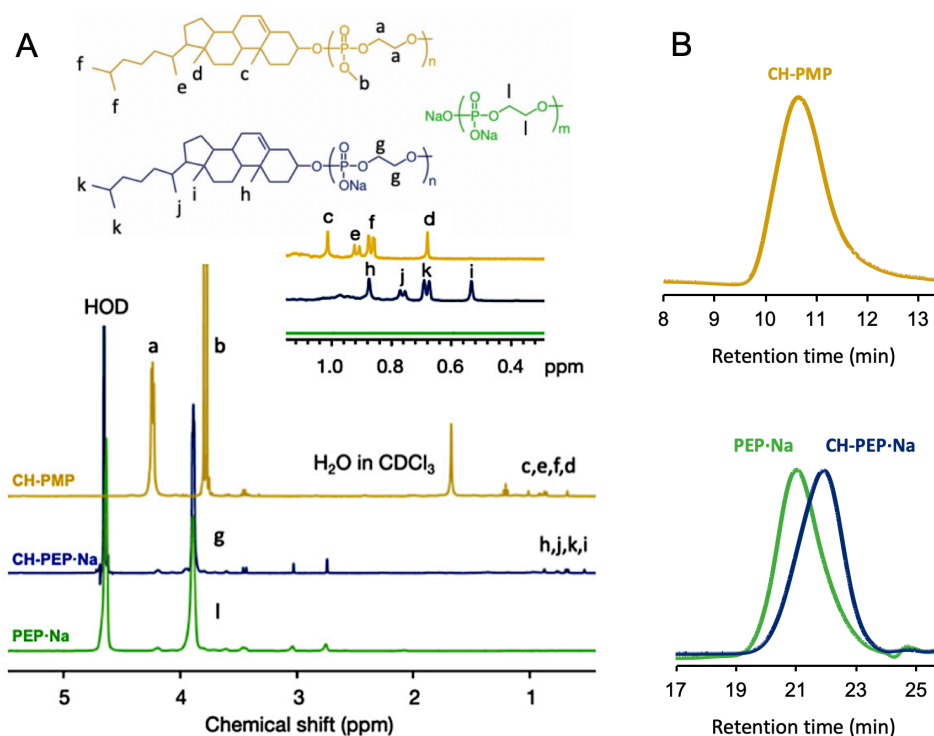
Figure 2.1 (A) ^{1}H NMR spectra of CH-PMP (yellow), CH-PEP·Na (blue), and PEP·Na (green). (B) GPC curves of CH-PMP eluting with chloroform (top) and CH-PEP·Na and PEP·Na eluting with acetate buffer (bottom).

Table 2.1 Molecular Characteristics of Polyphosphoesters.

Polymer	$M_{n, NMR}$ [a] ($\times 10^3$)	$M_{n, GPC}$ [b] ($\times 10^3$)	DP [a]	M_w/M_n [b]	Demethylation [a] (%)	cmc (g/L)
CH-PEP·Na	11.1	9.5	73	1.48	98	0.04
PEP·Na	−	8.1	−	1.25	97	−
CH-PMP	12.2	8.8	86	1.46	−	0.01

[a] Estimated by ^{1}H NMR analysis. [b] Determined by GPC.

2.3.2 Complexation of protein–PPE

BSA was used as a guest protein for complexing with PPEs. By heating at 90 °C, BSA was rapidly aggregated because of thermal denaturation, presenting cloudy suspension (**Figure 2.2A**). In contrast, the BSA suspensions exhibited transparency in the presence of amphiphilic CH-PEP·Na. The complex suspensions became more transparent with increasing the CH-PEP·Na, reaching a transmittance of almost 100% as BSA without heat. Upon the thermal treatment, BSA structure initially unfold and the exposed hydrophobic regions of denatured BSA then led to protein aggregation. After the addition of CH-PEP·Na, the hydrophobic parts of the denaturing protein interacted with the cholesteryl appendages at the polymeric chain ends, while the anionic PEP·Na chains, which were exposed to the surrounding aqueous medium, prevented protein aggregation because of electrostatic repulsion and steric stabilization.[43,51] The other two polymers, CH-PMP and PEP·Na, did not exhibit any thermal stabilization property for the protein; for the case of PEP·Na, in particular, the complexes showed the lowest transmittance because of the absence of nonpolar molecules. Although CH-PMP is an amphiphilic PPE as CH-PEP·Na, it could not efficiently inhibit the protein aggregation because of the lower hydrophilicity of PMP compared with PEP·Na and the absence of electrostatic repulsions. Another well-known hydrophilic polymer, PEG, harboring cholesteryl groups at the chain ends (CH-PEG) was also employed to form a complex with BSA (BSA/CH-PEG ratios of 1:2, 1:5, and 1:10). After heat treatment, the BSA–PEG complexes exhibited a turbid appearance for all BSA/CH-PEG ratios (**Figure 2.3A-E**), revealing the thermal aggregation of BSA at 90 °C. According to the phase separation of PEG in PBS,[95] hydrophobic PEG aggregates at high temperatures[96] as shown in **Figure 2.3G**. Consequently, CH-PEG (M_w 5×10^3) lost its hydrophilicity to stabilize the protein upon heating. Circular dichroism (CD) measurements were also performed (**Figure 2.3H**) to confirm that CH-PEG does not suppress the thermal denaturation of the protein according to no significant change of the complex spectra compared with heated BSA without PEG-CH.
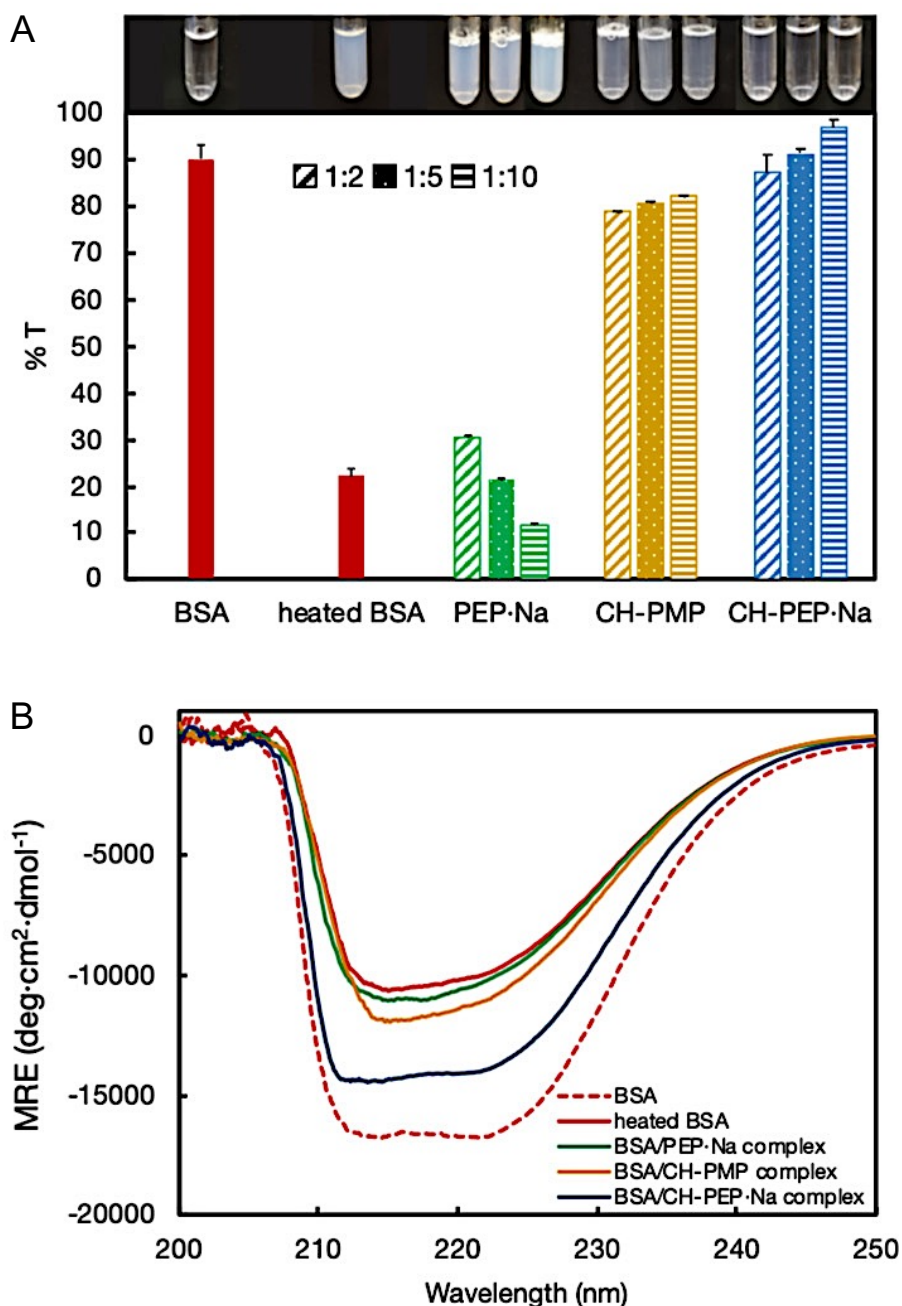
Figure 2.2 (A) Transmittance (%) and observation images (inset) of native BSA, heated BSA, and BSA–PPE complexes with different BSA/polymer molar ratios (1:2, 1:5, and 1:10). (B) CD spectra of native BSA, heated BSA, and BSA–PPE complexes with a molar ratio of 1:10. Mean residual ellipticities were plotted as a function of wavelength.
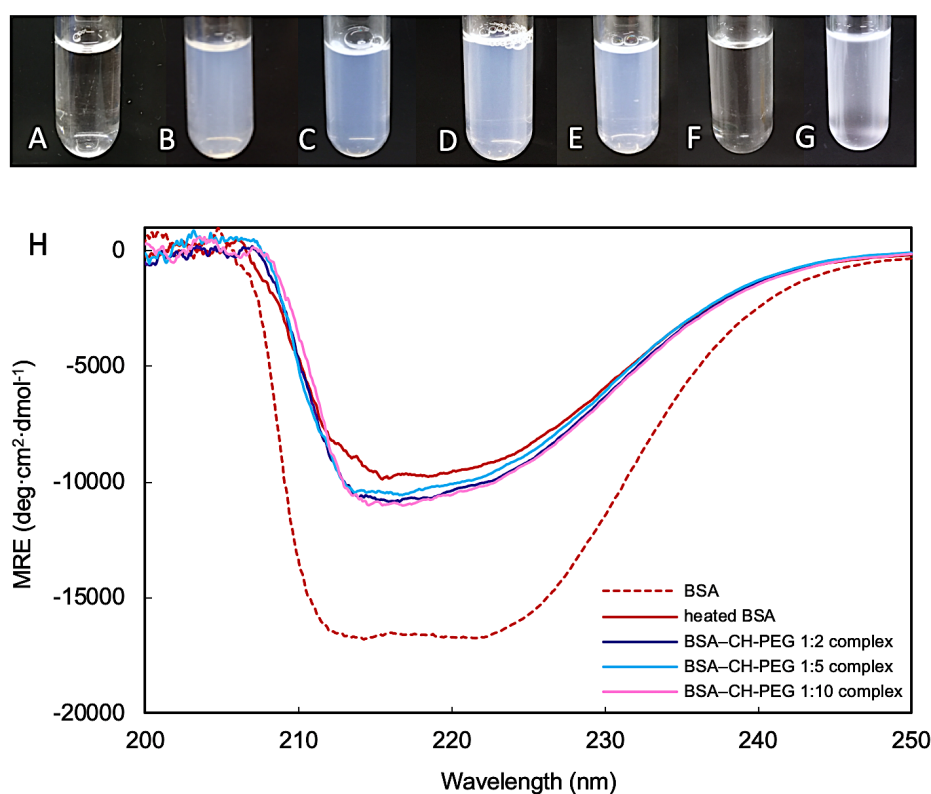
Figure 2.3 Appearance photographs of (A) native BSA, (B) heated BSA, thermally Assisted BSA–CH-PEG complexes with ratios of (C) 1:2, (D) 1:5, and (E)1:10, CH-PEG solution at (F) ambient temperature and (G) after thermal treatment (Figure 3G was photographed immediately before the turbid suspension reversibly become transparent again as Figure 3F). Heating temperature was 90°C for 15 mins. CD spectra (H) of BSA and BSA–CH-PEG complexes.

By elucidating the effect of different PPEs, the secondary structural alteration of complexed BSA was performed using CD measurements as depicted in **Figure 2.2B**. The CD spectrum of native BSA showed two negative peaks, at 212 and 222 nm, at 37 °C, and the heated BSA exhibited a large reduction in the CD intensity, indicating a decrease of the α-helices and a denaturation of BSA during the thermal treatment.[97] The signals of BSA–CH-PMP and BSA–PEP·Na did not remarkably differ from that of the heated BSA, suggesting that neither CH-PMP nor PEP·Na could preserve the conformational structure of BSA. In the presence of CH-PEP·Na (BSA/CH-PEP·Na ratio of 1:10; the other ratios are displayed in **Figure 2.4**), the loss in the negative band was interestingly much smaller compared to that observed for the heated BSA and the other complexes, implying that only CH-PEP·Na could

stabilize the complexed BSA, for the same reason described before. Thereby, amphiphilic CH-PEP·Na can be considered an effective excipient for suppression of thermal denaturation and aggregation.
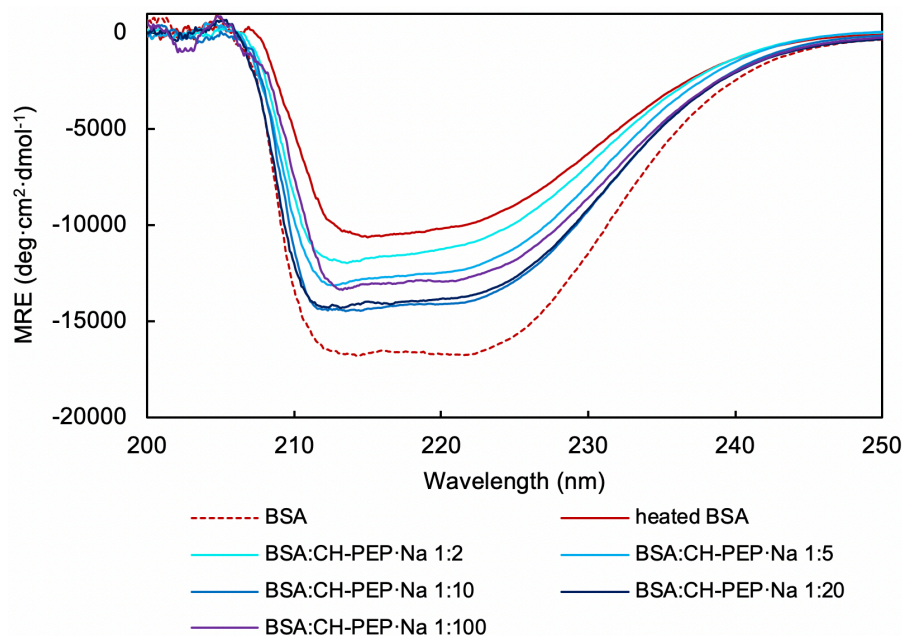
Figure 2.4 CD spectra of BSA and BSA–CH-PEP·Na complexes at different ratio.

The complexation of BSA and CH-PEP·Na was further confirmed by GPC (**Figure 2.5A**); native BSA, the BSA–CH-PEP·Na (1:10) complex, and the unheated mixture of BSA and CH-PEP·Na (1:10) were eluted with PBS. The GPC traces revealed a decrease in the retention time and a peak broadening was observed after thermal treatment with the polymer, indicating the complex formation. In our study, it is notable that the complexation could not occur without thermal inducement, that is, CH-PEP·Na did not interact with BSA at ambient temperature. As shown in **Figure 2.5B**, BSA and CH-PEP·Na formed spherical-like complexes under thermal treatment in an aqueous medium. However, a small amount of free BSA still remained in the complex solution observed from a tiny peak of the complex trace at the retention time of 14 min (solid line, **Figure 2.5A**). Percentage of complex purity reached 94% derived from the area under its GPC trace of noncomplexed and complexed BSA. In addition, BSA/CH-PEP·Na composition in the complexes was estimated from the bicinchoninic acid (BCA) assay. The BSA/CH-PEP·Na ratio in the complexes was 1:12.7 (by mol), resembling feeding ratios of 1:10.0 equiv. The BSA–CH-PEP·Na (1:10) complex with M_w of 1.9×10^5

g/mol was obtained as evaluated by size exclusion chromatography with multiangle light scattering (SEC-MALS) measurement (**Figure 2.6**). On the basis of the data derived from the BCA assay and SEC-MALS, we could estimate that a complex comprised one BSA molecule with 13 chains of CH-PEP·Na. This result verified that CH-PEP·Na had a great ability to prevent protein aggregation.
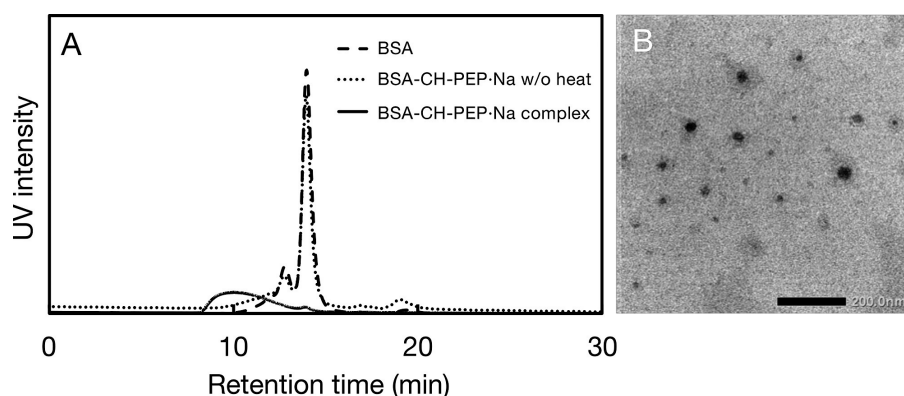
Figure 2.5 (A) GPC elution profiles of native BSA, heated BSA–CH-PEP·Na (1:10) complex, and a mixture of BSA and CH-PEP·Na at 25 °C in PBS. (B) TEM image of the BSA–CH-PEP·Na (1:10) complex (scale bar 200 nm).
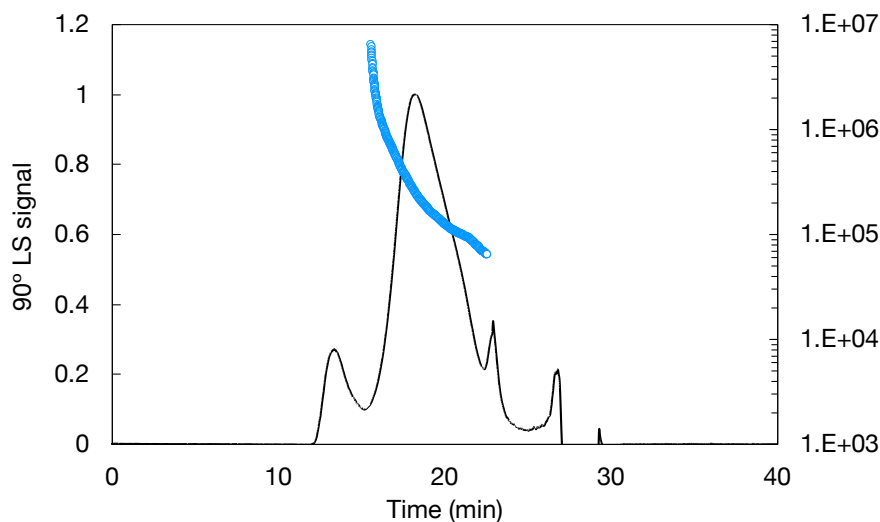
Figure 2.6 SEC-MALS chromatogram of BSA–CH-PEP·Na (1:10) complex in PBS. Open circle, molar mass; solid line, 90° light-scattering signal.

The complex formation by heat treatment at 90 °C was further characterized by dynamic light scattering (DLS). The average size of native BSA at room temperature was detected as 11 nm and the larger size (158 nm) after heat at 90 °C was observed on account of thermal aggregation BSA. BSA–CH-PEP·Na complexes with different feeding CH-PEP·Na ratios were also carried out as demonstrated in **Figure 2.7**. By increasing the amphiphilic CH-PEP·Na, the size of the complex decreased from 51 to 27 nm. This is because, at higher CH-PEP·Na portions, the polymer chains probably stabilized the whole surface of the heat-denatured proteins, resulting in inhibition of large protein aggregation and subsequent formation of smaller complexes. Blocking of protein aggregation by high polymeric content was also previously described, that thermal aggregation of lysozyme was suppressed with an increase in polymeric concentrations by functioning as a molecular shield.[98] It is consistent with the prior result showing the inhibition of the protein thermal aggregation by CH-PEP·Na. Due to biodegradability of PPE analogues, the stability during long-term storage was investigated. Steinbach and coworkers reported a high stability of degradable poly(ethyl ethylene phosphate)–protein conjugates during storage at 4 °C for 1 year.[13] In our study, the size and polydispersity index (PDI) values derived from the DLS data did not notably change and undesirable aggregates were not found over 1 month of storage at room temperature. Hence, BSA–CH-PEP·Na complexes can ensure a high stability in aqueous solution for long-term storage.
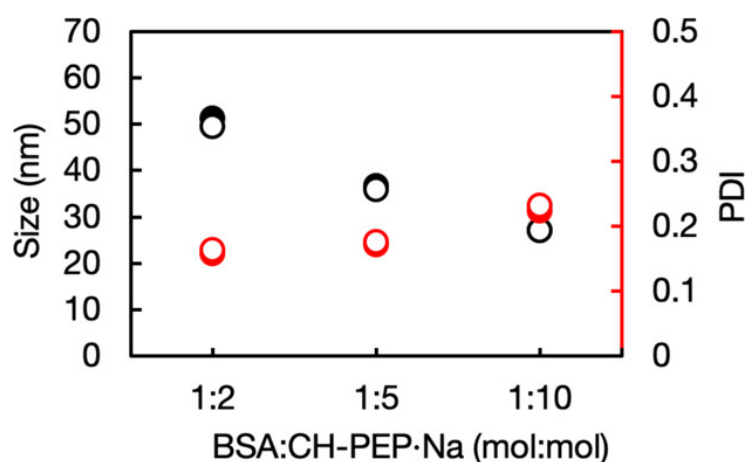
Figure 2.7 Size (black) and PDI (red) of BSA–CH-PEP·Na complex suspended in PBS before (closed circles) and after (open circles) storage for 1 month at ambient temperature.

2.3.3 Complex stability against proteolytic digestion

The BSA–CH-PEP·Na complexes and BSA were subjected to proteolytic condition using a stealth polymer to shelter the sensitive protein from proteolytic attacks. After the complexes and the naked BSA were incubated with trypsin solution in buffer pH 8 at 37 °C, each sample was collected to analyze with matrix-assisted laser desorption/ionization time-of-flight (MALDI-TOF) mass spectroscopy. The mass spectra confirmed that noncomplexed BSA from both neat BSA and BSA/CH-PEP·Na mixture without heat (**Figure 2.8A, B**) were readily digested by trypsin, affording several BSA peptides which were reported by Jaskolla et al (**Table 2.2**).[99] Interestingly, the BSA–CH-PEP·Na (1:10) complex did not show any discernible signals (**Figure 2.8C**), demonstrating an excellent stability in the presence of trypsin. The protective ability of CH-PEP·Na against trypsin digestion was further evaluated by DLS technique as exhibited in **Figure 2.8D, E**. Other polymers, such as poly(ethylene glycol)monomethyl ether methacrylate-*co*-poly(nitrophenylcarbonate) (PEGMA-*co*-PNPC)[93], poly(ethylene glycol)-*block*-poly(*N*-2-hydroxypropylmethacrylamide) (PEG-*b*-PHPMA)[46], and carbohydrate-*block*-poly(propylene glycol)[100], have the potential ability to protect the guest proteins. CH-PEP·Na can be considered as a promising protective carrier for protein delivery under proteolytic conditions.

Figure 2.8 MALDI TOF MS of (A) unprotected BSA and (B) mixture of BSA and CH-PEP·Na (1:10) and (C) thermally assisted complex of BSA–CH-PEP·Na (1:10) under trypsin digestion. DLS profile of (D) unprotected BSA and (E) BSA–CH-PEP·Na (1:10) complex in the presence of trypsin over time.

Table 2.2 Main peptide fragments of BSA from trypsin digest detected by MALDI TOF MS.

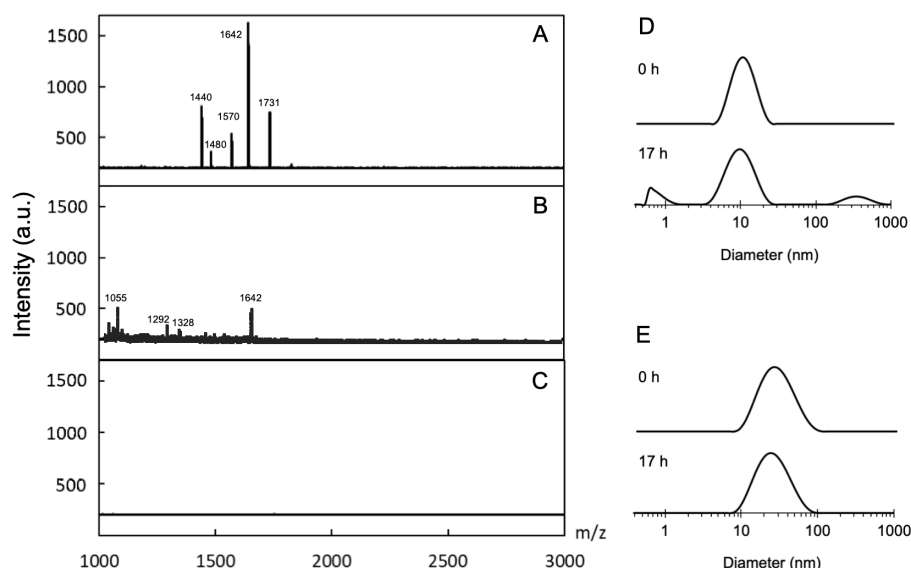| m/z (detected)	Typical fragments	Amino acid sequences
1055	460-468	(R) CCTKPESER (M)
1292	300-309	(K) ECCDKPLLEK (S)
1328	198-209	(K) GACLLPKIETMR (E)
1440	361-371	(R) RHPEYAVSVLLR (L)
1480	421-433	(K) LGEYGFQNALIVR(Y)
1570	347-359	(K) DAFLGSFLYEYSR (R)
1642	437-451	(R) KVPQVSTPTLVEVSR (S)
1731	469-482	(R) MPCTEDYLSLILNR (L)

2.3.4 Binding affinity of FITC-BSA–CH-PEP·Na complexes for HAp surfaces

HAp ($Ca_{10}(PO_4)_6OH_2$) is the major mineral component in bones and teeth.[101] It contains two species of binding sites, anionic phosphate and cationic calcium. As our previous reports, PEP·Na exhibited excellent affinity for both HAp substrates[8,102] and *in vivo* mouse bones.[7] Consequently, BSA-fluoresce in isothiocyanate conjugate (FITC-BSA)–CH-PEP·Na complexes were prepared in order to adsorb onto HAp surface to continue this complex platform for teeth/bone-targeting nanomedicine. Firstly, HAp was soaked into a FITC-BSA–CH-PEP·Na suspension for 3 h. As albumin concentration in human serum is in the range of 3.3–5.2 g/dL[103], the concentrations of 2.5-5.5 g/dL were used in our experiment to investigate the effect of albumin on the affinity of the complexes toward HAp. The coverage ratio and quantity of the adsorbed complexes per unit amount of HAp was estimated by comparing the final complex concentration in the supernatant with that in the original solution before immersion with HAp microparticles. As exhibited in **Figure 2.9A**, both stable plots of coverage ratio ($1.8\text{-}2.0 \times 10^{-3}$) and the amount of adsorbed complex (26.6–28.4 μg/mg HAp) revealed no significant changes in the values upon increasing the albumin concentration, thus implying that the FITC-BSA–CH-PEP·Na complexes strongly deposited on the HAp surface and the albumin could not obstruct the interaction between the complexes and the HAp particles. The uncomplexed FITC-BSA (**Figure 2.9B**), however, exhibited a decrease in affinity for HAp as the albumin concentration increased because of the competitive adsorption of that protein. This

phenomenon could be confirmed by the fluorescence micrographs of HAp treated with FITC-BSA and FITC-BSA–CH-PEP·Na complexes. The green fluorescence signal of FITC-BSA-treated HAp disappeared in the presence of free albumin, whereas that of the complex-treated HAp with and without albumin remained steady (**Figure 2.10**). Therapeutic proteins have been recently developed for osteopathic[93,104] and dental treatments[105,106]; due to the versatilities of CH-PEP·Na, our protein–CH-PEP·Na complexes could be potentially used as therapeutic carriers with proteolytic stability for such bio-applications.
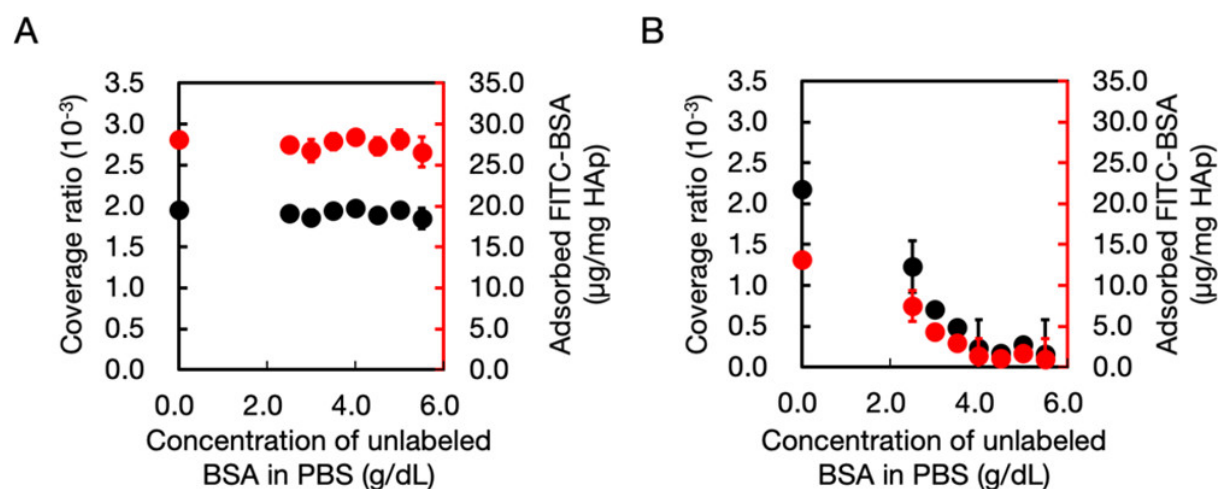
Figure 2.9 Surface coverage ratio (black circles) and quantity (red circles) of (A) complex and (B) FITC-BSA adsorbed on HAp, treated, respectively, with FITC-BSA–CH-PEP·Na (1:10) complex and FITC-BSA, in the absence and presence of free albumin at different concentrations.
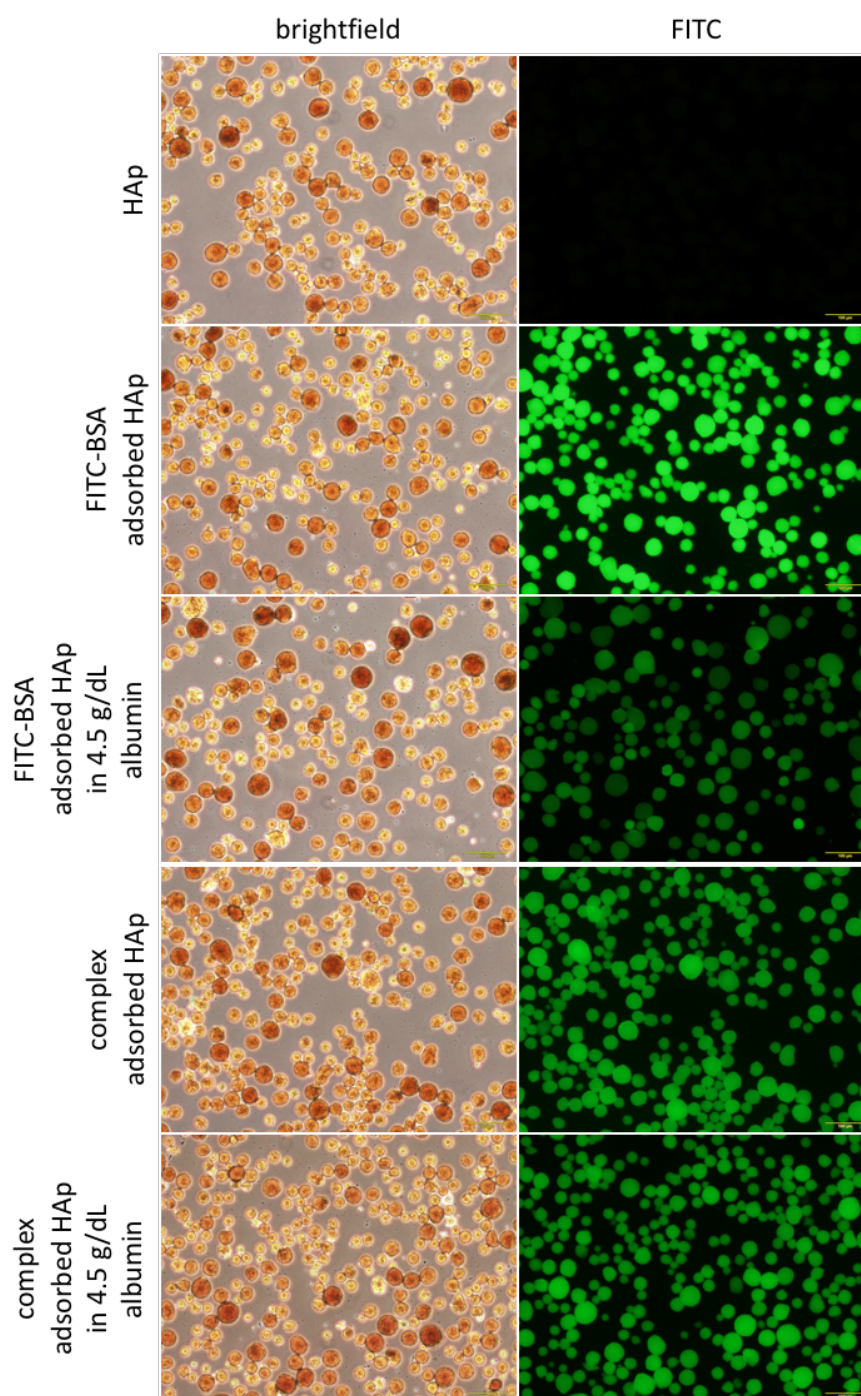
Figure 2.10 Fluorescence micrographs of untreated HAp, FITC-BSA-treated HAp, and complex-treated HAp in the absence and presence of albumin (4.5 g/dL) after washing with PBS (the scale bar is 100 am).

2.4 conclusions

Amphiphilic CH-PEP·Na was selected to fabricate protein–polymer complexes through a facile method as heat treatment. This noncovalent conjugation was created by utilizing the hydrophobic interaction of partial proteins and cholesteryl appendages. To compare with the other two polyphosphoesters, namely, PEP·Na and CH-PMP, CH-PEP·Na provided a superior thermal stabilization ability to the protein resulting from its amphiphilicity and anionic backbone. The BSA–CH-PEP·Na complexes with monodisperse size were obtained at 90 °C for 15 mins, as verified by DLS and TEM. The CH-PEP·Na chains were able to protect the complexed BSA in the presence of protease and excellently maintain the complex size stability for 1 month in aqueous media, indicating long-term stability. In addition, FITC-BSA–CH-PEP·Na complexes have a binding affinity toward HAp surfaces even in the presence of interference of free albumin. It is suggested that this study should be further extended on the complexation of other proteins with CH-PEP·Na for osteopathic and dental cares.

CHAPTER III

THERMALLY ASSISTED GENERATION OF PROTEIN–POLY(ETHYLENE SODIUM PHOSPHATE) CONJUGATES WITH HIGH MINERAL AFFINITY

3.1 Introduction

Oral ailments such as dental caries are serious health problems for all over the world caused by biofilm formation from pathogenic bacteria such as *Streptococcus mutans* (*S. Mutans*). During bacterial adhesion, dental enamel is exposed to acid produced by bacterial metabolism and fermentation leading to enamel demineralization and subsequent decay.[73,107,108] Consequently, hindering of initial stage of bacterial adhesion is necessary to block cariogenic biofilm buildup. In this sense, one of alternative strategies to control bacterial interface is the surface modification with antifouling polymers. Several antifouling polymers such as, poly(ethylene glycol) (PEG)[109,110], zwitterionic polymers[111–114] etc., have been widely studied to generate fouling-resistant surfaces owing to their hydration layers which hinder bacterial attachment. Particularly, immobilization of zwitterionic 2-methacryloyloxyethyl phosphorylcholine (MPC) polymers exhibited effective performance in bacterial repellence on some types of materials.[113,115–117] However, the surface modification mineral substrates with MPC polymers has been rarely studied. To increase the affinity of polymers for mineral surfaces, adornment of phosphate or phosphonate groups in polymers is an effective approach by reason of the strong chelation with mineral ions.[4,101] Poly(ethylene sodium phosphate) (PEP·Na) is a class of water-soluble polyphosphoesters (PPEs) possessing degradable anionic phosphodiester backbone. In our previous works, PEP·Na showed high affinity for hydroxyapatite (HAp) and bone with great cell viability against bone cells.[7–9,72,102] PEP·Na also create a protective barrier for apatite surface against acid erosion.[76,102]

Thanks to the previous researches described above, this study aimed to prepare PPEs bearing zwitterionic phosphorylcholine (PC) groups as antifouling coating polymers that have affinity to mineral surfaces. To introduce PC moieties to the PPEs, thio-yne click reaction was employed because thiol-yne click reaction is a versatile route proceeded under mild condition without byproducts and side reactions.[14] There have been former literatures describing reaction of propargyl or butynyl groups embedded in phosphotriester PPEs with cysteine through UV-assisted thiol-yne click reaction. The reaction was stoichiometrically occurred and applied for preparation of biodegradable PPE-antimicrobial peptide conjugates[18] and zwitterionic PPEs for protection of gold nanoparticles[57]. Therefore, preparation of mineral-binding PPEs harboring zwitterionic PC moieties were carried out using phosphodiester or phosphotriester copolymers having butynyl groups. The alkyne-functional PPEs were reacted with thiol-terminated PC (PC-SH) by thiol-yne click chemistry to afford zwitterionic PPEs. The composition of PC

groups in the PPEs was varied to obtain both the resistance of bacterial adhesion and coating stability of PPEs on mineral substrates. To scrutinize binding capability of the zwitterionic PPEs on HAp surface, amount of adsorbed the polymers and resorption of HAp immobilized with the polymers in acidic media were investigated. Cytotoxicity of the polymers was confirmed by cell viability test with mouse fibroblast cells. Finally, we also assessed inhibition of the polymer toward adhesion and biofilm formation of *S. Mutans*, the main causative bacteria of tooth decay in the human oral cavity. **Scheme 3.1** was shown representation of HAp surface with and without immobilization of zwitterionic PPE and their subsequent effect against bacteria.
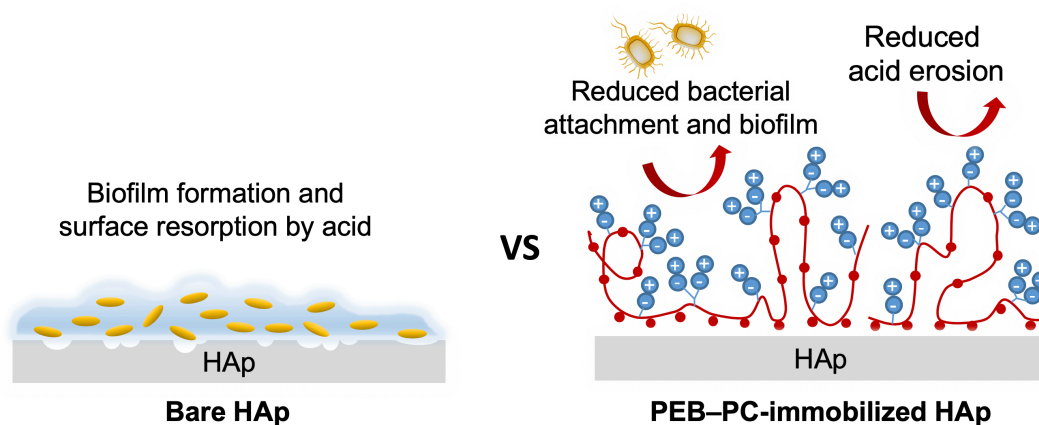
Scheme 3.1 Bacterial adhesion effect of HAp surface with and without immobilization of zwitterionic PPE.

3.2 Materials and methods

3.2.1 Materials

2-Methacryloyloxyethyl phosphorylcholine (MPC) and 2-chloro-2-oxo-1,3,2-dioxaphospholane (COP) were kindly donated by NOF Co., Ltd., Tokyo, Japan. The water used throughout the experiments was purified using a Millipore Milli-Q system (resistivity 18.2 MΩ·cm), involving ultraviolet irradiation, ion exchange, and filtration. Ceramic hydroxyapatite, type II, 80 μm (Bio-Rad) and apatite plate (HOYA Technosurgical, Inc., Tokyo, Japan) were used as substrates for polymer adsorption. 1,8-Diazabicy-clo[5.4.0]-undec-7-ene (DBU) was purchased from FUJIFILM Wako Pure Chemical Co., Osaka, Japan and distilled under reduced pressure, where the fraction with a bp of 130 °C/3.0 mmHg (lit.: bp 80 °C/0.6 mmHg) was collected. 2,6-Lutidine was purified by vacuum distillation. Ion exchange Amberlite IR-120 (Merck KGaA) was rinsed with water before use. An aqueous solution of trimethylamine (TMA) (30%) was purchased from Nacalai Tesque, Tokyo, Japan. Azide-fluor 488 and albumin–fluorescein isothiocyanate conjugate protein bovine (FITC-BSA) were purchased from Sigma-Aldrich Co., St. Louis, MO, USA. Brain–heart infusion (BHI) broth and BHI agar powder were purchased from Becton Dickinson, Sparks, MD, USA. Human saliva was collected from one of the authors and was filtered using a membrane filter (0.2 μm) before use. Other chemicals were purchased from FUJIFILM Wako Pure Chemical Co., Osaka, Japan and used without further purification. An artificial saliva solution was used for mimicking the mixture in oral cavity prepared by dissolving $CaCl_2$ (1.5 mM), KH_2PO_4 (0.9 mM), KCl (130 mM), NaN_3 (1.0 mM), and HEPES (20 mM) and adjusted the solution to pH 7.0 with KOH (1 M)[110].

3.2.2 Synthesis of monomers

3.2.2.1 Synthesis of 2-methoxy-2-oxo-1,3,2-dioxaphospholane (MP)

Toluene (500 mL), distilled 2,6-Lutidine (0.51 mol, 1 eq.), and dehydrated methanol (0.51 mol, 1 eq.) were added into a round-bottom flask in an ice bath and were then mixed by homogenizer. COP (0.51 mol, 1 eq.) was dropwise added into the mixture. After homogenizing for 3 h, vacuum filtration was carried out to eliminate the by-product. After that toluene was remove by evaporation and the product was purified by distillation under reduced pressure condition. The product was obtained as colorless liquid and stored at 4 °C.

3.2.2.2 Synthesis of 2-(but-3-yn-1-yloxy)-2-oxo-1,3,2-dioxaphospholane (BYP)

BYP was synthesized following the MP method using toluene (400 mL), distilled 2,6-lutidine (38.2 mL, 0.33 mol, 1 eq.), 3-Butyn-1-ol (25.0 mL, 0.33 mol, 1eq.), and COP (47.1 g, 0.33 mol, 1 eq.). The product was obtained as light-yellow liquid and stored at 4 °C.

3.2.3 Preparation and characterization of materials for immobilization of zwitterionic PPEs on HAp substrates

3.2.3.1 Synthesis and characterization of PPE copolymers

Various compositions of copolymers of MP with BYP, termed PMB, were prepared by ROP according to a previously reported procedure.[7] Typically, MP (0.31 g, 2.26 mmol, 1 eq.) and BYP (3.62 g, 20.34 mmol, 9 eq.) were placed in a round bottom flask and dried under reduced pressure for 1 h. Benzyl alcohol (34 μL, 0.32 mmol) and DBU (45 μL, 0.32 mmol) were added into the flask. The mixture was dissolved in dehydrated dichloromethane (1 mL) and the reaction was allowed to proceed under an argon atmosphere in an ice bath for 1 h and was then subsequently stirred at ambient temperature for a further 2 h before adding acetic acid to quench the polymerization. Then, the polymers were purified by reprecipitation in toluene followed by diethyl ether and dried under vacuum.

To synthesize the copolymer of EP·Na and BYP (PEB), the demethylation of PMB (1.25 g, 1.04 mol MP) was also performed *via* reaction with TMA (0.41 g, 2.08 mol) and a cation-exchange resin, respectively. PEB was then obtained after neutralization with NaOH solution and dialysis against deionized water using a dialysis tubing with MWCO of 3500. Using a similar method, another PEB copolymer with a different composition was prepared using an [MP]/[TMA] ratio of 1:2.

3.2.3.2 Synthesis of thiol-terminated phosphorylcholine (PC–SH)

PC–SH was synthesized as reported in a previous study.[69,118] Briefly, MPC (14.76 g, 50 mmol, 1 eq.) and 1,6-hexanedithiol (15.29 mL, 100 mmol, 2 eq.) were dissolved in degassed chloroform (100 mL). Diisopropylamine (139.4 μL, 1.0 mmol, 0.02 eq.) was subsequently added to the resulting solution mixture with stirring at ambient temperature for 22 h. The solution was purified by reprecipitation in acetone and then dried under vacuum. Finally, the product was dissolved in degassed water and lyophilized.

3.2.3.3 Modification of PPEs *via* a thiol-yne click reaction with PC–SH

PC-modified PPEs was synthesized *via* a thiol-yne click reaction according to a modified version of a previously reported procedure.[57] Briefly, PEB (0.31 g, 1.23 mmol BYP), PC–SH (5.48 g, 12.3 mmol), and 2,2-dimethoxy-2-phenylacetophenone (DMPA, 94.6 mg, 0.37 mmol) were dissolved in degassed methanol/water. The mixture was exposed to ultraviolet (UV) light (365 nm) irradiated by a Handy UV lamp (LUV-16, AS ONE, Tokyo, Japan) for 3 h with stirring at ambient temperature. The solvent was evaporated and the product was then re-dissolved in methanol. PC-modified PPEs, namely PMB–PC and PEB–PC, were obtained after re-precipitating them in chloroform five times.

3.2.3.4 Characterization of the zwitterionic PPEs

To determine the chemical structure of PMB–PC and PEB–PC, ^{1}H NMR spectra were obtained using a JEOL spectrometer (Tokyo, Japan) operating at 400 MHz. Molecular weights and the dispersity of the PMB–PC and PEB–PC were analyzed by GPC in methanol/water mixture (7:3) containing 50 mM LiBr at 25 °C using an JASCO apparatus, Tokyo, Japan and a refractive index detector (RI-2031, JASCO, Tokyo, Japan). PEG (standard sample of 0.75-140 kDa, Tosoh, Tokyo, Japan) was used to generate a calibration curve.

3.2.3.5 Immobilization and characterization of zwitterionic PPEs on HAp surfaces

Each HAp disc was immersed in 1 mL of polymer solution (0.75 wt%) at 37 °C for 30 min and then dried under vacuum. This step was repeated twice and the product was rinsed with milli-Q water. The hydrophilicity of the HAp surface was investigated by carrying out dynamic water contact angle measurements (First Ten Angstrom model FT-125, goniometer, USA). The reported increasing and decreasing angles are derived from an average of three repeated measurements of different areas in each sample. Surface elemental analysis of the HAp surface was investigated by X-ray photoelectron spectroscopy (XPS) using an ESCA-3400 spectrometer (Shimadzu, Kyoto, Japan) equipped with a Mg Kα X-ray source.

3.2.3.6 Fluorescein labeling of the zwitterionic PPEs and determination of the amount of the adsorbed polymer on the HAp microparticles

PC-modified polyphosphoesters labeled with azide-fluor 488 were synthesized by Cu-catalyzed azide-alkyne cycloaddition.[15,119] PEB–PC (100.67 mg) was dissolved in a 1:4

mixture (2.5 mL) of water and methanol. 42 μL of azide-fluor 488 in DMSO, aqueous sodium L-ascorbate (2.6 M; 12.8 μL), and aqueous $CuSO_4 \cdot 5H_2O$ (0.8 M; 4 μL) were added to the solution. The reaction proceeded at room temperature in the dark for 24 h. The product was dialyzed against water for 1 day (MWCO 3500) before being lyophilized.

In order to determine the quantity of adsorbed polymer on the HAp surface, HAp microparticles (average size 80 μm, 30 mg) were suspended in 0.5 mL of Tris buffer (pH 7.4) containing the relevant fluorescent labeled polymer (1 mg/mL) and each suspension was incubated for 1 h at 37 °C. A calibration curve was determined between the fluorescence intensity and concentration of each fluorescent polymer. The fluorescence intensity of the centrifuged supernatants was measured on a FP-6200 spectrofluorometer (JASCO, Tokyo, Japan) and derived from the initial value to determine the amount of polymer adsorbed on the HAp, where the excitation and emission wavelengths used were 505 and 510 nm, respectively.

3.2.3.7 Inhibition of HAp resorption

To analyze the inhibition of HAp resorption, HAp microparticles (30 mg) were suspended in 1 mL of 0.05 M Tris buffer (pH 7.4) containing zwitterionic PPE (0.75 wt%). After 8 h of incubation at 37 °C, the supernatant was withdrawn. The treated HAp particles were washed with milli-Q water and subsequently resuspended in pH 5 acetate buffer (10 mL). After incubation at 37 °C for 24 h, aliquots were removed, filtered, and analyzed for quantity of calcium ions by an AA-7000 atomic absorption spectrophotometer (Shimadzu, Kyoto, Japan).

3.2.3.8 Cell viability

Mouse fibroblast L929 cells were cultured in Roswell Park Memorial Park (RPMI) 1640 medium (Gibco, Life Technologies, New York) supplemented with 10% (v/v) fetal bovine serum (biowest, Perth, Australia) and 1% antibiotic-antimycotic (Gibco, Life Technologies, New York). The cells were then seeded at approximately 5×10^4 cells/ml (100 μL/well) into a 96-well tissue culture plate. Various concentrations of the polymers (0.16–20 mg/mL) were incubated with the cells at 37 °C under a 5% CO_2-containing atmosphere for 24 h. A Cell Counting Kit-8 (CCK-8; Dojindo, Kumamoto, Japan) was added (10 μL/well) and incubated for 2 h in the dark before measuring the absorbance using a microplate reader (Bio-

Rad, USA) at 450 nm. The experiment was repeated three times. The cell viability percentage was calculated according to the following formula:

$$\text{cell viability (\%)} = (A_{sample} - A_{blank})/(A_{control} - A_{blank}) \times 100\%$$

3.2.3.9 Bacterial anti-attachment of the HAp surface with immobilization of zwitterionic PPEs

To evaluate the bacterial growth in contact with the surface on the zwitterionic PPE-immobilized HAp discs, the samples were first sterilized using ethylene oxide gas (EOG) and each specimen was treated with 500 µL of salivary proteins in a 24-well plate for 2 h at 37 °C. Then, the specimens were washed with 1.0 mL of PBS. *Streptococus mutans* (*S. mutans*) NTCT10449 was cultured in BHI broth and adjusted to approximately 1×10^6 colony-forming units (CFU)/mL. The bacterial suspension (2.0 mL/well) was then inoculated on the discs and incubated at 37 °C for 24 h in anaerobic condition with agitating at 100 rpm. The discs were washed twice with sterilized water to remove loosely-bound bacteria. The adhered bacteria were then transferred to fresh BHI broth medium by a microbrush. 100 µL of the bacterial suspension was spread on a BHI agar plate. After anaerobic incubation at 37 °C for 24 h, number of bacterial colonies was counted.

3.2.3.10 Biofilm formation on PEB-PC-immobilized HAp surface

The sterilized specimens were placed in a 24-well plate for saliva treatment as the same method described above and were incubated with *S. mutans* suspension (1×10^6 CFU/mL) in BHI broth supplemented with 1% (w/v) sucrose. After anaerobic incubation at 37 °C for 6 h with shaking, the *S. mutans*-containing specimens were transferred to new wells with fresh bacterial suspension (1×10^6 CFU/mL; 2 mL) and incubated under anaerobic conditions for 18 h. The specimens were again transferred into new wells containing fresh bacterial suspension for a further 24 h of incubation. In order to observe biofilm formation on the HAp surface, the specimens were gently irrigated with PBS (2 mL) to remove any unattached bacteria followed by staining of the biofilm with a LIVE/DEAD® BacLightTM bacterial viability kit (L7007, Molecular Probes, Eugene, OR, USA). Briefly, 2 µL of component A (SYTO 9 dye, 1.67 mM/propidium iodide, 1.67 mM) and 2 µL of component B (SYTO 9 dye, 1.67 mM/propidium iodide, 18.3 mM) were mixed in 1 mL of water. The solution (150 µL) was dropped onto the

samples that where then subsequently incubated in the dark at 37 °C for 15 min. After irrigating with deionized water, the samples were observed by confocal laser scanning microscopy (CLSM; LSM 700, Carl Zeiss, Oberkochen, Germany) at excitation wavelengths of 488 and 553 nm, and emission wavelengths of 520 and 568 nm. The images were analyzed using the ZEN 2011 SP7 (Carl Zeiss, Oberkochen, Germany) and Imaris (Bitplane, Zurich, Switzerland) software packages to determine the biofilm thickness.

3.3 Results and discussion

3.3.1 Synthesis and characterization of monomers
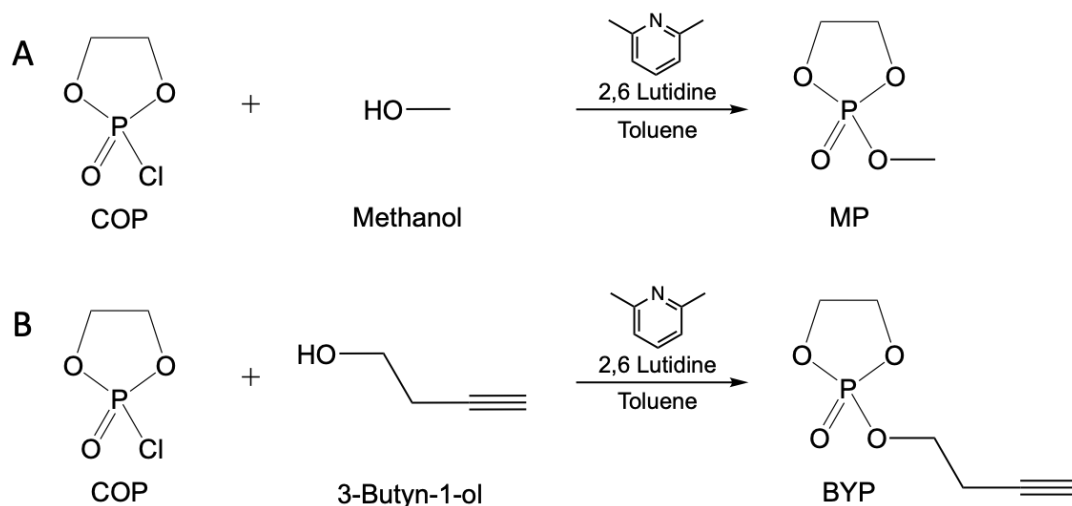
Figure 3.1 Synthesis of (A) MP and (B) BYP.

2-methoxy-2-oxo-1,3,2-dioxaphospholane (MP) was synthesized by 2-chloro-2-oxo-1,3,2-dioxaphospholane (COP) and methanol (**Figure 3.1A**) using 2,6-lutidine as catalyst at room temperature providing dimethylpyridinium as the byproduct. In the same way, COP was allowed to react with 3-butyn-1-ol to prepare another monomer, 2-(but-3-yn-1-yloxy)-2-oxo-1,3,2-dioxaphospholane (BYP) (**Figure 3.1B**). The structure of MP and BYP were confirmed by ^{1}H NMR spectra as depicted in **Figure 3.2**.

Figure 3.2 ^{1}H NMR spectra in CDCl$_3$ of (A) COP, (B) MP, and (C) BYP.

3.3.2 Synthesis and characterization of PPEs

Poly(2-methoxy-2-oxo-1,3,2-dioxaphospholane-*co*-2-(but-3-yn-1-yloxy)-2-oxo-1,3,2-dioxaphospholane) (PMB) was successfully synthesized by ring-opening polymerization (ROP) of MP and BYP at different rat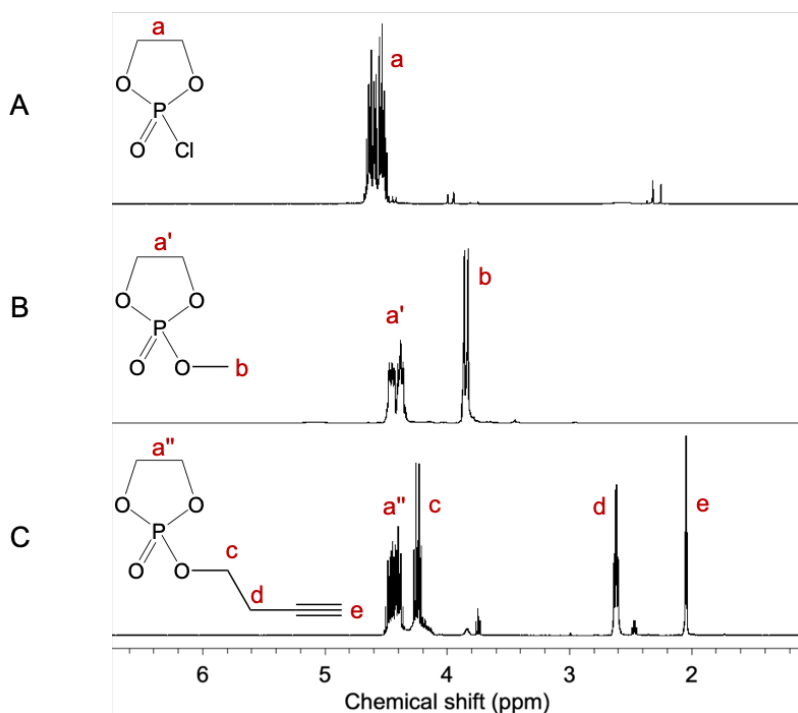ios using benzyl alcohol as an initiator and 1,8-diazabicyclo[5.4.0]-undec-7-ene (DBU) as a catalyst. After purification, demethylation, and neutralization step, poly(ethylene sodium phosphate-*co*-2-(but-3-yn-1-yloxy)-2-oxo-1,3,2-dioxaphospholane) (PEB) was obtained as the synthetic route revealed in **Figure 3.3**. The copolymer structures of PMB and PEB were proved by ^{1}H NMR spectroscopy (**Figure 3.4**). The spectrum of PMB shows chemical shift at 3.8 ppm, which can be attribute to the proton of methoxy groups while such peak of PEB (3.6 ppm) obviously reduced after trimethylamine (TMA) treatment. Notably, BYP signal could be still observed after the severe conditions. The molecular characteristics were evaluated by ^{1}H NMR and GPC (**Table 3.1 and Table 3.2**). The monomer ratio in all copolymers of PMB closely resembles the feeding ratio for target degree of polymerization of 70. Also, % demethylation of PEB reached almost 100% indicating that the transformation of triester PMB to diester PEB was nearly complete for all 5 compositions.
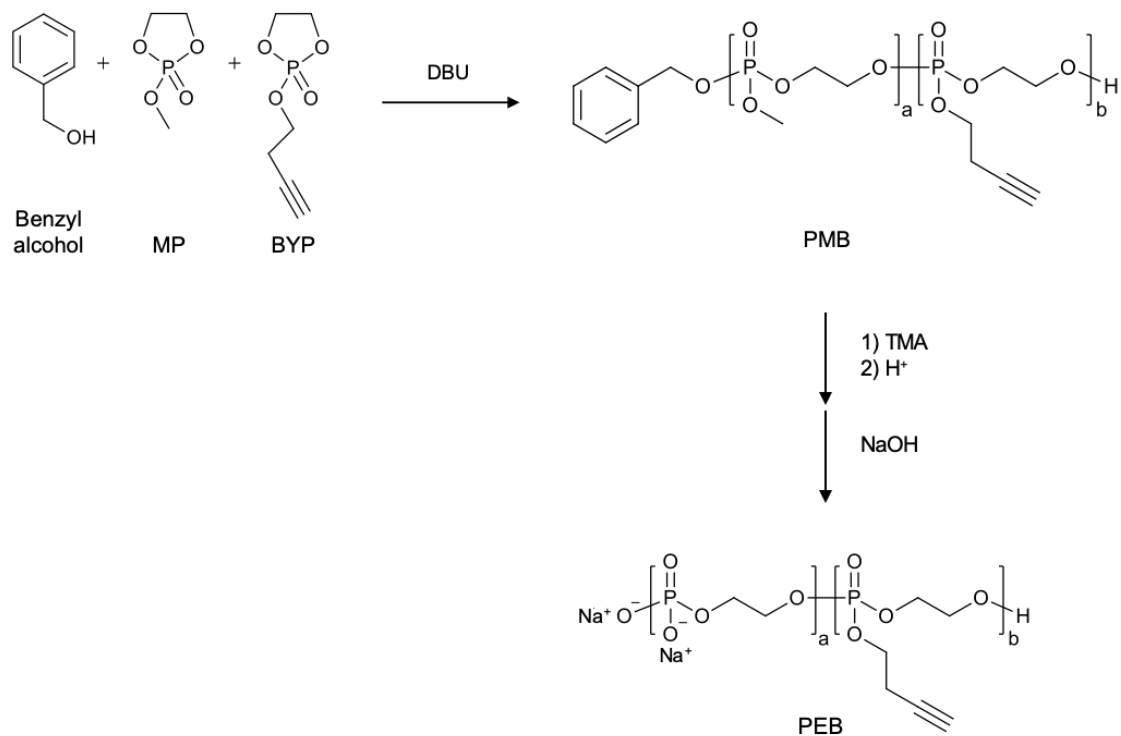
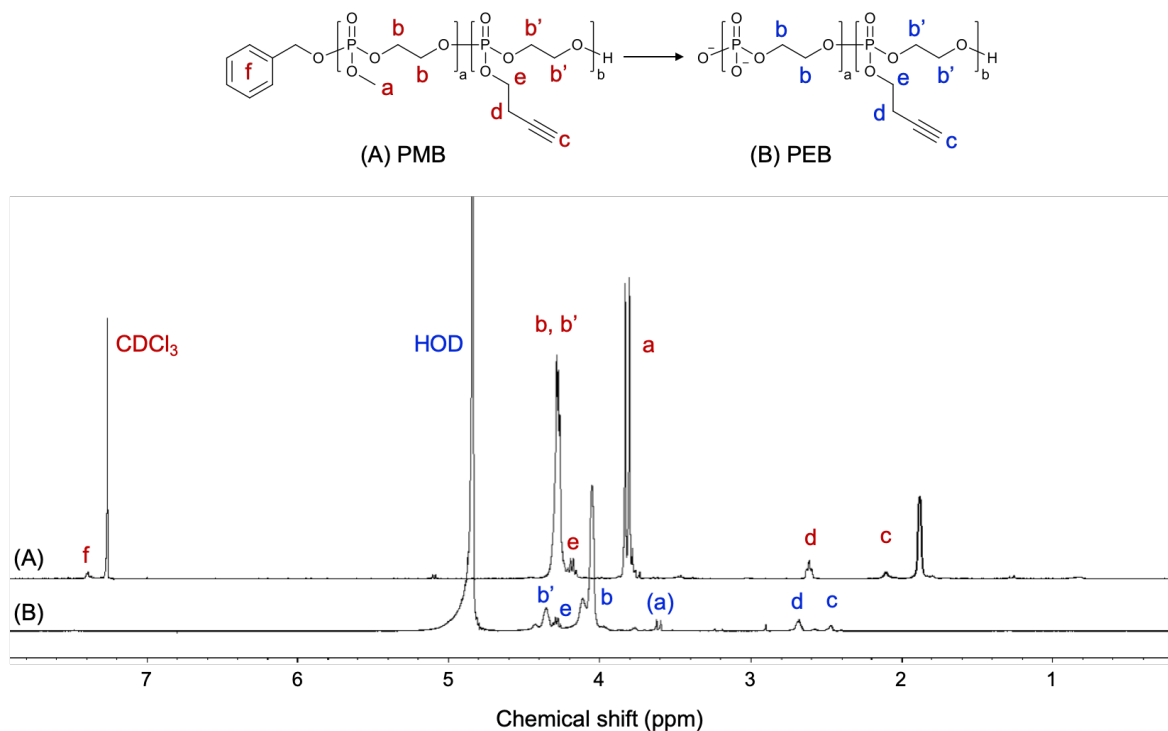**Figure 3.3** Synthetic route of PMB and PEB.

Figure 3.4 ^{1}H NMR spectra of (A) PMB and (B) PEB.

Table 3.1 Molecular characteristic of PMB at different ratios.

Polymer	MP:BYP ratio		[M]/[I]	DP[a]	$M_{n,\,\text{NMR}}$ [a] $(\times 10^3)$	$M_{n,\,\text{GPC}}$ [b] $(\times 10^3)$	M_w/M_n [b]
	In feed	In copolymer[a]					
PMB1/9	0.1:0.9	0.1:0.9	70	70	12.3	8.4	1.41
PMB3/7	0.3:0.7	0.3:0.7	70	75	12.6	9.1	1.28
PMB5/5	0.5:0.5	0.5:0.5	70	68	10.9	7.4	1.36
PMB7/3	0.7:0.3	0.7:0.3	70	70	10.6	7.1	1.43
PMB9/1	0.9:0.1	0.9:0.1	70	71	10.3	5.3	1.47

DP: degree of polymerization.
[a] Determined by ^{1}H NMR in CDCl$_3$.
[b] Determined by GPC elution in CHCl$_3$.

Table 3.2 Molecular characteristic of PEB at different ratios.

Polymer	MP: EP·Na :BYP[a]	% Demethylation[a]	$M_{n,\,\text{NMR}}$ [a] $(\times 10^3)$	$M_{n,\,\text{GPC}}$ $(\times 10^3)$	M_w/M_n
PEB1/9	0.01:0.09:0.90	92	12.2	15.8[b]	1.32[b]
PEB3/7	0.03:0.31:0.66	92	12.6	24.3[b]	1.29[b]
PEB5/5	0.04:0.47:0.49	92	10.9	7.4[c]	1.36[c]
PEB7/3	0.03:0.66:0.31	96	10.8	8.7[c]	1.45[c]
PEB9/1	0.04:0.86:0.10	96	10.6	7.7[c]	1.35[c]

[a] Determined by ^{1}H NMR in D$_2$O.
[b] Determined by GPC elution in methanol/water (7:3).
[c] Determined by GPC elution in acetate buffer.

3.3.3 Synthesis of thiol-terminated phosphorylcholine (PC-SH)

Thiol-terminated phosphorylcholine PC-SH was successfully synthesized through thiol-ene reaction using 2-methacryloyloxyetyl hexanedithiol and phosphorylcholine (MPC). The successful product was confirmed by ^{1}H NMR spectrum of PC-SH (**Figure 3.5**) with no emergence of methylene proton signal arising from MPC precursor. Matrix assisted laser desorption ionization time of flight mass spectrometer (MALDI TOF MS) revealed that PC-SH was a major product (m/z = 446.54) while there were side products with PC-S-(CH$_2$)$_6$-S-PC (m/z = 741.74) and disulfide dimer, PC-S-(CH$_2$)$_6$-S-S-(CH$_2$)$_6$-S-PC (m/z = 891.32).
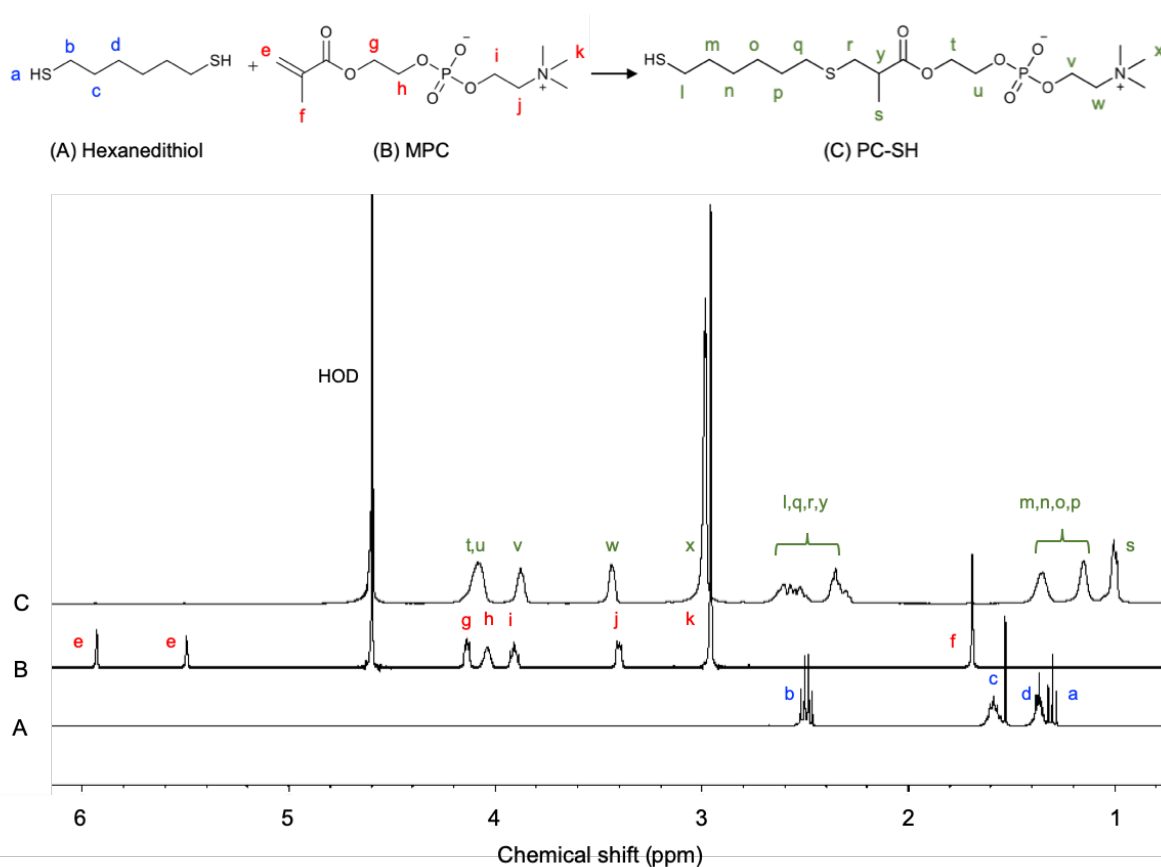
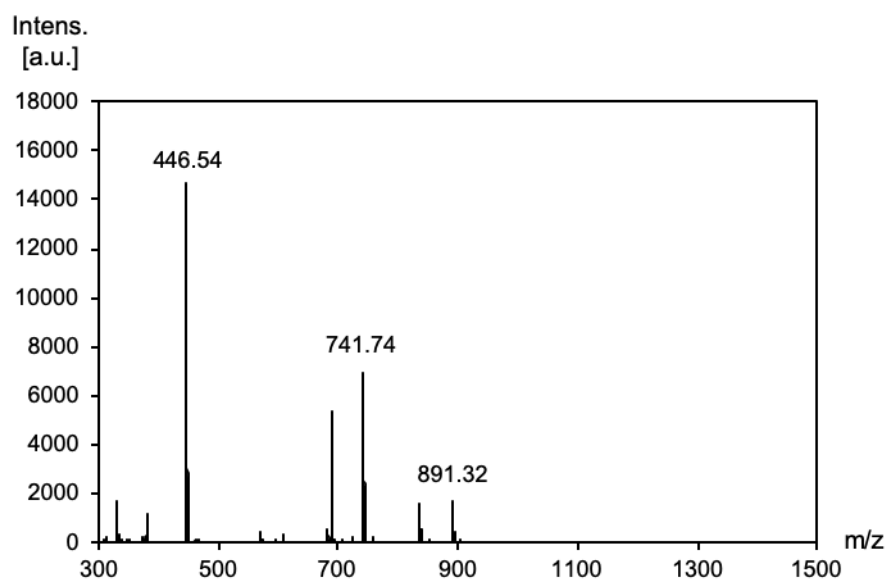**Figure 3.5** ^{1}H NMR spectra of (A) hexanedithiol, (B) MPC, and (C) PC-SH.

Figure 3.6 MALDI TOF MS spectra for the product of the reaction between MPC and 1,6-hexanedithiol.

3.3.4 Synthesis and characterization of zwitterionic PPEs through thiol-yne click reaction

Zwitterionic PPEs, PC-modified PMB (PC-PMB), and PC-modified PEB (PEB–PC) with two composition ratios of the MP and BYP units (1:9 and 3:7) were prepared through the thiol-yne click reaction of the BYP moieties of PMB and PEB with PC–SH, respectively (**Figure 3.7**). ^{1}H NMR was used to verify the successful conjugation, evidenced by characteristic peaks arising from the PPE backbone and pendant PC motifs (**Figure 3.8**). ^{1}H NMR, alongside GPC, were then used to measure the molecular weights, the dispersity, and PC fraction in each copolymer (**Table 3.3**). The reaction of the BYP and PC–SH successfully proceeded to give both the monoaddition (1-arm PC) and biaddition (2-arm PC) products, whereas some BYP portions still remained unreacted because of the steric hindrance of the pendant PC.[120] However, the products with 2-arm PC groups made up the highest proportion of the four copolymers compared with the 1-arm product and remained BYP, indicating that zwitterionic PPEs were successfully synthesized by click conjugation.
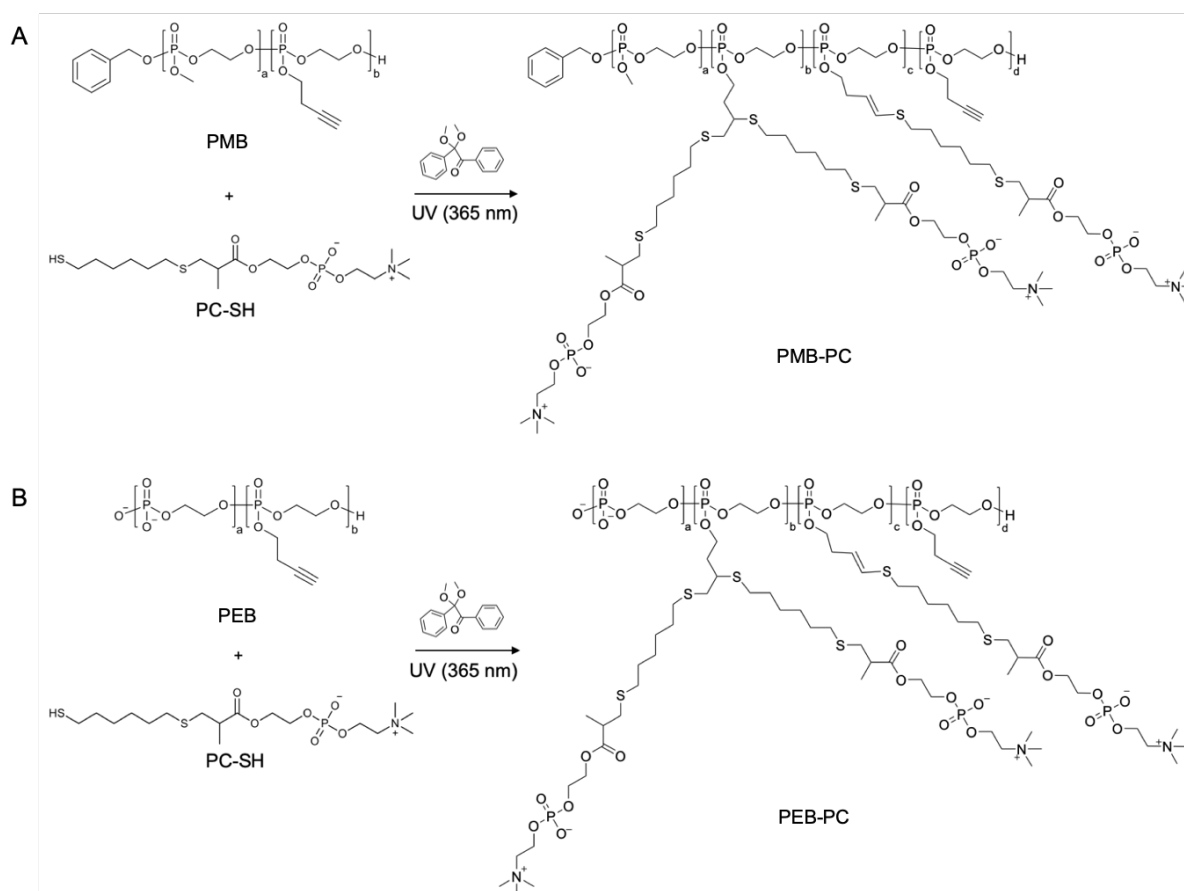

Figure 3.7 Overview of the synthesis of PMB–PC and PEB–PC via a thiol-yne click reaction.
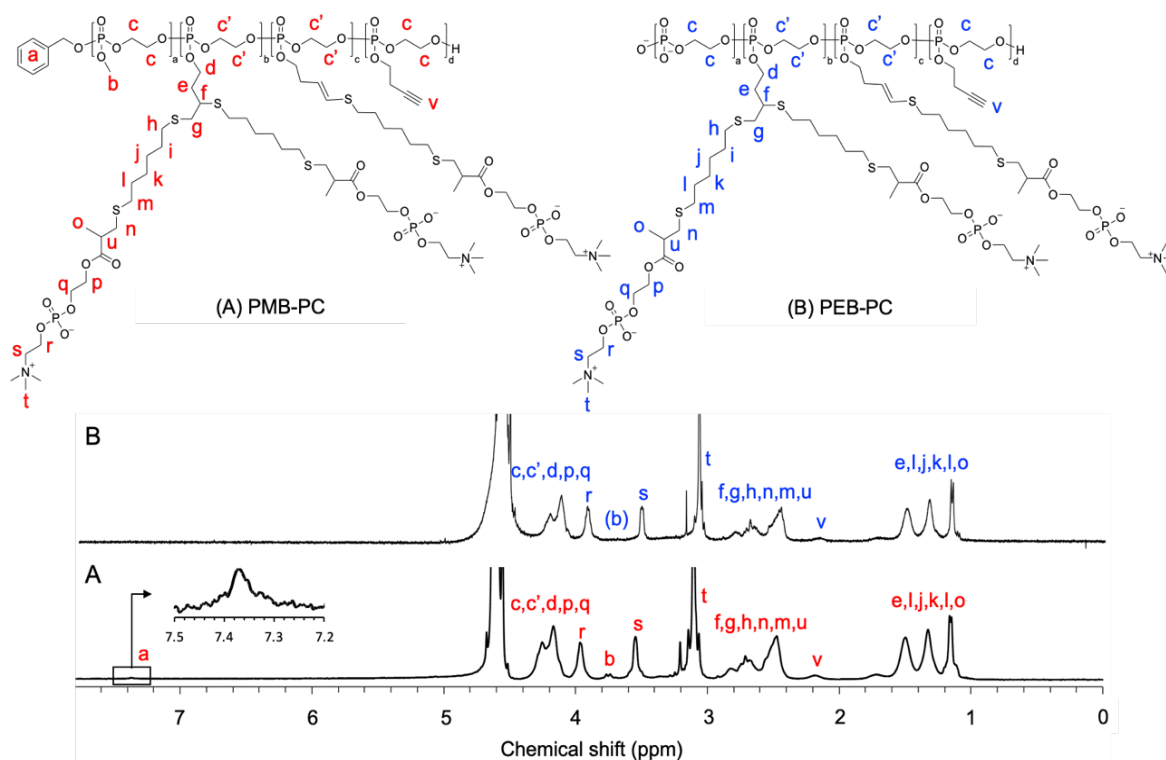
Figure 3.8 ^{1}H NMR spectra in D_2O of (A) PMB–PC and (B) PEB–PC.

Table 3.3 Characterization of the zwitterionic PPEs prepared in this study.

Polymer	M_n[a] ($\times 10^3$)	M_w/M_n[a]	Molar fractions in polymer[b]				
			MP	EP·Na	1-arm PC	2-arm PC	BYP
PMB1/9–PC	15.2	1.48	0.10	-	0.20	0.49	0.21
PMB3/7–PC	13.3	1.45	0.33	-	0.13	0.38	0.16
PEB1/9–PC	12.4	1.44	0.01	0.09	0.21	0.46	0.23
PEB3/7–PC	15.2	1.42	0.02	0.31	0.08	0.39	0.20

[a] Determined by GPC elution in methanol/water (7:3).
[b] Derived from ^{1}H NMR spectra in D_2O.

3.3.5 Immobilization and characterization of zwitterionic PPEs on HAp surfaces

After HAp discs were immobilized with the four zwitterionic PPEs, wettability of the PMB–PC and PEB–PC-immobilized HAp surfaces were determined by the contact angle measurement in order to clarify that the zwitterionic PPEs adsorb on a HAp substrate to create a hydrophilic surface (**Figure 3.9A**). The water contact angle data was decreased by

immobilization with the zwitterionic PPEs from 84° to 47-51° for advancing and from 51° to 24-31° for receding, respectively. Accordingly, this data indicated their highly hydrophilic characters on the HAp surface after the polymeric immobilization.

Moreover, X-ray photoelectron spectroscopy (XPS) measurements were carried out to confirm the immobilization of the zwitterionic PPEs on a HAp surface. Comparing with the bare HAp, the spectra of the immobilized HAp show the appearance of a N_{1s} signal (403 eV) corresponding to nitrogen, arising from the PC groups (**Figure 3.9B**).
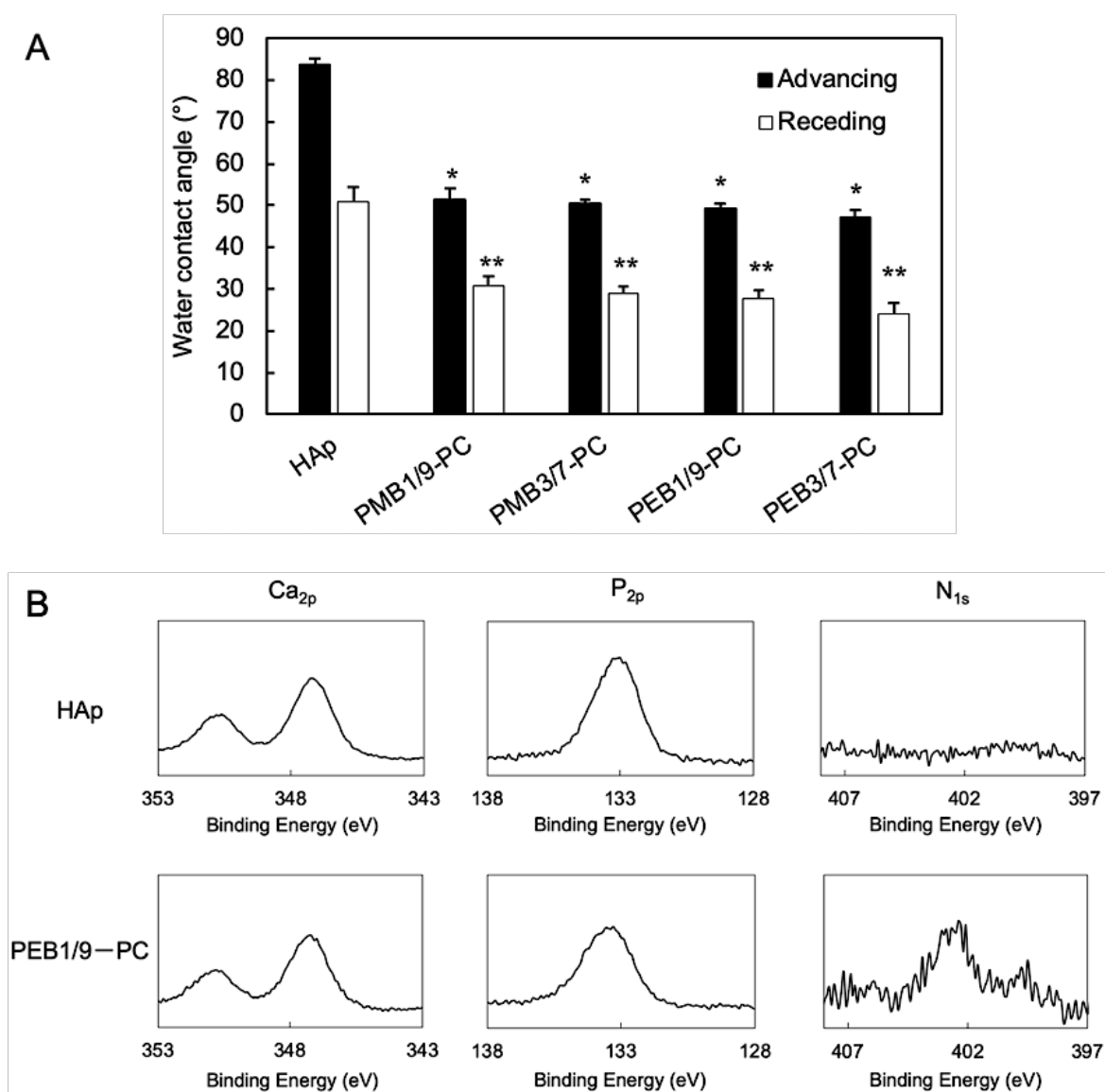

Figure 3.9 (A) Water contact angle data for non-immobilized and immobilized HAp discs. * and ** *p* < 0.01 vs. HAp, *t*-test (n=3). (B) XPS spectra of bare HAp and HAp with immobilization of PEB1/9−PC.

3.3.6 Fluorescein labeling of the zwitterionic PPEs

A copper-mediated azide-alkyne click conjugation was performed to further adorn fluorescent probe on the zwitterionic PPEs by the reaction between the remaining BYP groups in each polymer and a fluorescent azide (**Figure 3.10**). The densities of the labeled fluorescence (**Table 3.4**) on the zwitterionic PPEs were determined by fluorescence spectroscopy using calibration curves of free azide-fluor 488.
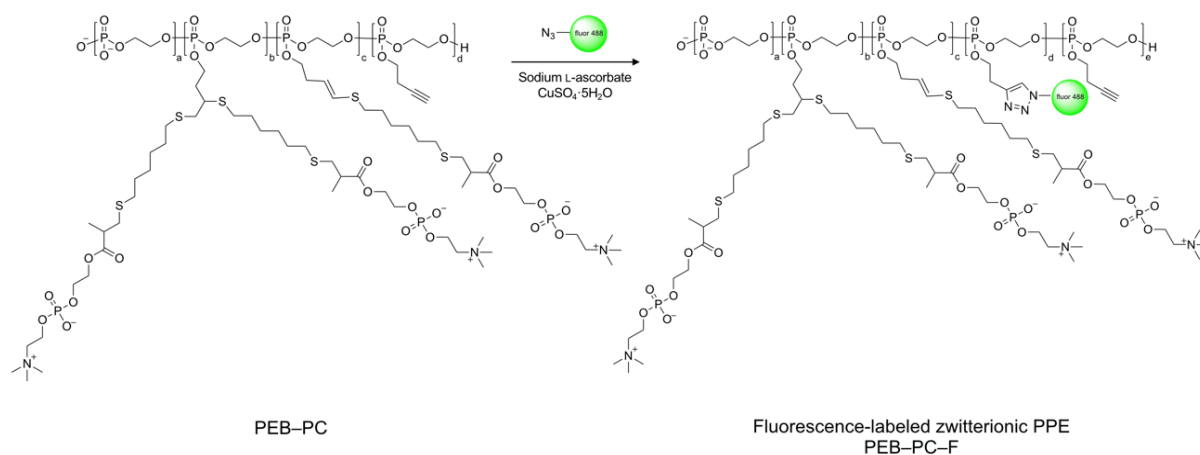
Figure 3.10 Preparation of fluorescence-labeled polymer by azide-alkyne click reaction.

Table 3.4 Densities of the fluorescent probe (fluor 488) immobilized with zwitterionic PPEs.

Sample	Densities of fluor 488 (%; mol/mol)
PMB1/9–PC–F	0.43
PMB3/7–PC–F	0.22
PEB1/9–PC–F	0.50
PEB3/7–PC–F	0.64

3.3.7 Determination of the quantity of the adsorbed polymer on the HAp microparticles

In **Figure 3.11B**, the quantity of the adsorbed polymer and pendant PC on HAp microparticles was estimated by comparing the fluorescent intensity between the final fluorescence-labeled polymer in the supernatant and that in the initial solution before being incubated with HAp microparticles. Calibration curves between fluorescent intensity and

concentration of each fluorescent polymer were exhibited in **Figure 3.11A**. Fluorescence-tagged PEB–PC (PEB–PC–F) shows higher adsorption on a HAp surface than the PMB–PC–F, especially PEB3/7–PC–F (128 $\mu g/m^2$), the adsorption of which is double the values of the PMB–PC–F on account of PEB3/7–PC–F containing the most content of anionic phosphate moieties. Even though the PEB1/9–PC–F did not show superior adsorption over PEB3/7–PC–F, PEB1/9–PC–F contains the highest pendant PC at 30 $\mu g/m^2$, derived from the ^{1}H NMR integration of PC fraction in each polymer. It is accordant with our previous study, which showed that the anionic PPE enhance the adsorption on HAp particle,[102] a result that was confirmed in this study from fluorescence images of PEB1/9–PC–F (**Figure 3.12**). According to the fluorescence micrographs, the HAp particles reveal green fluorescence after immobilization of the fluorescence-labeled polymers.

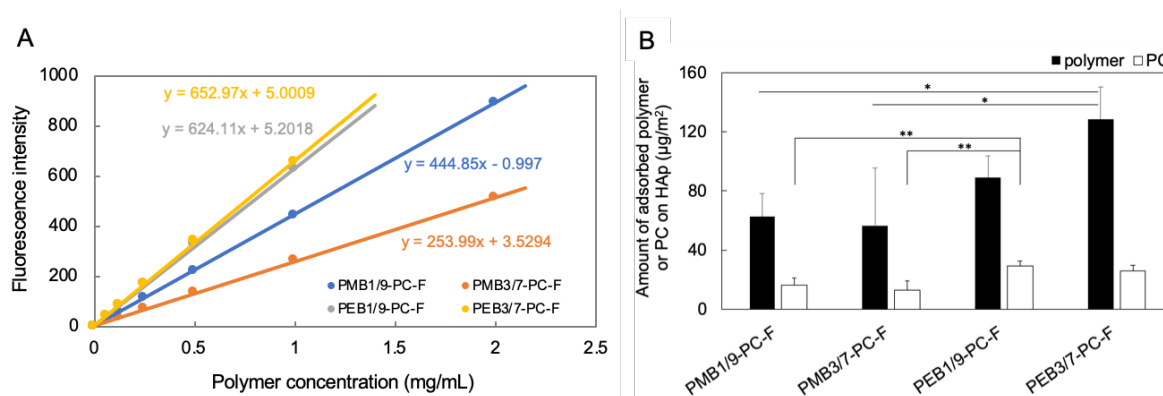**Figure 3.11** (A) Calibration curves of fluorescence intensity as a function of the polymer concentration in Tris buffer (pH 7.4). (B) Amounts of PPE–PC–F and PC moieties adsorbed on HAp microparticles. * and ** $p < 0.05$, *t*-test (n = 3).
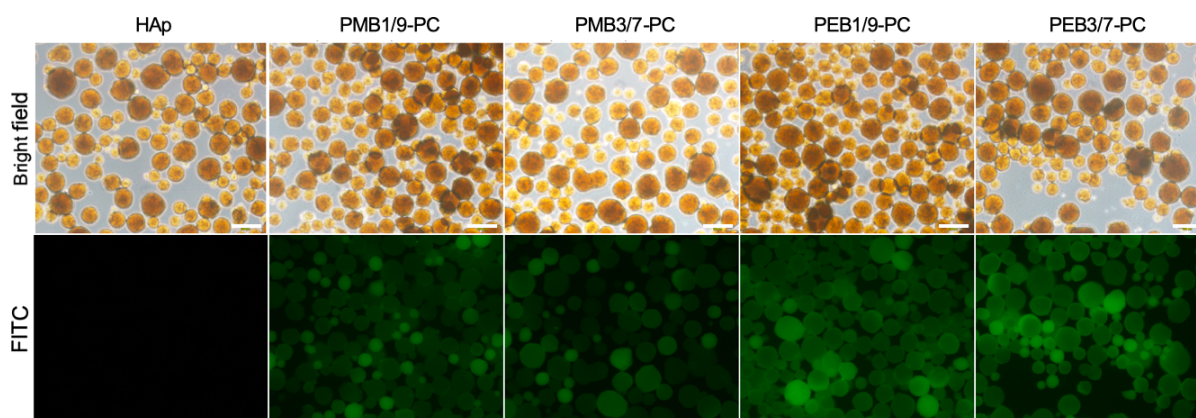
Figure 3.12 Representative fluorescence micrographs of non-immobilized and immobilized HAp microparticles (the scale bar 200 μm).

3.3.8 Stability of HAp surface with the immobilization of the zwitterionic PPEs in artificial saliva

The stability of the immobilized HAp surfaces was investigated in artificial saliva containing $CaCl_2$, KH_2PO_4, KCl, NaN_3, HEPES, and KOH. After incubation in artificial saliva at 37 °C for 1 week, the water contact angles (**Figure 3.13A**) and the fluorescence signal of the HAp surface (**Figure 3.13B**) with the immobilization of PEB1/9-PC and fluorescent polymers, respectively, were found to have hardly changed, indicating that the immobilized zwitterionic PPE on HAp substrate is stable in mimetically salivary condition.

Figure 3.13 Water contact angles (A) and fluorescence micrographs (B) of the bare HAp and immobilized HAp surfaces before and after incubation in artificial saliva at 37°C for 1 week. Scale bar is 200 μm.

3.3.9 Inhibition of HAp resorption under acidic condition
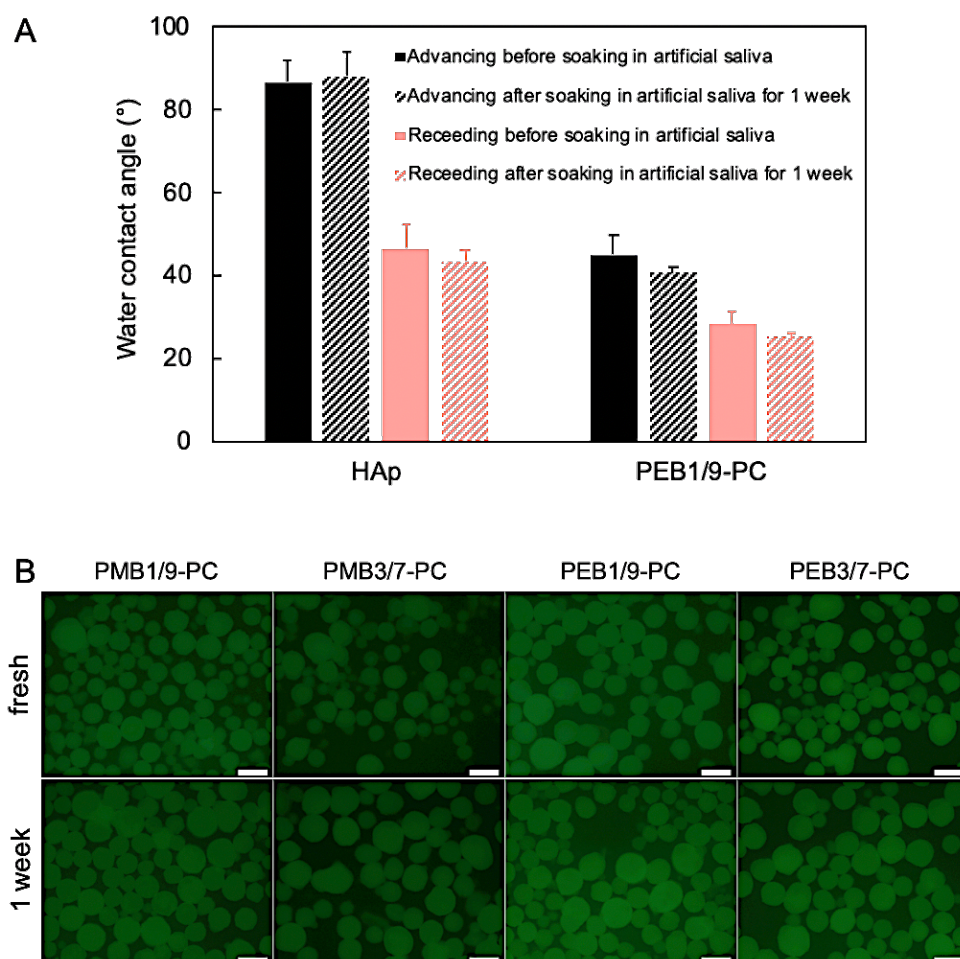
One of crucial factors in maintaining healthy teeth is pH. According to critical pH for enamel demineralization is around 5.2-5.5[121], loss of enamel can be caused by highly acidic microenvironments generated by bacteria attached on dental surfaces.[73,107] In addition, regurgitated food from stomach and consumption of acidic foods and beverages, such as soft drinks, negatively affect teeth.[29] Therefore, preventive efficiency of zwitterionic PPEs against acid was investigated using HAp microparticles as tooth model. After surface immobilization on HAp microparticles, the microparticles were immersed in acetate buffer pH 5 for 24 h to evaluate concentration of released calcium from HAp by atomic absorption spectrometry (**Figure 3.14**). As high as 1.98 mM calcium eroded by acid was detected from non-immobilized HAp (0.10 mM was detected at pH 7.4) while 1.12, 0.99, 0.67, and 0.65 mM of released calcium were observed from the immobilization of PMB1/9–PC, PMB3/7–PC, PEB1/9–PC, and PEB3/7–PC, respectively. The resorption of HAp in acidic condition was significantly decreased by the surface immobilization with the zwitterionic PPEs. In the presence of PMB–PC immobilization, the mineral loss was reduced by 44-50% in comparison with non-immobilized HAp surface while 66-67% reduction was observed in PEB–PC-immobilized HAp. This phenomenon suggested that PEB–PC showed superior performance as anti-erosive agent in order to decrease the dissolution of HAp to that of PMB–PC because high adsorption amount of PEB–PC on HAp surface as described in **Figure 3.11B**. This is consistent with the previous report that phosphate-containing polymer could protect HAp surface against acidic attack.[76] Poly(methyl methacrylate-*block*-methacryloyloxyethyl phosphate) was synthesized as non-fluoride agent to prevent acidic erosion. After polymer treatment on HAp discs at pH 7.0, the discs were immersed in 1% acetic acid (pH 3.8). Calcium release detected by atomic absorption spectrometry was reduced by 46% as compared to the bare HAp.
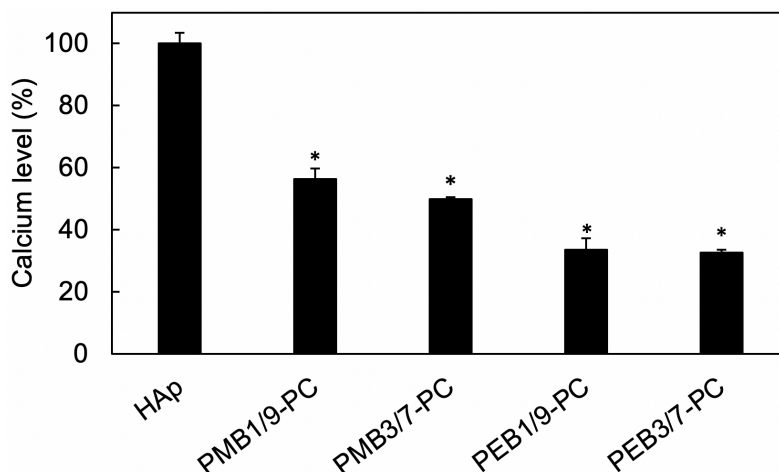
Figure 3.14 Effect of zwitterionic PPEs on resorption of HAp microparticles in acetate buffer pH 5. *$p < 0.01$ vs. HAp, *t*-test (n = 3).

3.3.10 Cell viability test

The influence of the different zwitterionic PPEs on cell viability was examined by 24 h incubation against L929 cells in different concentration of the polymer solutions followed by Cell counting kit-8 (CCK-8) determination. Interestingly, PEB1/9–PC exhibited the most excellent biocompatibility even with 10 mg/mL PEB1/9–PC, the cell viability was still higher than 77% as displayed in **Figure 3.15A**. Due to the superior biocompatibility of PMB1/9–PC, it did not exhibit IC_{50} value to L929 cells within the tested concentration range (0.625-20 mg/mL), the other three polymers (PMB1/9–PC, PMB3/7–PC, and PEB3/7–PC) had IC_{50} values as summarized in **Figure 3.15B**. To compare with poly(ethylene glycol) (PEG) is widely accepted as highly cytocompatible polymer, IC_{50} values for the identical cell line, estimated by CCK-8, are approximately 12.4-22.5 mg/ml depending on molecular weight of PEG (M_n 150-4000).[122] These values are close to that of the synthesized polymer, indicating that biocompatibility of the zwitterionic PPE that can be well applied for biomedical-related applications.
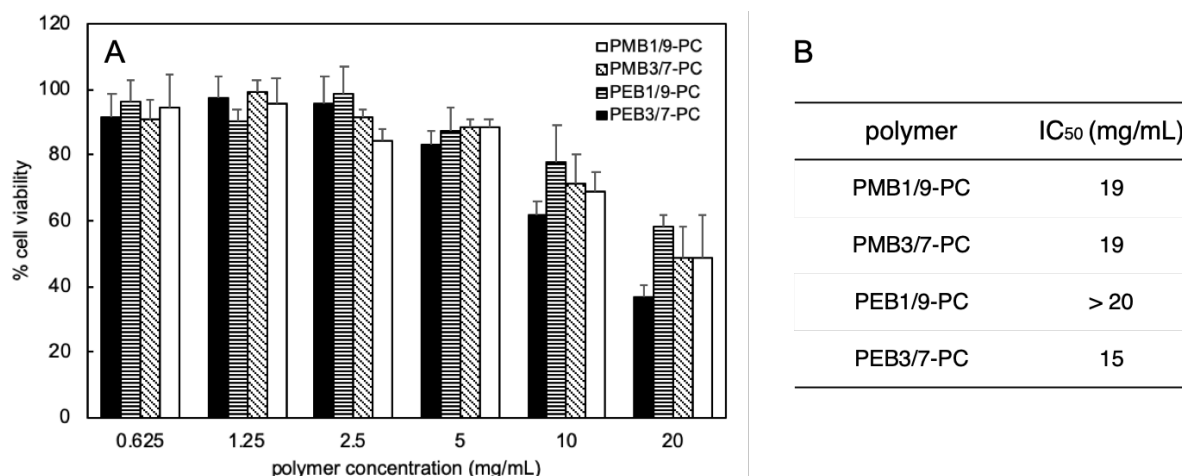
Figure 3.15 Cytotoxicity (A) of the zwitterionic PPEs to fibroblast L929 cells and summary of IC_{50} values (B).

3.3.11 Anti-attachment effect on protein and bacteria

Oral bacteria generally adhere on dental surface through physical interactions as hydrophobic and electrostatic force. Also, the bacteria can recognize a characteristic of dental pellicles which are formed by salivary proteins on enamels.[67] In order to reduce both the nonspecific and specific adhesion of the bacteria on tooth, creating PC layer on the tooth surface can prevent physical interactions not only the bacterial surfaces but also salivary proteins.

The effect of polymer immobilization against protein adsorption was observed by fluorescence microscope using albumin–fluorescein isothiocyanate conjugate protein bovine (FITC-BSA) as a representative salivary protein in artificial saliva environment (**Figure 3.16A-F**). The HAp microparticles with and without the polymer immobilization were soaked in FITC-BSA and were then rinsed with water before scrutinizing green fluorescence due to FITC-BSA. The HAp with the polymer immobilization presents super low fluorescent signal in comparison with maximum intensity of the bare HAp, suggesting that PC moieties of the PPE-PC had a strong effect to effectively reduce protein adsorption on HAp surfaces.

The bacterial anti-attachment effects of the polymer-immobilized HAp materials was investigated *via* the adhesion of *Streptococcus mutans* (*S. mutans*). HAp discs were first treated with human saliva, with the oral bacteria removed prior to the experiment by filtration, to allow salivary proteins to attach on the HAp surface, which would subsequently induce adhesion of bacteria on the surface of a tooth. After anaerobic incubation, the number of colonies attached

on the disc was counted (Figure 4A). The immobilization of PMB–PC on HAp led to inefficient inhibition of bacterial adhesion compared with an untreated HAp, probably due to lack of phosphate anions, meaning that PMB–PC could not strongly deposit on the HAp surface. However, because of its strong attachment to the HAp surface as a result of the anionic content, PEB1/9–PC exhibited relatively high bacterial anti-attachment efficacy and the presence of PC moieties also led to the material having antifouling properties that reduce the bacterial adhesion.
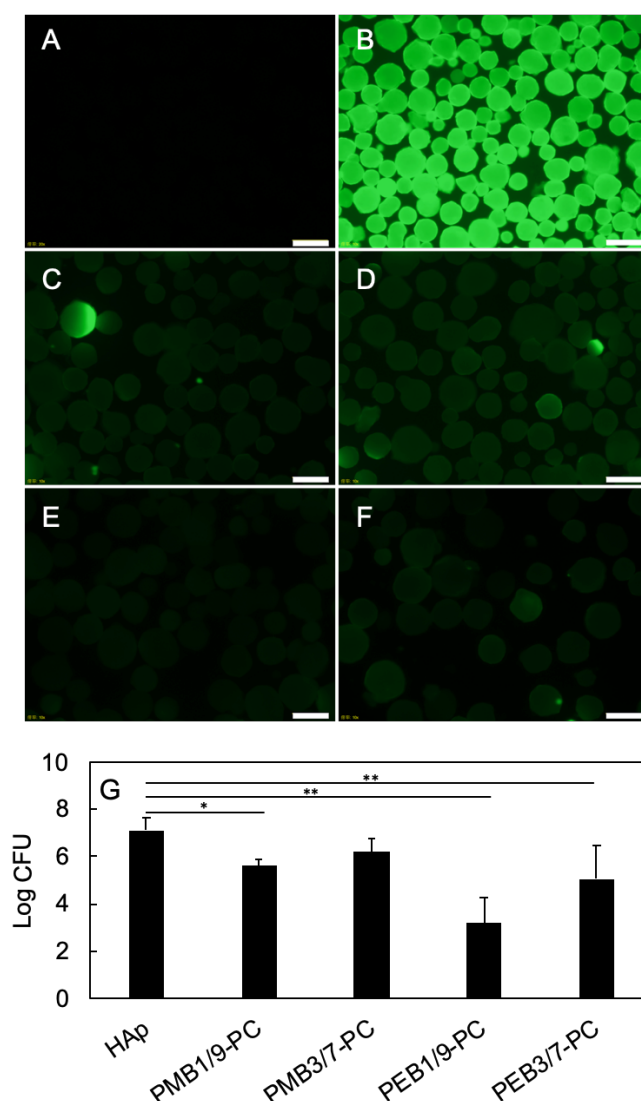
Figure 3.16 Effect of polymer immobilization on HAp against protein and bacterial attachment. Fluorescence images of bare HAp without (A) and with (B) protein immersion, PMB1/9–PC-(C), PMB3/7–PC-(D), PEB1/9–PC-(E), and PEB3/7–PC-(F) immobilized HAp after being immersed in a solution of FITC-BSA in artificial saliva. (scale bar 200 μm). (G) Number of viable *S. mutans* adhered to the immobilized HAp. * $p < 0.05$ and ** $p < 0.01$, *t*-test (n = 4).

3.3.12 Biofilm formation

To observe whether a biofilm can form on the HAp surfaces with the immobilization of the zwitterionic PPEs, the substrates were inoculated with a suspension of *S. mutans* for 48 h in the presence of dietary sucrose. In general, *S. mutans* secrete extracellular polymeric substances (EPSs) into their environment from the sugar in order to provide structural support and protection for the biofilm formation.[72] After the inoculation followed by Live/Dead staining, the biofilms on the specimens were observed by confocal laser scanning microscopy (CLSM). The surface with the immobilized polymer shows relatively denser bacterial adhesion than the bare HAp (**Figure 3.17A, B**). The projections of the individual components, including the dead, live, and merged channels, in the biofilms are depicted in **Figure 3.18**. Both live and dead bacteria were observed for a bare HAp surface and a HAp surface immobilized with PEB1/9–PC. Since the synthesized polymer does not have inherent bactericidal activities to kill bacteria, live bacteria can be observed as green fluorescence for the PEB–PC-immobilized HAp. In contrast, the dead bacteria observed probably died by lack of nutrients in the multilayered biofilm formed by the bacteria.[113] Consequently, the inhibition of the biofilm development by the immobilized PEB–PC also proves that the biofilm is not very thick. It can be seen from **Figure 3.17C** that the thickness of the biofilm on the PEB1/9–PC–immobilized HAp is 4 μm, noticeably thinner than the 23 μm biofilm on the bare HAp surface, suggesting the effective anti-attachment properties brought about by immobilizing a polymer on the HAp surface in terms of reduced bacterial adhesion and inhibition of biofilm formation.

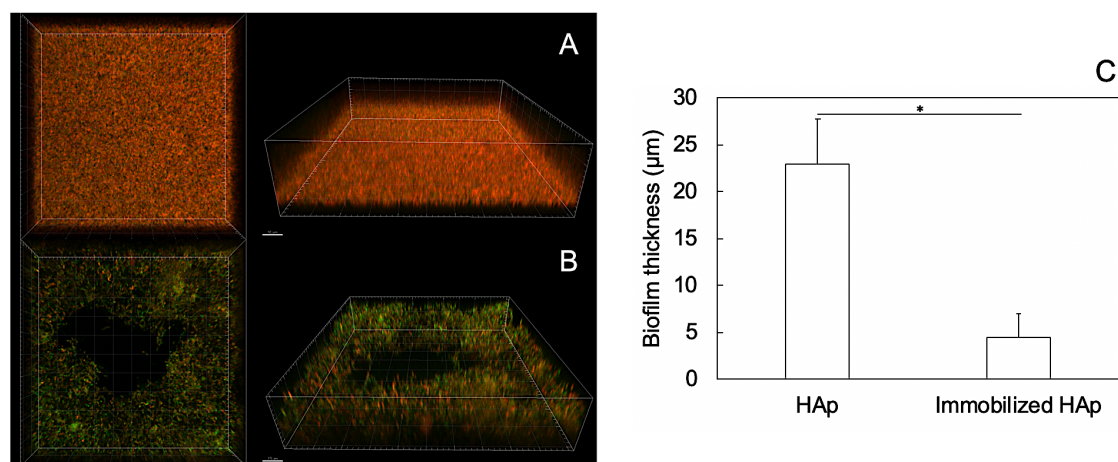**Figure 3.17** The CLSM biofilm structure in top view and side view of *S. Mutans* on HAp (A) and PEB–PC-immobilized HAp (B) (scale bar 10 µm). Biofilm thickness (C) of non-immobilized HAp and PEB–PC-immobilized HAp. * $p < 0.05$, *t*-test, n = 15 of 5 areas × 3 samples.
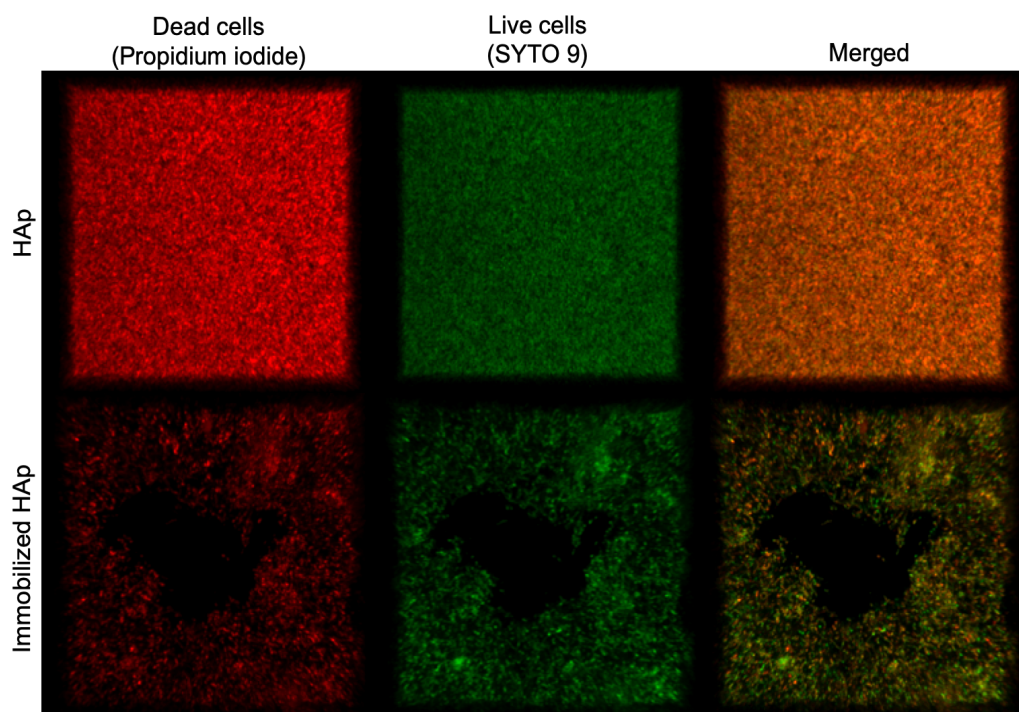

Figure 3.18 3D projections of individual components in biofilms formed by *S. Mutans* on HAp (top) and PEB1/9–PC-immobilized HAp (bottom).

3.4 Conclusions

PPEs with pendant PC moieties were first synthesized *via* thiol-yne click chemistry of thiol-terminated PC with PMB or PEB copolymers. All synthesized PPE-PC were highly biocompatible with mouse fibroblast cells. After the immobilization of the zwitterionic PPE on HAp, the immobilized polymers were stable on the substrates in mimetically salivary condition for 1 week. PEB–PC showed high affinity for HAp surface, leading to the protection of the HAp surface against acid erosion. Furthermore, PEB1/9–PC revealed efficient performance in reducing the bacterial adhesion and biofilm formation on HAp substrate in comparison with triester PMB–PC. It is anticipated that PEB1/9–PC can be applied for dental cares to prevent carries by the binding of the PPE to mineral that found in teeth, exploiting the fouling-resistant activity of its PC motifs. Additionally, there is the potentiality that the remaining alkyne domains can be further functionalized with azide- or thiol-bearing molecules, such as antimicrobial peptides (AMPs), to create desired antibacterial materials.

64

CHAPTER IV

CONCLUDING REMARKS

Biodegradable PEP·Na is an anionic polymer inspired by natural nucleic acid possessing excellent biocompatibility and a binding affinity for apatite substrates. Several types of PEP·Na analogs can be conveniently prepared, including homopolymer PEP·Na, amphiphilic PEP·Na with terminated hydrophobic groups for self-assemblies, and a clickable copolymer of PEP·Na and butynyl BYP in accordance with the modifications desired.

Amphiphilic CH-PEP·Na is able to form nanocomplexes with BSA assisted by thermal treatment without aggregation of denatured proteins due to the thermal stabilization capacity of the polymer. The BSA–CH-PEP·Na complex exhibited complex size stability in long-term storage. The polymer could also behave as a protective barrier for the complex proteins, shielding them from proteolytic enzymes. Despite the addition of free albumin in the environment, the BSA–CH-PEP·Na complex possessed an affinity to the mineral surface.

In another study, PC groups were successfully introduced to alkyne-pendant PEB as novel zwitterionic PEB–PC through thiol-yne click chemistry with great cytocompatibility against fibroblast cells. The remaining BYP of PEB–PC could be easily further tailored *via* azide–alkyne click reaction with an azide-fluorescent probe. After immobilization of PEB–PC onto the HAp surface, the polymer ionically adsorbed onto the HAp, as evidenced by XPS, water contact angle, and fluorescence microscopy. A decrease in the mineral release from HAp caused by acid diffusion toward the HAp surface was observed, and the PEB–PC immobilization efficiently minimized bacterial adhesion and biofilm formation on HAp.

Interestingly, PEP·Na moieties still exhibited binding ability toward the HAp surface whether the polymer assembled with proteins as spherical particles or whether it was functionalized with antifouling PC motifs and a fluorescent probe. This proved the advantages of PEP·Na derivatives that can be useful as an intermediate for the complexation of proteins and can fabricate into several types of materials but still have a strong mineral affinity.

Motivated by the capacity of amphiphilic PEP·Na as a protein carrier and the anti-adhesion properties of PEB–PC, pH-responsive antimicrobial peptide (AMP)-encapsulated PEB–PC nanoparticles are being designed for tooth coating; these will show calcium affinity due to EP·Na and the synergistic partnership of AMP and PC groups for improved bactericidal and anti-adhesive activities, respectively. However, the detail of potential clinical applications and possible industrial developments need to be further investigated.

REFERENCES

(1)   Friedman, A. D.; Claypool, S. E.; Liu, R. The Smart Targeting of Nanoparticles. *Curr. Pharm. Des.* **2013**, *19* (35), 6315–6329. https://doi.org/10.2174/13816128113199990375.

(2)   Kang, M.; Kim, S.; Kim, H.; Song, Y.; Jung, D.; Kang, S.; Seo, J. H.; Nam, S.; Lee, Y. Calcium-Binding Polymer-Coated Poly(Lactide-Co-Glycolide) Microparticles for Sustained Release of Quorum Sensing Inhibitors to Prevent Biofilm Formation on Hydroxyapatite Surfaces. *ACS Applied Materials and Interfaces*. 2019, pp 7686–7694. https://doi.org/10.1021/acsami.8b18301.

(3)   Cui, X.; Koujima, Y.; Seto, H.; Murakami, T.; Hoshino, Y.; Miura, Y. Inhibition of Bacterial Adhesion on Hydroxyapatite Model Teeth by Surface Modification with PEGMA-Phosmer Copolymers. *ACS Biomater. Sci. Eng.* **2016**, *2* (2), 205–212. https://doi.org/10.1021/acsbiomaterials.5b00349.

(4)   Steinbach, T.; Wurm, F. R. Poly(Phosphoester)s: A New Platform for Degradable Polymers. *Angew. Chemie - Int. Ed.* **2015**, *54* (21), 6098–6108. https://doi.org/10.1002/anie.201500147.

(5)   Bauer, K. N.; Tee, H. T.; Velencoso, M. M.; Wurm, F. R. Main-Chain Poly(Phosphoester)s: History, Syntheses, Degradation, Bio-and Flame-Retardant Applications. *Prog. Polym. Sci.* **2017**, *73*, 61–122. https://doi.org/https://doi.org/10.1016/j.progpolymsci.2017.05.004.

(6)   Steinbach, T.; Wurm, F. R. Degradable Polyphosphoester-Protein Conjugates: "PPEylation" of Proteins. *Biomacromolecules* **2016**, *17* (10), 3338–3346. https://doi.org/10.1021/acs.biomac.6b01107.

(7)   Iwasaki, Y.; Yokota, A.; Otaka, A.; Inoue, N.; Yamaguchi, A.; Yoshitomi, T.; Yoshimoto, K.; Neo, M. Bone-Targeting Poly(Ethylene Sodium Phosphate). *Biomater. Sci.* **2018**, *6* (1), 91–95. https://doi.org/10.1039/c7bm00930e.

(8)   Hirano, Y.; Iwasaki, Y. Bone-Specific Poly(Ethylene Sodium Phosphate)-Bearing Biodegradable Nanoparticles. *Colloids Surfaces B Biointerfaces* **2017**, *153*, 104–110. https://doi.org/10.1016/j.colsurfb.2017.02.015.

(9)   Noree, S.; Iwasaki, Y. Thermally Assisted Generation of Protein-Poly(Ethylene Sodium Phosphate) Conjugates with High Mineral Affinity. *ACS Omega* **2019**, *4* (2), 3398–3404. https://doi.org/10.1021/acsomega.8b03585.

(10) Wang, Y.-C.; Yuan, Y.-Y.; Du, J.-Z.; Yang, X.-Z.; Wang, J. Recent Progress in Polyphosphoesters: From Controlled Synthesis to Biomedical Applications. *Macromol. Biosci.* **2009**, *9* (12), 1154–1164. https://doi.org/10.1002/mabi.200900253.

(11) Monge, S.; Canniccioni, B.; Graillot, A.; Robin, J.-J. Phosphorus-Containing Polymers: A Great Opportunity for the Biomedical Field. *Biomacromolecules* **2011**, *12* (6), 1973–1982. https://doi.org/10.1021/bm2004803.

(12) Penczek, S.; Pretula, J.; Kubisa, P.; Kaluzynski, K.; Szymanski, R. Reactions of H3PO4 Forming Polymers. Apparently Simple Reactions Leading to Sophisticated Structures and Applications. *Prog. Polym. Sci.* **2015**, *45*, 44–70. https://doi.org/https://doi.org/10.1016/j.progpolymsci.2015.01.001.

(13) Steinbach, T.; Becker, G.; Spiegel, A.; Figueiredo, T.; Russo, D.; Wurm, F. R. Reversible Bioconjugation: Biodegradable Poly(Phosphate)-Protein Conjugates. *Macromol. Biosci.* **2017**, *17* (10), 1–9. https://doi.org/10.1002/mabi.201600377.

(14) Zhang, S.; Li, A.; Zou, J.; Lin, L. Y.; Wooley, K. L. Facile Synthesis of Clickable, Water-Soluble, and Degradable Polyphosphoesters. *ACS Macro Lett.* **2012**, *1* (2), 328–333. https://doi.org/10.1021/mz200226m.

(15) Otaka, A.; Iwasaki, Y. Endocytosis of Poly(Ethylene Sodium Phosphate) by Macrophages and the Effect of Polymer Length on Cellular Uptake. *J. Ind. Eng. Chem.* **2019**, *75*, 115–122. https://doi.org/10.1016/j.jiec.2019.03.010.

(16) Kootala, S.; Tokunaga, M.; Hilborn, J.; Iwasaki, Y. Anti-Resorptive Functions of Poly(Ethylene Sodium Phosphate) on Human Osteoclasts. *Macromol. Biosci.* **2015**, *15* (12), 1634–1640. https://doi.org/10.1002/mabi.201500166.

(17) Wang, Y.-C.; Yuan, Y.-Y.; Wang, F.; Wang, J. Syntheses and Characterization of Block Copolymers of Poly(Aliphatic Ester) with Clickable Polyphosphoester. *J. Polym. Sci. Part A Polym. Chem.* **2011**, *49* (2), 487–494. https://doi.org/10.1002/pola.24462.

(18) Pranantyo, D.; Xu, L. Q.; Kang, E.-T.; Mya, M. K.; Chan-Park, M. B. Conjugation of Polyphosphoester and Antimicrobial Peptide for Enhanced Bactericidal Activity and Biocompatibility. *Biomacromolecules* **2016**, *17* (12), 4037–4044. https://doi.org/10.1021/acs.biomac.6b01452.

(19) Iwasaki, Y.; Akiyoshi, K. Design of Biodegradable Amphiphilic Polymers: Well-Defined Amphiphilic Polyphosphates with Hydrophilic Graft Chains via ATRP. *Macromolecules* **2004**, *37* (20), 7637–7642. https://doi.org/10.1021/ma049043g.

(20) Iwasaki, Y.; Akiyoshi, K. Synthesis and Characterization of Amphiphilic

Polyphosphates with Hydrophilic Graft Chains and Cholesteryl Groups as Nanocarriers. *Biomacromolecules* **2006**, *7* (5), 1433–1438. https://doi.org/10.1021/bm050917w.

(21)   Iwasaki, Y.; Wachiralarpphaithoon, C.; Akiyoshi, K. Novel Thermoresponsive Polymers Having Biodegradable Phosphoester Backbones. *Macromolecules* **2007**, *40* (23), 8136–8138. https://doi.org/10.1021/ma0715573.

(22)   Hiranphinyophat, S.; Asaumi, Y.; Fujii, S.; Iwasaki, Y. Surface Grafting Polyphosphoesters on Cellulose Nanocrystals To Improve the Emulsification Efficacy. *Langmuir* **2019**, *35* (35), 11443–11451. https://doi.org/10.1021/acs.langmuir.9b01584.

(23)   Lim, Y. H.; Heo, G. S.; Rezenom, Y. H.; Pollack, S.; Raymond, J. E.; Elsabahy, M.; Wooley, K. L. Development of a Vinyl Ether-Functionalized Polyphosphoester as a Template for Multiple Postpolymerization Conjugation Chemistries and Study of Core Degradable Polymeric Nanoparticles. *Macromolecules* **2014**, *47* (14), 4634–4644. https://doi.org/10.1021/ma402480a.

(24)   Liu, J.; Huang, W.; Zhou, Y.; Yan, D. Synthesis of Hyperbranched Polyphosphates by Self-Condensing Ring-Opening Polymerization of HEEP without Catalyst. *Macromolecules* **2009**, *42* (13), 4394–4399. https://doi.org/10.1021/ma900798h.

(25)   Liu, J.; Huang, W.; Pang, Y.; Zhu, X.; Zhou, Y.; Yan, D. Hyperbranched Polyphosphates for Drug Delivery Application: Design, Synthesis, and In Vitro Evaluation. *Biomacromolecules* **2010**, *11* (6), 1564–1570. https://doi.org/10.1021/bm100188h.

(26)   Song, W.-J.; Du, J.-Z.; Liu, N.-J.; Dou, S.; Cheng, J.; Wang, J. Functionalized Diblock Copolymer of Poly(ε-Caprolactone) and Polyphosphoester Bearing Hydroxyl Pendant Groups: Synthesis, Characterization, and Self-Assembly. *Macromolecules* **2008**, *41* (19), 6935–6941. https://doi.org/10.1021/ma801043m.

(27)   Feng, X. Chemical and Biochemical Basis of Cell-Bone Matrix Interaction in Health and Disease. *Curr. Chem. Biol.* **2009**, *3* (2), 189–196. https://doi.org/10.2174/187231309788166398.

(28)   Müller, W. E. G.; Ackermann, M.; Neufurth, M.; Tolba, E.; Wang, S.; Feng, Q.; Schröder, H. C.; Wang, X. A Novel Biomimetic Approach to Repair Enamel Cracks/Carious Damages and to Reseal Dentinal Tubules by Amorphous Polyphosphate. *Polymers (Basel).* **2017**, *9* (4), 120. https://doi.org/10.3390/polym9040120.

(29)   Cui, X.; Murakami, T.; Hoshino, Y.; Miura, Y. Anti-Biofouling Phosphorylated HEMA and PEGMA Block Copolymers Show High Affinity to Hydroxyapatite. *Colloids Surfaces B Biointerfaces* **2017**, *160*, 289–296.

https://doi.org/10.1016/j.colsurfb.2017.09.038.

(30) Ishikawa, K.; Miyamoto, Y.; Tsuchiya, A.; Hayashi, K.; Tsuru, K.; Ohe, G. Physical and Histological Comparison of Hydroxyapatite, Carbonate Apatite, and β-Tricalcium Phosphate Bone Substitutes. *Materials (Basel).* **2018**, *11* (10), 1–12. https://doi.org/10.3390/ma11101993.

(31) Dorozhkin, S. V. Dissolution Mechanism of Calcium Apatites in Acids: A Review of Literature. *World J. Methodol.* **2012**, *2* (1), 1. https://doi.org/10.5662/wjm.v2.i1.1.

(32) Zétola, A.; Ferreira, F. M.; Larson, R.; Shibli, J. A. Recombinant Human Bone Morphogenetic Protein-2 (RhBMP-2) in the Treatment of Mandibular Sequelae after Tumor Resection. *Oral Maxillofac. Surg.* **2011**, *15* (3), 169—174. https://doi.org/10.1007/s10006-010-0236-7.

(33) Yamamoto, M.; Takahashi, Y.; Tabata, Y. Enhanced Bone Regeneration at a Segmental Bone Defect by Controlled Release of Bone Morphogenetic Protein-2 from a Biodegradable Hydrogel. *Tissue Eng.* **2006**, *12* (5), 1305–1311. https://doi.org/10.1089/ten.2006.12.1305.

(34) Tong, Z.; Guo, J.; Glen, R. C.; Morrell, N. W.; Li, W. A Bone Morphogenetic Protein (BMP)-Derived Peptide Based on the Type I Receptor-Binding Site Modifies Cell-Type Dependent BMP Signalling. *Sci. Rep.* **2019**, *9* (1), 13446. https://doi.org/10.1038/s41598-019-49758-x.

(35) Poon, B.; Kha, T.; Tran, S.; Dass, C. R. Bone Morphogenetic Protein-2 and Bone Therapy: Successes and Pitfalls. *J. Pharm. Pharmacol.* **2016**, *68* (2), 139–147. https://doi.org/10.1111/jphp.12506.

(36) Kelly, M. P.; Vaughn, O. L. A.; Anderson, P. A. Systematic Review and Meta-Analysis of Recombinant Human Bone Morphogenetic Protein-2 in Localized Alveolar Ridge and Maxillary Sinus Augmentation. *J. Oral Maxillofac. Surg.* **2016**, *74* (5), 928–939. https://doi.org/https://doi.org/10.1016/j.joms.2015.11.027.

(37) Park, S.-Y.; Kim, K.-H.; Kim, S.; Lee, Y.-M.; Seol, Y.-J. BMP-2 Gene Delivery-Based Bone Regeneration in Dentistry. *Pharmaceutics* **2019**, *11* (8). https://doi.org/10.3390/pharmaceutics11080393.

(38) Ning, H.; Wu, X.; Wu, Q.; Yu, W.; Wang, H.; Zheng, S.; Chen, Y.; Li, Y.; Su, J. Microfiber-Reinforced Composite Hydrogels Loaded with Rat Adipose-Derived Stem Cells and BMP-2 for the Treatment of Medication-Related Osteonecrosis of the Jaw in a Rat Model. *ACS Biomater. Sci. Eng.* **2019**, *5* (5), 2430–2443.

https://doi.org/10.1021/acsbiomaterials.8b01468.

(39) Dogan, S.; Fong, H.; Yucesoy, D. T.; Cousin, T.; Gresswell, C.; Dag, S.; Huang, G.; Sarikaya, M. Biomimetic Tooth Repair: Amelogenin-Derived Peptide Enables in Vitro Remineralization of Human Enamel. *ACS Biomater. Sci. Eng.* **2018**, *4* (5), 1788–1796. https://doi.org/10.1021/acsbiomaterials.7b00959.

(40) Paine, M. L.; White, S. N.; Luo, W.; Fong, H.; Sarikaya, M.; Snead, M. L. Regulated Gene Expression Dictates Enamel Structure and Tooth Function. *Matrix Biol.* **2001**, *20* (5), 273–292. https://doi.org/https://doi.org/10.1016/S0945-053X(01)00153-6.

(41) Mukherjee, K.; Ruan, Q.; Nutt, S.; Tao, J.; De Yoreo, J. J.; Moradian-Oldak, J. Peptide-Based Bioinspired Approach to Regrowing Multilayered Aprismatic Enamel. *ACS Omega* **2018**, *3* (3), 2546–2557. https://doi.org/10.1021/acsomega.7b02004.

(42) Ruan, Q.; Liberman, D.; Bapat, R.; Chandrababu, K. B.; Phark, J.-H.; Moradian-Oldak, J. Efficacy of Amelogenin-Chitosan Hydrogel in Biomimetic Repair of Human Enamel in PH-Cycling Systems. *J. Biomed. Eng. Informatics* **2015**, *2* (1), 119. https://doi.org/10.5430/jbei.v2n1p119.

(43) Sadhukhan, N.; Muraoka, T.; Ui, M.; Nagatoishi, S.; Tsumoto, K.; Kinbara, K. Protein Stabilization by an Amphiphilic Short Monodisperse Oligo(Ethylene Glycol). *Chem. Commun.* **2015**, *51* (40), 8457–8460. https://doi.org/10.1039/C4CC10301G.

(44) Martin, S. R.; Schilstra, M. J. B. T.-M. in C. B. Circular Dichroism and Its Application to the Study of Biomolecules. In *Biophysical Tools for Biologists, Volume One: In Vitro Techniques*; Academic Press, 2008; Vol. 84, pp 263–293. https://doi.org/https://doi.org/10.1016/S0091-679X(07)84010-6.

(45) Zhang, M.; Zhao, J.; Zheng, J. Molecular Understanding of a Potential Functional Link between Antimicrobial and Amyloid Peptides. *Soft Matter* **2014**, *10* (38), 7425–7451. https://doi.org/10.1039/C4SM00907J.

(46) Blackman, L. D.; Varlas, S.; Arno, M. C.; Houston, Z. H.; Fletcher, N. L.; Thurecht, K. J.; Hasan, M.; Gibson, M. I.; O'Reilly, R. K. Confinement of Therapeutic Enzymes in Selectively Permeable Polymer Vesicles by Polymerization-Induced Self-Assembly (PISA) Reduces Antibody Binding and Proteolytic Susceptibility. *ACS Central Science*. 2018, pp 718–723. https://doi.org/10.1021/acscentsci.8b00168.

(47) Alconcel, S. N. S.; Baas, A. S.; Maynard, H. D. FDA-Approved Poly(Ethylene Glycol)–Protein Conjugate Drugs. *Polym. Chem.* **2011**, *2* (7), 1442–1448. https://doi.org/10.1039/C1PY00034A.

(48)   Bendele, A.; Seely, J.; Richey, C.; Sennello, G.; Shopp, G. Short Communication: Renal Tubular Vacuolation in Animals Treated with Polyethylene-Glycol-Conjugated Proteins. *Toxicol. Sci.* **1998**, *42* (2), 152–157. https://doi.org/https://doi.org/10.1006/toxs.1997.2396.

(49)   Pelosi, C.; Duce, C.; Russo, D.; Tiné, M. R.; Wurm, F. R. PPEylation of Proteins: Synthesis, Activity, and Stability of Myoglobin-Polyphosphoester Conjugates. *Eur. Polym. J.* **2018**, *108*, 357–363. https://doi.org/https://doi.org/10.1016/j.eurpolymj.2018.09.019.

(50)   Wu, Y.; Ng, D. Y. W.; Kuan, S. L.; Weil, T. Protein-Polymer Therapeutics: A Macromolecular Perspective. *Biomater. Sci.* **2015**, *3* (2), 214–230. https://doi.org/10.1039/c4bm00270a.

(51)   Akiyoshi, K.; Sasaki, Y.; Sunamoto, J. Molecular Chaperone-Like Activity of Hydrogel Nanoparticles of Hydrophobized Pullulan: Thermal Stabilization with Refolding of Carbonic Anhydrase B. *Bioconjug. Chem.* **1999**, *10* (3), 321–324. https://doi.org/10.1021/bc9801272.

(52)   Moradian-Oldak, J. Protein-Mediated Enamel Mineralization. *Front. Biosci. (Landmark Ed.* **2012**, *17*, 1996–2023. https://doi.org/10.2741/4034.

(53)   Lowe, A. B. Thiol–Ene "Click" Reactions and Recent Applications in Polymer and Materials Synthesis: A First Update. *Polym. Chem.* **2014**, *5* (17), 4820–4870. https://doi.org/10.1039/C4PY00339J.

(54)   Hoyle, C. E.; Bowman, C. N. Thiol–Ene Click Chemistry. *Angew. Chemie Int. Ed.* **2010**, *49* (9), 1540–1573. https://doi.org/10.1002/anie.200903924.

(55)   Jewett, J. C.; Bertozzi, C. R. Cu-Free Click Cycloaddition Reactions in Chemical Biology. *Chem. Soc. Rev.* **2010**, *39* (4), 1272–1279. https://doi.org/10.1039/B901970G.

(56)   Sletten, E. M.; Bertozzi, C. R. Bioorthogonal Chemistry: Fishing for Selectivity in a Sea of Functionality. *Angew. Chemie Int. Ed.* **2009**, *48* (38), 6974–6998. https://doi.org/10.1002/anie.200900942.

(57)   Li, R.; Elsabahy, M.; Song, Y.; Wang, H.; Su, L.; Letteri, R. A.; Khan, S.; Heo, G. S.; Sun, G.; Liu, Y.; et al. Functional, Degradable Zwitterionic Polyphosphoesters as Biocompatible Coating Materials for Metal Nanostructures. *Langmuir* **2019**, *35* (5), 1503–1512. https://doi.org/10.1021/acs.langmuir.8b02033.

(58)   Zhang, S.; Zou, J.; Zhang, F.; Elsabahy, M.; Felder, S. E.; Zhu, J.; Pochan, D. J.; Wooley, K. L. Rapid and Versatile Construction of Diverse and Functional Nanostructures

Derived from a Polyphosphoester-Based Biomimetic Block Copolymer System. *J. Am. Chem. Soc.* **2012**, *134* (44), 18467–18474. https://doi.org/10.1021/ja309037m.

(59)   Ishihara, K.; Ueda, T.; Nakabayashi, N. Preparation of Phospholipid Polylners and Their Properties as Polymer Hydrogel Membranes. *Polym. J.* **1990**, *22* (5), 355–360. https://doi.org/10.1295/polymj.22.355.

(60)   Ishihara, K.; Ziats, N. P.; Tierney, B. P.; Nakabayashi, N.; Anderson, J. M. Protein Adsorption from Human Plasma Is Reduced on Phospholipid Polymers. *J. Biomed. Mater. Res.* **1991**, *25* (11), 1397–1407. https://doi.org/10.1002/jbm.820251107.

(61)   Ishihara, K.; Fukumoto, K.; Iwasaki, Y.; Nakabayashi, N. Modification of Polysulfone with Phospholipid Polymer for Improvement of the Blood Compatibility. Part 2. Protein Adsorption and Platelet Adhesion. *Biomaterials* **1999**, *20* (17), 1553–1559. https://doi.org/https://doi.org/10.1016/S0142-9612(98)00206-3.

(62)   Iwasaki, Y.; Ishihara, K. Cell Membrane-Inspired Phospholipid Polymers for Developing Medical Devices with Excellent Biointerfaces. *Sci. Technol. Adv. Mater.* **2012**, *13* (6), 64101. https://doi.org/10.1088/1468-6996/13/6/064101.

(63)   Ishihara, K. Blood-Compatible Surfaces with Phosphorylcholine-Based Polymers for Cardiovascular Medical Devices. *Langmuir* **2019**, *35* (5), 1778–1787. https://doi.org/10.1021/acs.langmuir.8b01565.

(64)   Ishihara, K. Revolutionary Advances in 2-Methacryloyloxyethyl Phosphorylcholine Polymers as Biomaterials. *J. Biomed. Mater. Res. Part A* **2019**, *107* (5), 933–943. https://doi.org/10.1002/jbm.a.36635.

(65)   Goda, T.; Kjall, P.; Ishihara, K.; Richter-Dahlfors, A.; Miyahara, Y. Biomimetic Interfaces Reveal Activation Dynamics of C-Reactive Protein in Local Microenvironments. *Adv. Healthc. Mater.* **2014**, *3* (11), 1733–1738. https://doi.org/10.1002/adhm.201300625.

(66)   Iwasaki, S.; Kawasaki, H.; Iwasaki, Y. Label-Free Specific Detection and Collection of C-Reactive Protein Using Zwitterionic Phosphorylcholine-Polymer-Protected Magnetic Nanoparticles. *Langmuir* **2019**, *35* (5), 1749–1755. https://doi.org/10.1021/acs.langmuir.8b01007.

(67)   Kang, S.; Lee, M.; Kang, M.; Noh, M.; Jeon, J.; Lee, Y.; Seo, J. H. Development of Anti-Biofouling Interface on Hydroxyapatite Surface by Coating Zwitterionic MPC Polymer Containing Calcium-Binding Moieties to Prevent Oral Bacterial Adhesion. *Acta Biomater.* **2016**, *40*, 70–77. https://doi.org/10.1016/j.actbio.2016.03.006.

(68) Ishihara, K. Bioinspired Polymeric Materials: Progress from Molecular Science to Medical Devices. In *Frontiers in Bioengineering and Biotechnology*. https://doi.org/10.3389/conf.FBIOE.2016.01.00252.

(69) Goda, T.; Tabata, M.; Sanjoh, M.; Uchimura, M.; Iwasaki, Y.; Miyahara, Y. Thiolated 2-Methacryloyloxyethyl Phosphorylcholine for an Antifouling Biosensor Platform. *Chem. Commun.* **2013**, *49* (77), 8683–8685. https://doi.org/10.1039/c3cc44357d.

(70) Sangsuwan, A.; Kawasaki, H.; Matsumura, Y.; Iwasaki, Y. Antimicrobial Silver Nanoclusters Bearing Biocompatible Phosphorylcholine-Based Zwitterionic Protection. *Bioconjug. Chem.* **2016**, *27* (10), 2527–2533. https://doi.org/10.1021/acs.bioconjchem.6b00455.

(71) E.A., T. Biofilms and Their Role in Infection Pathogenesis. *Postep. Mikrobiol.* **2008**, *47* (3), 353–357. https://doi.org/10.15406/jmen.2014.01.00014.The.

(72) Benoit, D. S. W.; Sims, K. R.; Fraser, D. Nanoparticles for Oral Biofilm Treatments. *ACS Nano* **2019**, *13* (5), 4869–4875. https://doi.org/10.1021/acsnano.9b02816.

(73) Helfman, M. Chemical Aspects of Dentistry. *J. Chem. Educ.* **1982**, *59* (6), 666–668. https://doi.org/10.1021/ed059p666.

(74) Varol, E.; Varol, S. Does Fluoride Toxicity Cause Hypertension in Patients with Endemic Fluorosis? *Biol. Trace Elem. Res.* **2012**, *150* (1–3), 1–2. https://doi.org/10.1007/s12011-012-9499-1.

(75) Bartlett, J. D.; Dwyer, S. E.; Beniash, E.; Skobe, Z.; Payne-Ferreira, T. L. Fluorosis: A New Model and New Insights. *J. Dent. Res.* **2005**, *84* (9), 832–836. https://doi.org/10.1177/154405910508400910.

(76) Lei, Y.; Wang, T.; Mitchell, J. W.; Zaidel, L.; Qiu, J.; Kilpatrick-Liverman, L. Bioinspired Amphiphilic Phosphate Block Copolymers as Non-Fluoride Materials to Prevent Dental Erosion. *RSC Adv.* **2014**, *4* (90), 49053–49060. https://doi.org/10.1039/C4RA08377F.

(77) Riehemann, K.; Schneider, S. W.; Luger, T. A.; Godin, B.; Ferrari, M.; Fuchs, H. Nanomedicine—Challenge and Perspectives. *Angew. Chemie Int. Ed.* **2009**, *48* (5), 872–897. https://doi.org/10.1002/anie.200802585.

(78) Ma, X.; Zhao, Y.; Liang, X.-J. Theranostic Nanoparticles Engineered for Clinic and Pharmaceutics. *Acc. Chem. Res.* **2011**, *44* (10), 1114–1122. https://doi.org/10.1021/ar2000056.

(79) Singh, R.; Lillard, J. W. Nanoparticle-Based Targeted Drug Delivery. *Exp. Mol. Pathol.*

2009, *86* (3), 215–223. https://doi.org/https://doi.org/10.1016/j.yexmp.2008.12.004.

(80) Torchilin, V. P. Multifunctional Nanocarriers. *Adv. Drug Deliv. Rev.* **2006**, *58* (14), 1532–1555. https://doi.org/https://doi.org/10.1016/j.addr.2006.09.009.

(81) Yan, Y.; Such, G. K.; Johnston, A. P. R.; Best, J. P.; Caruso, F. Engineering Particles for Therapeutic Delivery: Prospects and Challenges. *ACS Nano* **2012**, *6* (5), 3663–3669. https://doi.org/10.1021/nn3016162.

(82) Pisal, D. S.; Kosloski, M. P.; Balu-Iyer, S. V. Delivery of Therapeutic Proteins. *J. Pharm. Sci.* **2010**, *99* (6), 2557–2575. https://doi.org/https://doi.org/10.1002/jps.22054.

(83) Torchilin, V. P.; Lukyanov, A. N. Peptide and Protein Drug Delivery to and into Tumors: Challenges and Solutions. *Drug Discov. Today* **2003**, *8* (6), 259–266. https://doi.org/https://doi.org/10.1016/S1359-6446(03)02623-0.

(84) Chen, J.; Zhao, M.; Feng, F.; Sizovs, A.; Wang, J. Tunable Thioesters as "Reduction" Responsive Functionality for Traceless Reversible Protein PEGylation. *J. Am. Chem. Soc.* **2013**, *135* (30), 10938–10941. https://doi.org/10.1021/ja405261u.

(85) Duncan, R.; Spreafico, F. Polymer Conjugates: Pharmacokinetic Considerations for Design and Development. *Clin. Pharmacokinet.* **1994**, *27* (4), 290–306. https://doi.org/10.2165/00003088-199427040-00004.

(86) Pei, P.; Sun, C.; Tao, W.; Li, J.; Yang, X.; Wang, J. ROS-Sensitive Thioketal-Linked Polyphosphoester-Doxorubicin Conjugate for Precise Phototriggered Locoregional Chemotherapy. *Biomaterials* **2019**, *188*, 74–82. https://doi.org/https://doi.org/10.1016/j.biomaterials.2018.10.010.

(87) Simon, J.; Wolf, T.; Klein, K.; Landfester, K.; Wurm, F. R.; Mailänder, V. Hydrophilicity Regulates the Stealth Properties of Polyphosphoester-Coated Nanocarriers. *Angew. Chemie Int. Ed.* **2018**, *57* (19), 5548–5553. https://doi.org/10.1002/anie.201800272.

(88) Libiszowski, J.; Kałużynski, K.; Penczek, S. Polymerization of Cyclic Esters of Phosphoric Acid. VI. Poly(Alkyl Ethylene Phosphates). Polymerization of 2-Alkoxy-2-Oxo-1,3,2-Dioxaphospholans and Structure of Polymers. *J. Polym. Sci. Polym. Chem. Ed.* **1978**, *16* (6), 1275–1283. https://doi.org/10.1002/pol.1978.170160610.

(89) Ikeuchi, R.; Iwasaki, Y. High Mineral Affinity of Polyphosphoester Ionomer–Phospholipid Vesicles. *J. Biomed. Mater. Res. Part A* **2013**, *101A* (2), 318–325. https://doi.org/10.1002/jbm.a.34321.

(90) Zhang, S.; Wang, H.; Shen, Y.; Zhang, F.; Seetho, K.; Zou, J.; Taylor, J.-S. A.; Dove,

A. P.; Wooley, K. L. A Simple and Efficient Synthesis of an Acid-Labile Polyphosphoramidate by Organobase-Catalyzed Ring-Opening Polymerization and Transformation to Polyphosphoester Ionomers by Acid Treatment. *Macromolecules* **2013**, *46* (13), 5141–5149. https://doi.org/10.1021/ma400675m.

(91) Topel, Ö.; Çakır, B. A.; Budama, L.; Hoda, N. Determination of Critical Micelle Concentration of Polybutadiene-Block-Poly(Ethyleneoxide) Diblock Copolymer by Fluorescence Spectroscopy and Dynamic Light Scattering. *J. Mol. Liq.* **2013**, *177*, 40–43. https://doi.org/https://doi.org/10.1016/j.molliq.2012.10.013.

(92) McRae Page, S.; Martorella, M.; Parelkar, S.; Kosif, I.; Emrick, T. Disulfide Cross-Linked Phosphorylcholine Micelles for Triggered Release of Camptothecin. *Mol. Pharm.* **2013**, *10* (7), 2684–2692. https://doi.org/10.1021/mp400114n.

(93) Dutta, K.; Hu, D.; Zhao, B.; Ribbe, A. E.; Zhuang, J.; Thayumanavan, S. Templated Self-Assembly of a Covalent Polymer Network for Intracellular Protein Delivery and Traceless Release. *J. Am. Chem. Soc.* **2017**, *139* (16), 5676–5679. https://doi.org/10.1021/jacs.7b01214.

(94) Moroi, Y.; Nishikido, N.; Saito, M.; Matuura, R. The Critical Micelle Concentration of Ionic-Nonionic Detergent Mixtures in Aqueous Solutions. III. *J. Colloid Interface Sci.* **1975**, *52* (2), 356–363. https://doi.org/https://doi.org/10.1016/0021-9797(75)90210-6.

(95) Silva, L. H. M. da; Coimbra, J. S. R.; Meirelles, A. J. de A. Equilibrium Phase Behavior of Poly(Ethylene Glycol) + Potassium Phosphate + Water Two-Phase Systems at Various PH and Temperatures. *J. Chem. Eng. Data* **1997**, *42* (2), 398–401. https://doi.org/10.1021/je9602677.

(96) Chua, G. B. H.; Roth, P. J.; Duong, H. T. T.; Davis, T. P.; Lowe, A. B. Synthesis and Thermoresponsive Solution Properties of Poly[Oligo(Ethylene Glycol) (Meth)Acrylamide]s: Biocompatible PEG Analogues. *Macromolecules* **2012**, *45* (3), 1362–1374. https://doi.org/10.1021/ma202700y.

(97) Borzova, V. A.; Markossian, K. A.; Chebotareva, N. A.; Kleymenov, S. Y.; Poliansky, N. B.; Muranov, K. O.; Stein-Margolina, V. A.; Shubin, V. V; Markov, D. I.; Kurganov, B. I. Kinetics of Thermal Denaturation and Aggregation of Bovine Serum Albumin. *PLoS One* **2016**, *11* (4), 1–29. https://doi.org/10.1371/journal.pone.0153495.

(98) Rajan, R.; Matsumura, K. A Zwitterionic Polymer as a Novel Inhibitor of Protein Aggregation. *J. Mater. Chem. B* **2015**, *3* (28), 5683–5689. https://doi.org/10.1039/C5TB01021G.

(99) Jaskolla, T. W.; Lehmann, W. D.; Karas, M. 4-Chloro-α-Cyanocinnamic Acid Is an Advanced, Rationally Designed MALDI Matrix. *Proc. Natl. Acad. Sci. U. S. A.* **2008**, *105* (34), 12200–12205. https://doi.org/10.1073/pnas.0803056105.

(100) Nishimura, T.; Sasaki, Y.; Akiyoshi, K. Cancer Therapy: Biotransporting Self-Assembled Nanofactories Using Polymer Vesicles with Molecular Permeability for Enzyme Prodrug Cancer Therapy (Adv. Mater. 36/2017). *Adv. Mater.* **2017**, *29* (36). https://doi.org/10.1002/adma.201770258.

(101) Low, S. A.; Kopeček, J. Targeting Polymer Therapeutics to Bone. *Adv. Drug Deliv. Rev.* **2012**, *64* (12), 1189–1204. https://doi.org/10.1016/j.addr.2012.01.012.

(102) Iwasaki, Y.; Katayama, K.; Yoshida, M.; Yamamoto, M.; Tabata, Y. Comparative Physicochemical Properties and Cytotoxicity of Polyphosphoester Ionomers with Bisphosphonates. *J. Biomater. Sci. Polym. Ed.* **2013**, *24* (7), 882–895. https://doi.org/10.1080/09205063.2012.710823.

(103) Jang, Y.; Lee, S.-T.; Kim, T.-J.; Jun, J.-S.; Moon, J.; Jung, K.-H.; Park, K.-I.; Chu, K.; Lee, S. K. High Albumin Level Is a Predictor of Favorable Response to Immunotherapy in Autoimmune Encephalitis. *Sci. Rep.* **2018**, *8* (1), 1012. https://doi.org/10.1038/s41598-018-19490-z.

(104) Wang, Y.; Newman, M. R.; Benoit, D. S. W. Development of Controlled Drug Delivery Systems for Bone Fracture-Targeted Therapeutic Delivery: A Review. *Eur. J. Pharm. Biopharm.* **2018**, *127*, 223–236. https://doi.org/https://doi.org/10.1016/j.ejpb.2018.02.023.

(105) Nakashima, M.; Reddi, A. H. The Application of Bone Morphogenetic Proteins to Dental Tissue Engineering. *Nat. Biotechnol.* **2003**, *21* (9), 1025–1032. https://doi.org/10.1038/nbt864.

(106) Huq, N. L.; Cross, K. J.; Ung, M.; Myroforidis, H.; Veith, P. D.; Chen, D.; Stanton, D.; He, H.; Ward, B. R.; Reynolds, E. C. A Review of the Salivary Proteome and Peptidome and Saliva-Derived Peptide Therapeutics. *Int. J. Pept. Res. Ther.* **2007**, *13* (4), 547–564. https://doi.org/10.1007/s10989-007-9109-9.

(107) Featherstone, J. D. B. Dental Caries: A Dynamic Disease Process. *Aust. Dent. J.* **2008**, *53* (3), 286–291. https://doi.org/10.1111/j.1834-7819.2008.00064.x.

(108) Guo, L.; Hu, W.; He, X.; Lux, R.; McLean, J.; Shi, W. Investigating Acid Production by Streptococcus Mutans with a Surface-Displayed PH-Sensitive Green Fluorescent Protein. *PLoS One* **2013**, *8* (2), 1–10. https://doi.org/10.1371/journal.pone.0057182.

(109) Park, K. D.; Kim, Y. S.; Han, D. K.; Kim, Y. H.; Lee, E. H. B.; Suh, H.; Choi, K. S. Bacterial Adhesion on PEG Modified Polyurethane Surfaces. *Biomaterials* **1998**, *19* (7), 851–859. https://doi.org/https://doi.org/10.1016/S0142-9612(97)00245-7.

(110) Cui, X.; Murakami, T.; Tamura, Y.; Aoki, K.; Hoshino, Y.; Miura, Y. Bacterial Inhibition and Osteoblast Adhesion on Ti Alloy Surfaces Modified by Poly(PEGMA-r-Phosmer) Coating. *ACS Appl. Mater. Interfaces* **2018**, *10* (28), 23674–23681. https://doi.org/10.1021/acsami.8b07757.

(111) Chou, Y.-N.; Venault, A.; Cho, C.-H.; Sin, M.-C.; Yeh, L.-C.; Jhong, J.-F.; Chinnathambi, A.; Chang, Y.; Chang, Y. Epoxylated Zwitterionic Triblock Copolymers Grafted onto Metallic Surfaces for General Biofouling Mitigation. *Langmuir* **2017**, *33* (38), 9822–9835. https://doi.org/10.1021/acs.langmuir.7b02164.

(112) Venault, A.; Yang, H.-S.; Chiang, Y.-C.; Lee, B.-S.; Ruaan, R.-C.; Chang, Y. Bacterial Resistance Control on Mineral Surfaces of Hydroxyapatite and Human Teeth via Surface Charge-Driven Antifouling Coatings. *ACS Appl. Mater. Interfaces* **2014**, *6* (5), 3201–3210. https://doi.org/10.1021/am404780w.

(113) Sae-ung, P.; Wijitamornloet, A.; Iwasaki, Y.; Thanyasrisung, P.; Hoven, V. P. Clickable Zwitterionic Copolymer as a Universal Biofilm-Resistant Coating. *Macromol. Mater. Eng.* **2019**, *304* (9), 1970022. https://doi.org/10.1002/mame.201970022.

(114) Tanaka, M.; Iwasaki, Y. Corrigendum to "Photo-Assisted Generation of Phospholipid Polymer Substrates for Regiospecific Protein Conjugation and Control of Cell Adhesion" [Acta Biomater. 40 (2016) 54–61]. *Acta Biomater.* **2018**, *77*, 394. https://doi.org/https://doi.org/10.1016/j.actbio.2018.07.043.

(115) Chang, C.-C.; Kolewe, K. W.; Li, Y.; Kosif, I.; Freeman, B. D.; Carter, K. R.; Schiffman, J. D.; Emrick, T. Underwater Superoleophobic Surfaces Prepared from Polymer Zwitterion/Dopamine Composite Coatings. *Adv. Mater. Interfaces* **2016**, *3* (6), 1500521. https://doi.org/10.1002/admi.201500521.

(116) Tateishi, T.; Kyomoto, M.; Kakinoki, S.; Yamaoka, T.; Ishihara, K. Reduced Platelets and Bacteria Adhesion on Poly(Ether Ether Ketone) by Photoinduced and Self-Initiated Graft Polymerization of 2-Methacryloyloxyethyl Phosphorylcholine. *J. Biomed. Mater. Res. A* **2014**, *102* (5), 1342—1349. https://doi.org/10.1002/jbm.a.34809.

(117) Zhang, N.; Melo, M. A. S.; Bai, Y.; Xu, H. H. K. Novel Protein-Repellent Dental Adhesive Containing 2-Methacryloyloxyethyl Phosphorylcholine. *J. Dent.* **2014**, *42* (10), 1284—1291. https://doi.org/10.1016/j.jdent.2014.07.016.

(118) Sangsuwan, A.; Kawasaki, H.; Iwasaki, Y. Thiolated-2-Methacryloyloxyethyl Phosphorylcholine Protected Silver Nanoparticles as Novel Photo-Induced Cell-Killing Agents. *Colloids Surfaces B Biointerfaces* **2016**, *140*, 128–134. https://doi.org/https://doi.org/10.1016/j.colsurfb.2015.12.037.

(119) Rostovtsev, V. V; Green, L. G.; Fokin, V. V; Sharpless, K. B. A Stepwise Huisgen Cycloaddition Process: Copper(I)-Catalyzed Regioselective "Ligation" of Azides and Terminal Alkynes. *Angew. Chemie Int. Ed.* **2002**, *41* (14), 2596–2599. https://doi.org/10.1002/1521-3773(20020715)41:14<2596::AID-ANIE2596>3.0.CO;2-4.

(120) Kaur, S.; Zhao, G.; Busch, E.; Wang, T. Metal-Free Photocatalytic Thiol–Ene/Thiol–Yne Reactions. *Org. Biomol. Chem.* **2019**, *17* (7), 1955–1961. https://doi.org/10.1039/C8OB02313A.

(121) Surmont, P. A.; Martens, L. C. Root Surface Caries: An Update. *Clin. Prev. Dent.* **1989**, *11* (3), 14—20.

(122) Liu, G.; Li, Y.; Yang, L.; Wei, Y.; Wang, X.; Wang, Z.; Tao, L. Cytotoxicity Study of Polyethylene Glycol Derivatives. *RSC Adv.* **2017**, *7* (30), 18252–18259. https://doi.org/10.1039/C7RA00861A.

VITA

Miss Susita Noree was born on November 17th, 1991 in Thailand. She graduated with a Bachelor's degree of Science, majoring in Chemistry, Faculty of Science, Chulalongkorn University in 2012. In the same year, she started as a Master Degree student with a major in Chemistry, Faculty of Science, Chulalongkorn University and graduated in the academic year of 2016. She began her PhD study in Program of Graduate School of Science and Engineering, Department of Chemistry and Materials, Faculty of Chemistry, Materials and Bioengineering, Kansai University in academic year of 2017 and graduated in the academic year of 2019.

Grants and Fellowships

2018-2020	Otsuka Toshimi Scholarship Foundation in Japan
2017-2020	Research Assistant Fellowship in Science and Engineering, Kansai University
2017-2018	Japan Student Services Organization (JASSO) Scholarship
2015-2016	Research Assistantship Scholarship for Graduate Students from Faculty of Science, Chulalongkorn University
2009-2017	Science Achievement Scholarship of Thailand (SAST)

Presentations

2019	**"Inhibition of bacterial adhesion on zwitterionic polyphosphoester-coated apatite surfaces"** 68th Symposium on Macromolecules at University of Fukui, Japan (Poster)
2019	**"Zwitterionic Polyphosphoester Coating for Inhibition of Oral Bacterial Adhesion"** The 14th International Symposium in science and technology 2019 (ISST 2019) at Chulalongkorn University, Thailand (Poster)

Presentations (Continued)

2019   **"High mineral affinity of protein-poly(ethylene sodium phosphate) nanocomplexes"** 68th SPSJ Annual Meeting at Osaka International Convention Center, Japan (Poster)

2019   **"Thermo-assisted generation of protein-poly(ethylene sodium phosphate) conjugates having high mineral affinity"** KUMP International Symposium, Japan (Poster)

2018   **"Heat-induced nanocomplexation of proteins with amphiphilic poly(ethylene sodium phosphate)"** The International Conference on Advanced and Applied Petroleum, Petrochemicals, and Polymers (ICAPPP 2018) at Chulalongkorn University, Thailand (Oral)

2018   **"Design of thermally-assisted complexation of proteins with amphiphilic poly(ethylene sodium phosphate)"** 67th Symposium on Macromolecules at Hokkaido University, Japan (Oral)

2018   **"Thermally assisted complexation of proteins with amphiphilic poly(ethylene sodium phosphate) as versatile excipients"** 47th Medical Polymer Symposium at National Institute of Advanced Industrial Science and Technology, Japan (Poster)

2018   **"Suppression of heat-induced denaturation of proteins via complexation with amphiphilic poly(ethylene sodium phosphate)"** 67th annual meeting at Nagoya Congress Center, Japan (Oral)

2017   **"Heat-assisted complex formation of proteins with amphiphilic poly(ethylene sodium phosphate)"** 66th Symposium on Macromolecules at Ehime University, Japan (Poster)

2016   **"Dual responsive nanoparticles developed by tandem post-polymerization modification of poly(pentafluorophenyl methacrylate) for controlled release applications"** IUPAC-PSK40 at International Convention Center Jeju, Korea (Poster)

2016   **"PEG-containing amphiphilic copolymers: preparation by post-polymerization modification and micelles formation"** Pure and Applied Chemistry International Conference (PACCON 2016) at Bangkok International Trade and Exhibition Centre, Thailand (Poster)

Presentations (Continued)

2013   **"Preparation of in situ silica filled natural rubber by latex coagulation in acid"** 8th Conference on Science and Technology for Youths at Bangkok International Trade and Exhibition Centre, Thailand (Oral)

Publications

2019   **Noree S**, Thongthai P, Kitagawa H, Imazato S, Iwasaki Y. Reduction of acidic erosion and oral bacterial adhesion through the immobilization of zwitterionic polyphosphoesters on mineral substrates, *Chem. Lett*. 2019. (In press)

2019   **Noree S**, Iwasaki Y. Thermally assisted generation of protein–poly(ethylene sodium phosphate) conjugates with high mineral affinity, *ACS Omega* 2019, *4*, 3398-3404.

2017   **Noree S**, Tangpasuthadol V, Kiatkamjornwong S, Hoven V. P., Cascade post-polymerization modification of single pentafluorophenyl ester-bearing homopolymer as a facile route to redox-responsive nanogels, *J. Colloid Interface Sci.* 2017, *501*, 94-102.

ACKNOWLEDGEMENTS

Susita Noree